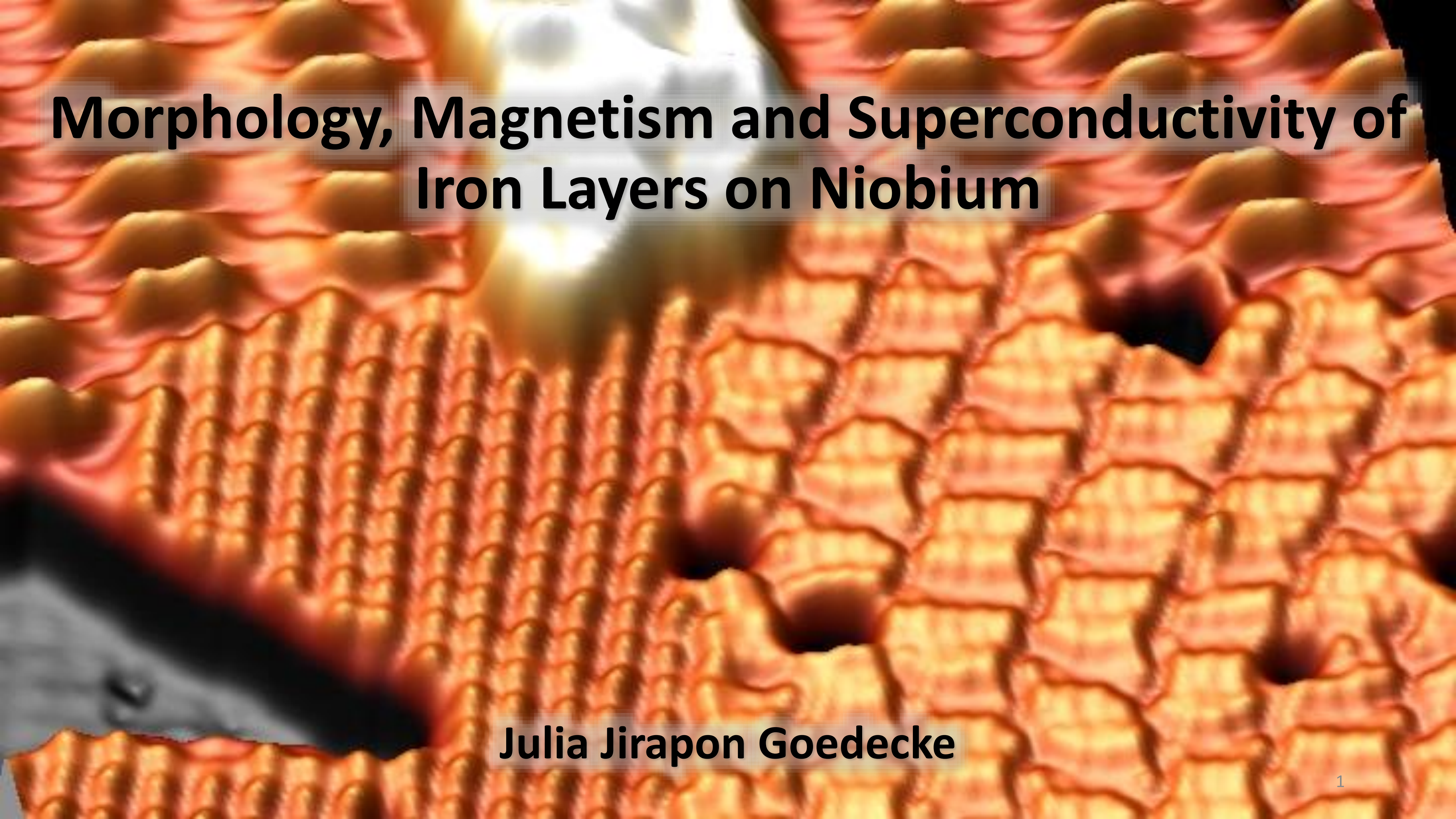

Morphology, Magnetism and Superconductivity of Iron Layers on Niobium

Julia Jirapon Goedecke

Motivation

- quantum computer
    - problem of decoherence: loss of superposition of a quantum state due to the environment

- new approaches: **topological qubits** - Majorana (quasi)particles
    - Majorana fermions origin in particle physics
    - particles which are their own antiparticles $\gamma = \gamma^\dagger$
    - search for Majorana fermions

- In solid state physics: **Majorana zero modes (MZM)**
    - charge- and spinless quasiparticles
    - in 2D: anyons obeying non-Abelian statistics

- In this work, physical systems were investigated to determine whether they are suitable for the realization of MZM

Source: IBM's Q System One

Fantastic Majoranas and where to find them

- e$^-$ and h$^+$ can be considered as particle and antiparticle
  - $c \neq c^\dagger$
- in superconductors (SC) $\gamma = uc + vc^\dagger$
  - the Majorana condition $\gamma = \gamma^\dagger$ is fulfilled for $u = v^*$
  - one expects Majorana excitations at $E = 0$

- taking spin into account leads to $\gamma_\uparrow \neq \gamma_\uparrow^\dagger$
  - make the equations somehow independent of spin
  - completely spin-polarizing all fermions ("spinless")
  - BSC SC: Cooper pairs comprised of superposition of spin-up and spin-down electrons
  - **p-wave SC** (Sr_2RuO_4 ???)

F. von Oppen, *et al*. Oxford Univ. Press (2014)

- artificially build a spinless p-wave SC:
  - the spin-degeneracy of an s-wave SC must be lifted -> spin orbit coupling
  - magnetic field -> separate two bands, fully spin-polarized

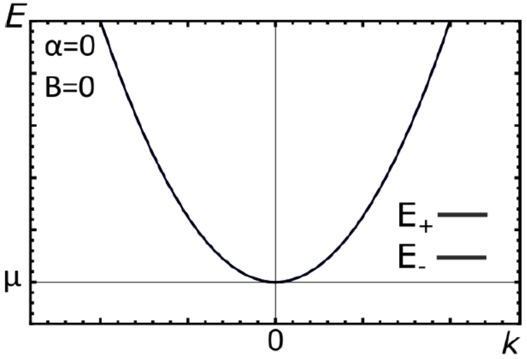

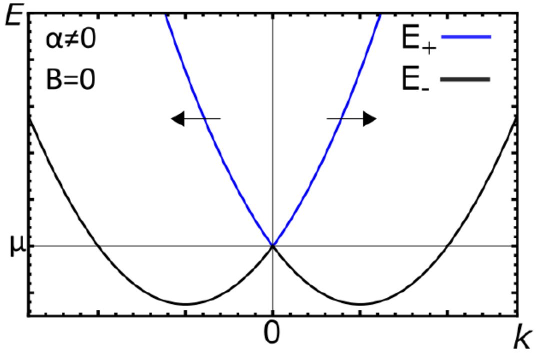

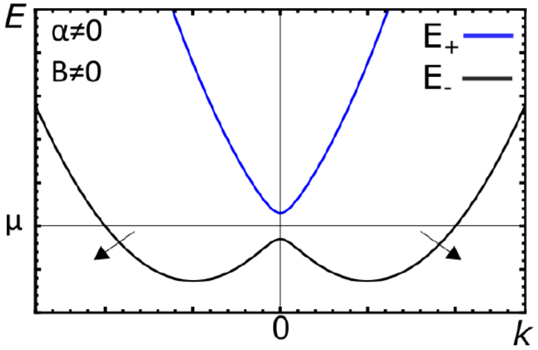

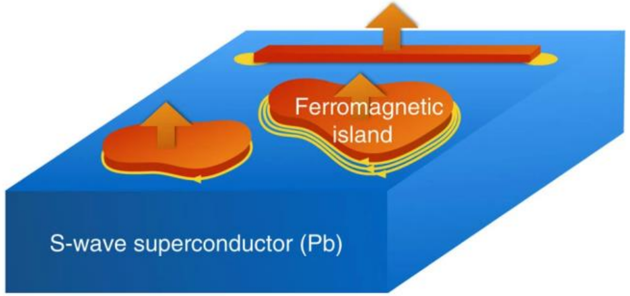

Li *et al.*, *Nat Commun* **7**, 12297 (2016)

Martin *et al. Semicond. Sci. Technol.* **27** 124003 (2012)

Practical realization of Majoranas via Yu-Shiba-Rusinov[1,2,3] states

Single magnetic impurity

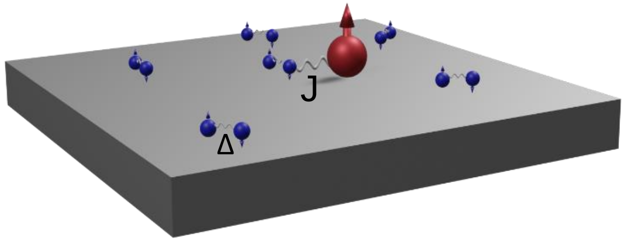

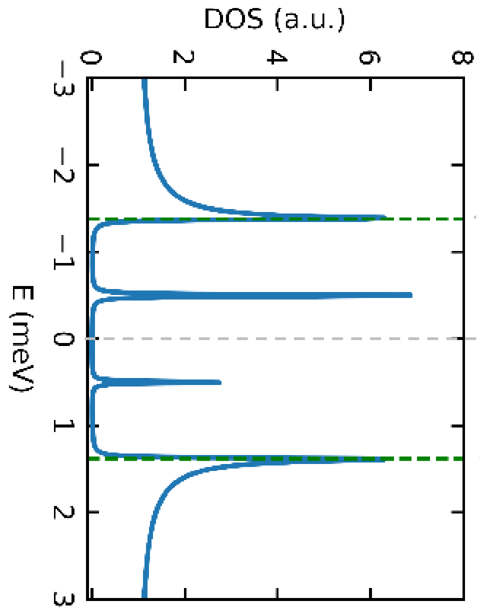

Multiple magnetic impurities

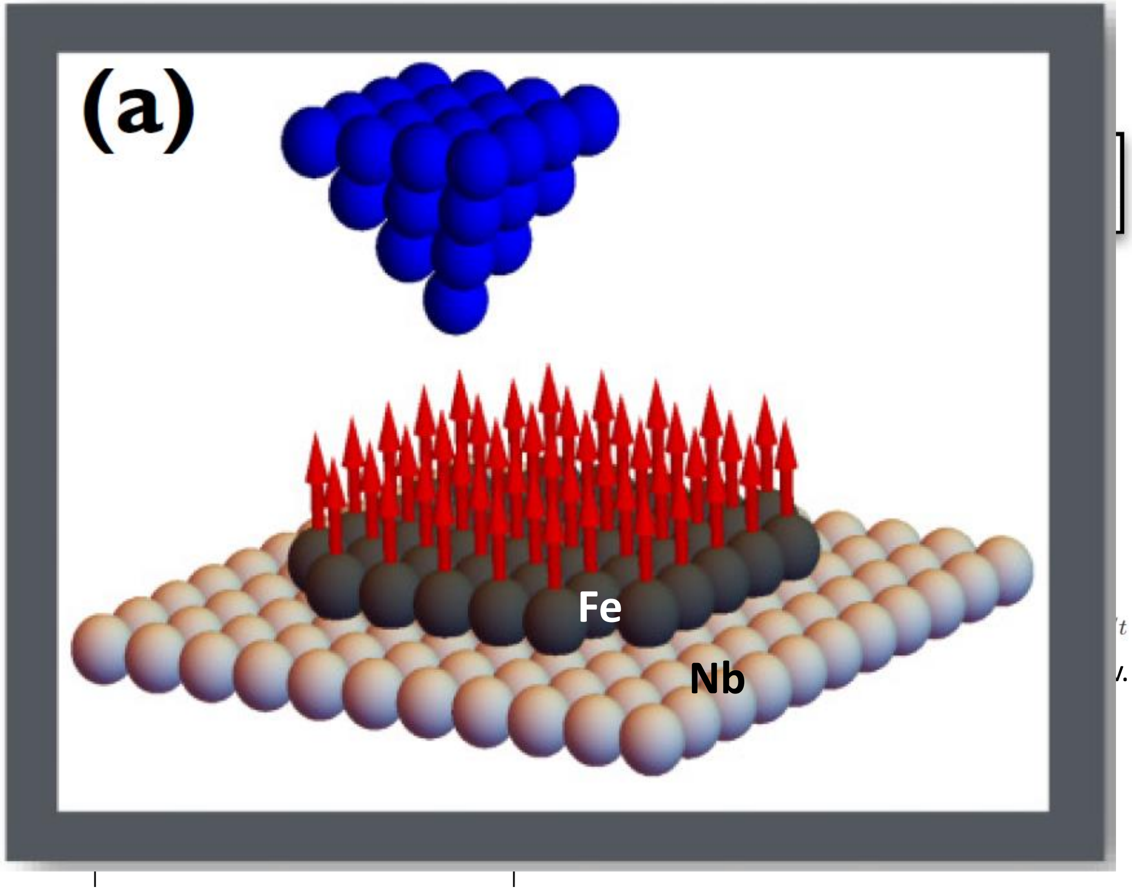

Inspired by F. von Oppen, *et al*. Oxford Univ. Press (2014)

2D Shiba lattice

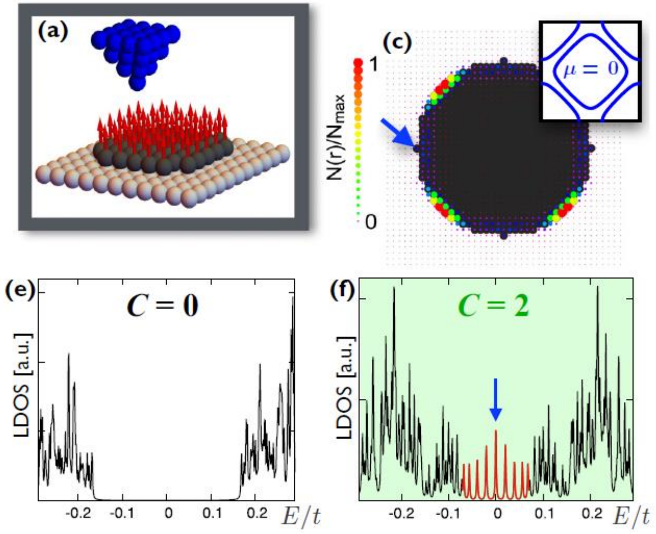

. B 96, 205131 (2017)

[1] Yu, Acta Phys. Sin., 1965, 21(1): 75-91; [2] Shiba, Prog of Theoretical Physics, (1968); [3] Rusinov, Eksp. Teor. Fiz 9, (1968) 146

Instrumentation: UHV system with scanning tunneling microscopy

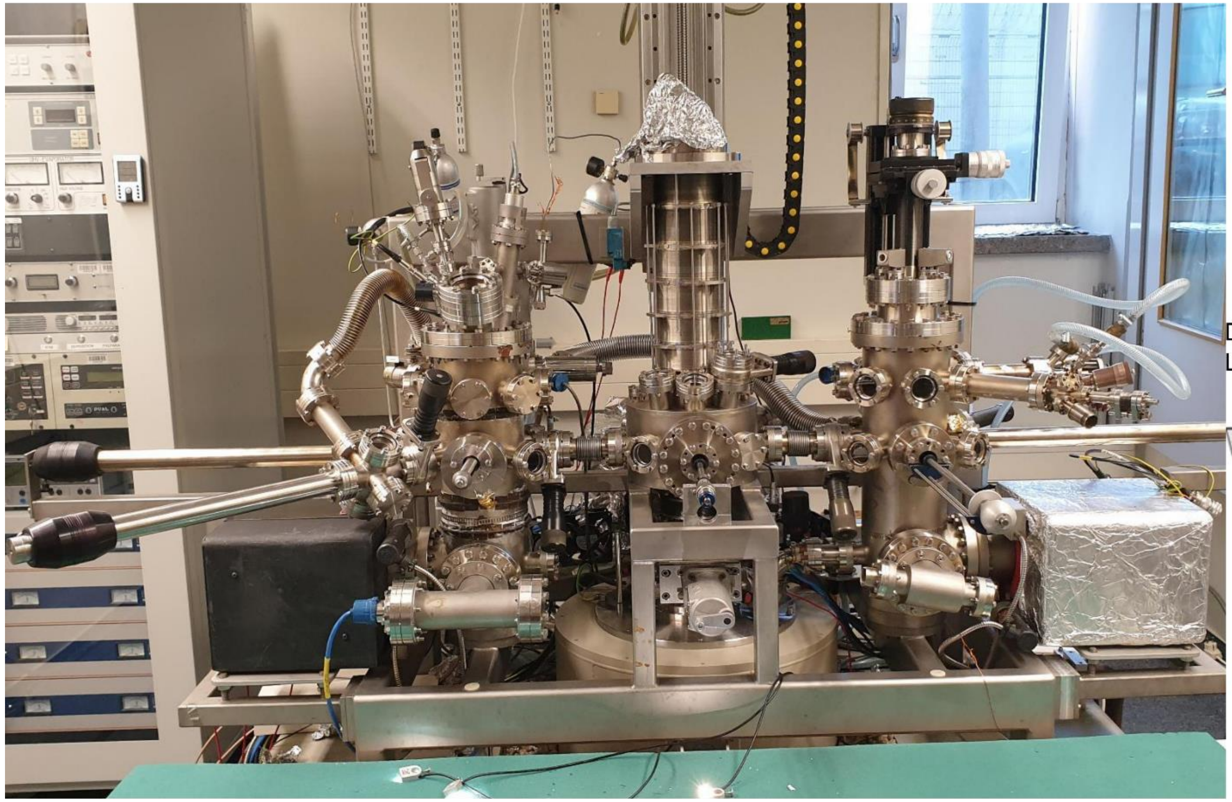

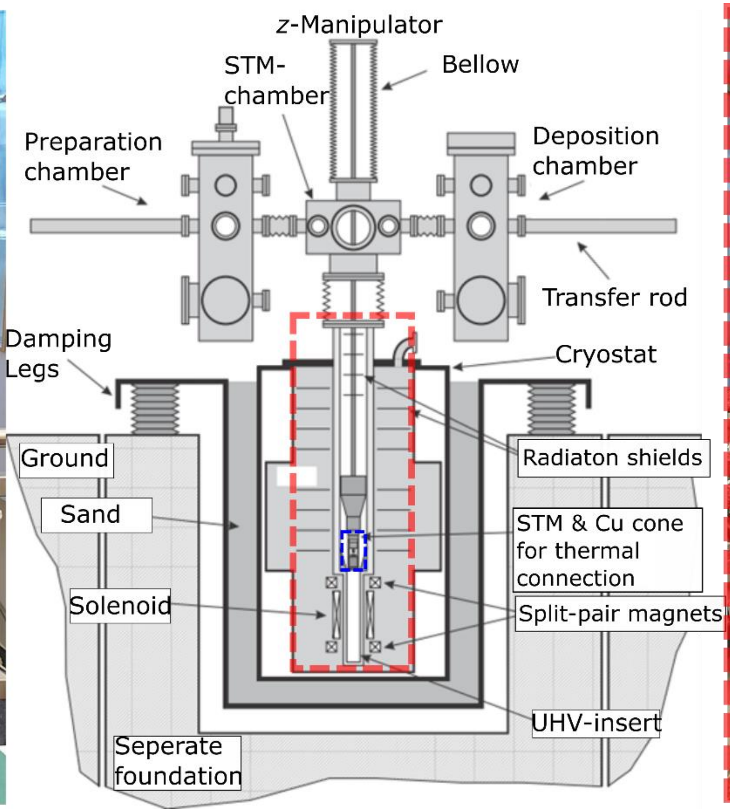

VT-STM

- ➢ UHV 10^{-10} mbar
- ➢ T = 25 K

He-bath STM System: Lab 014

- ➢ UHV 10^{-10} mbar
- ➢ T = 6.5 K
- ➢ $B_x = 2.5\ \mathrm{T}, B_z = 6\ \mathrm{T}$

JT-STM cryostat Specs Lab

- ➢ UHV 10^{-10} mbar
- ➢ T = 4 K
- ➢ $B_z = 2.8\ \mathrm{T}$

Scanning Tunneling Microscope (STM)

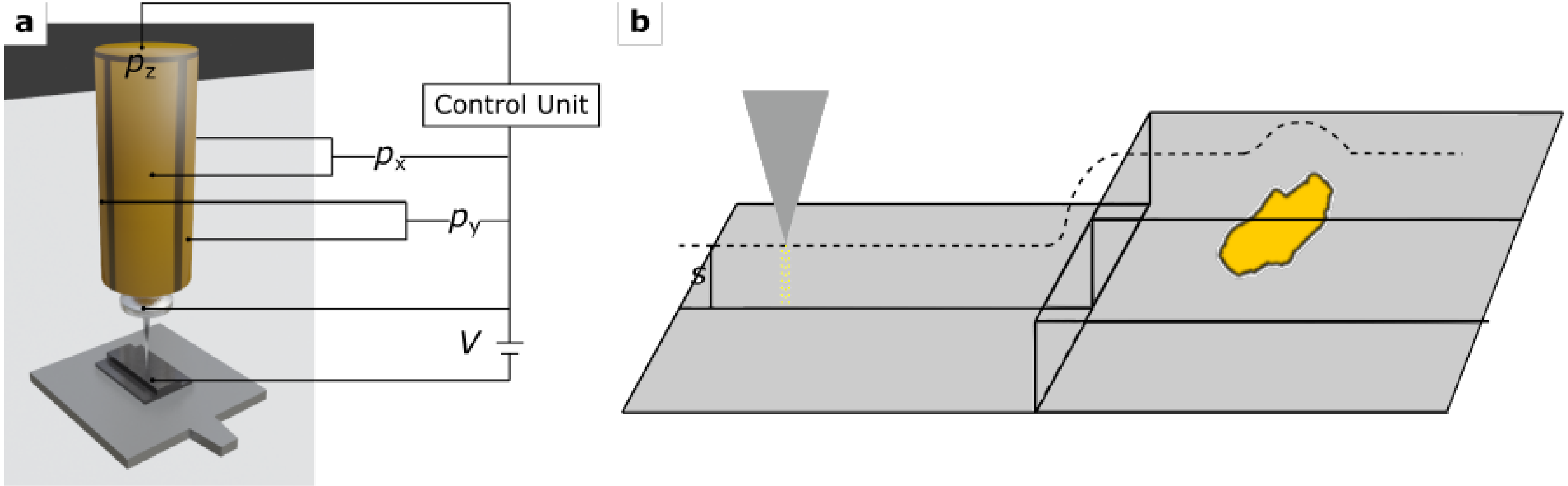

- sharp tip is raster-scanning a surface
- distance between the tip and the surface is only a few Angstrom
- wave function of the tip and the sample can overlap
  - electrons can tunnel from the tip to the sample
- if a voltage is applied between the tip and the sample, a net tunneling current in a define direction is obtained
- loop keeping I constant which is dependent of the distance
- from the vertical change of position of the tip the topography of the surface can be extracted
- STM can also be used for spectroscopic measurements by changing the bias voltage during the measurement

Niobium (Nb) as an s-wave superconductor

- Nb(110) twofold surface symmetry
- Nb(111) threefold surface symmetry
  - could favor the formation of chiral spin structures which might eliminate the need for strong spin-orbit coupling
- problem with Nb: high contamination with (mostly) oxygen
  - established process for Nb(110): cleaning by sputtering and annealing at very high temperature near the melting point
  - no established process for cleaning Nb(111)

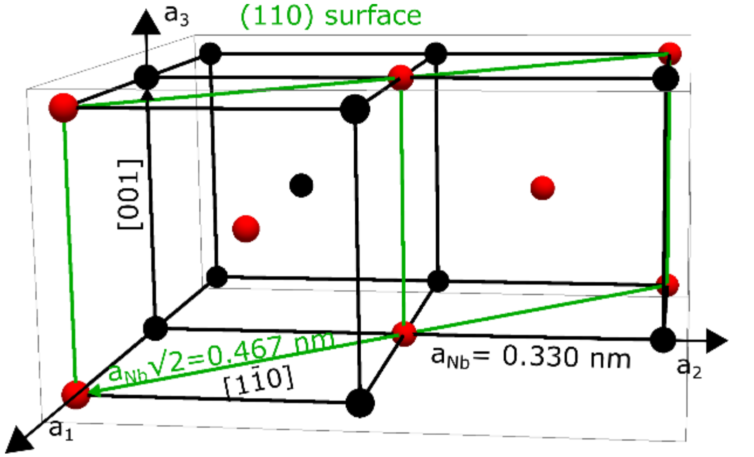

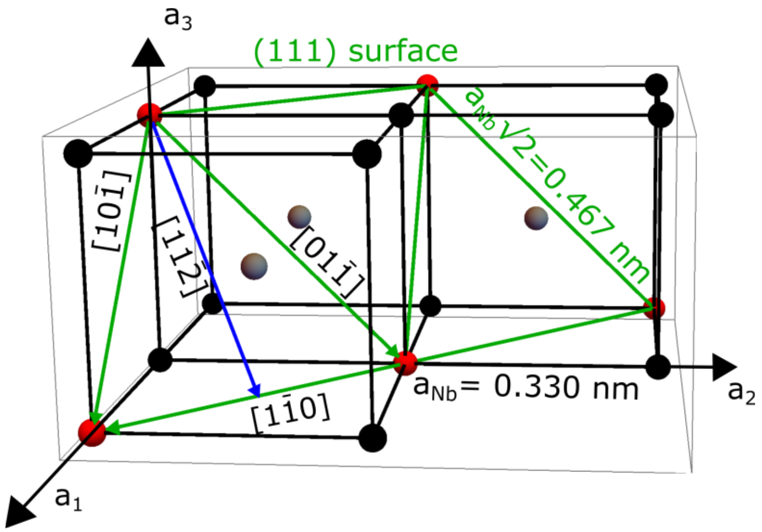

Attempts of cleaning Nb(111) by sputter-annealing cycles

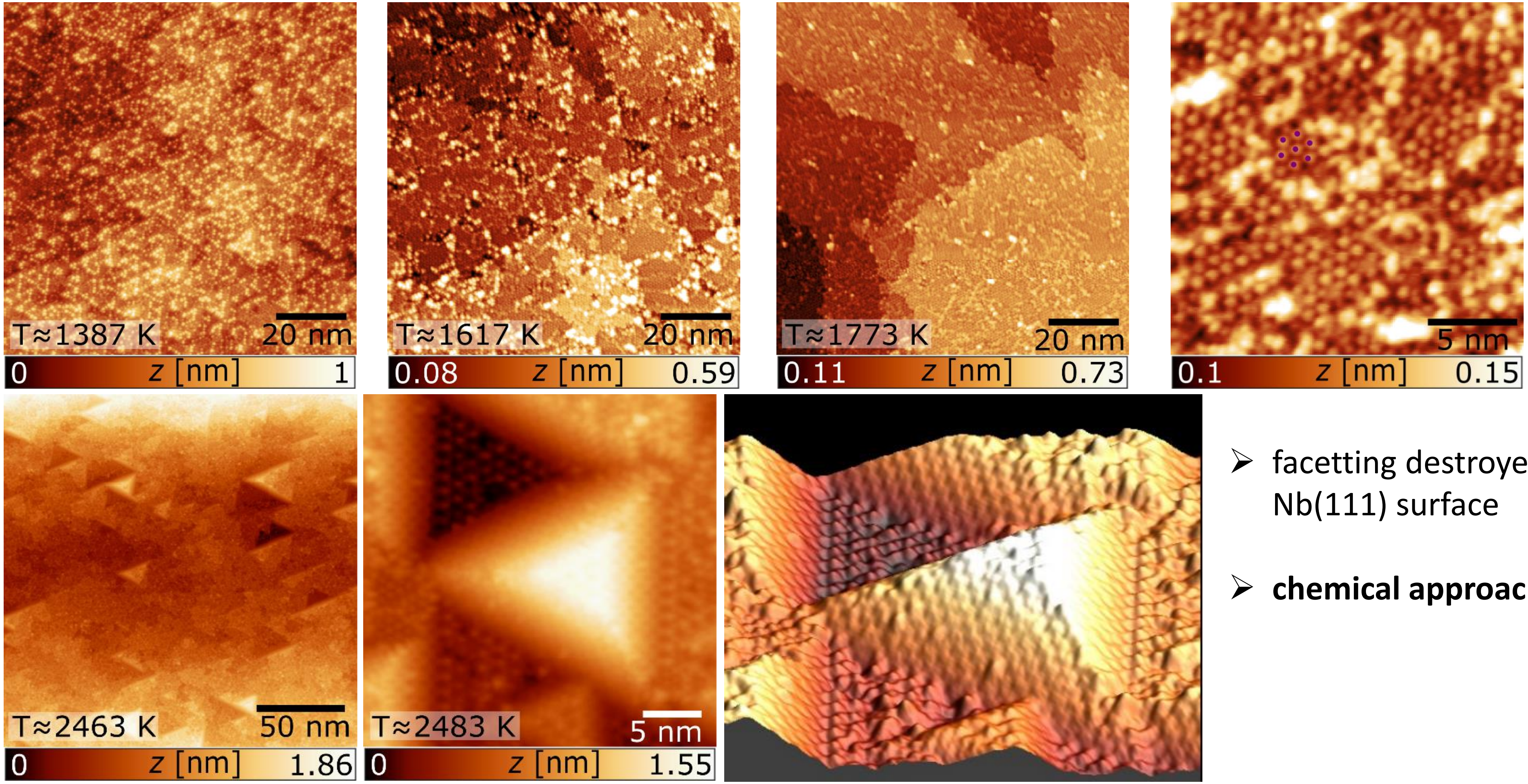

- ➢ facetting destroyed the Nb(111) surface
- ➢ **chemical approach**

Cleaning Nb(111) via atomic H treatment

- chemical reduction
  $\mathrm{NbO_x} + 2\mathrm{H} \rightarrow \mathrm{Nb} + \mathrm{H_2O}$

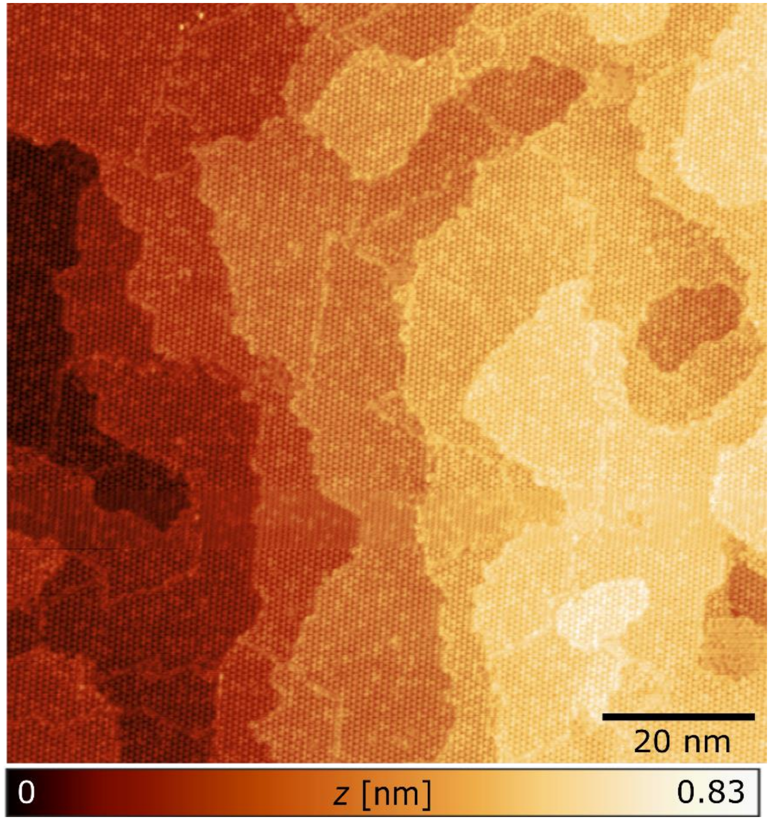

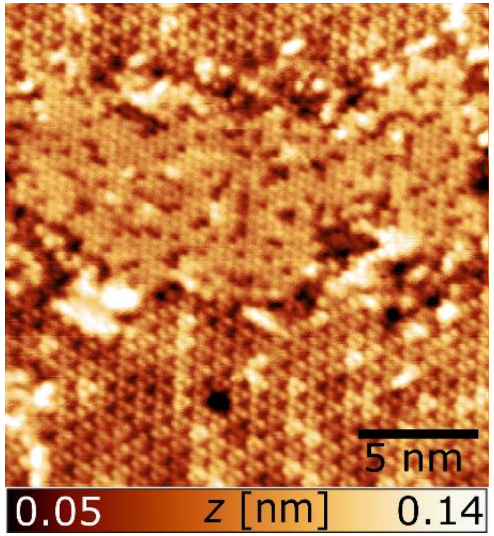

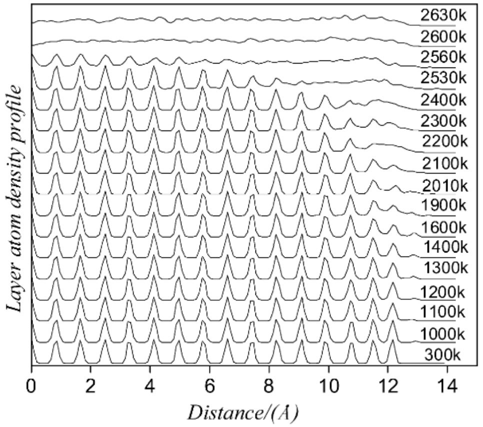

Fig. 1. The layer atomic density profiles with temperature for Nb(111) plane.

X. Yang et al., Physics Letters A 365 (2007) 161–165

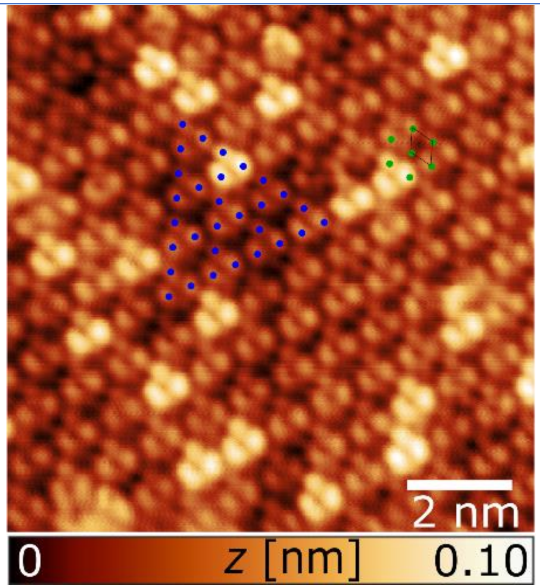

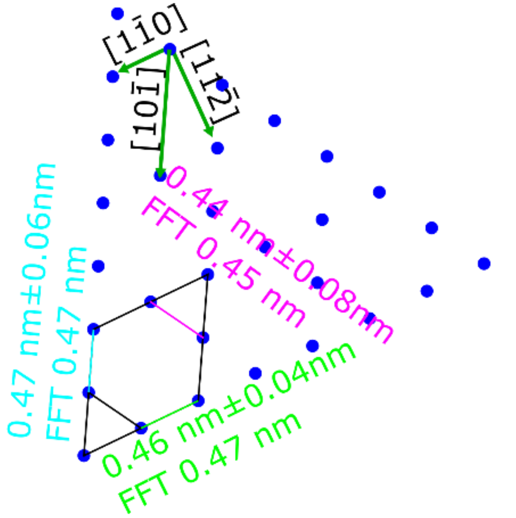

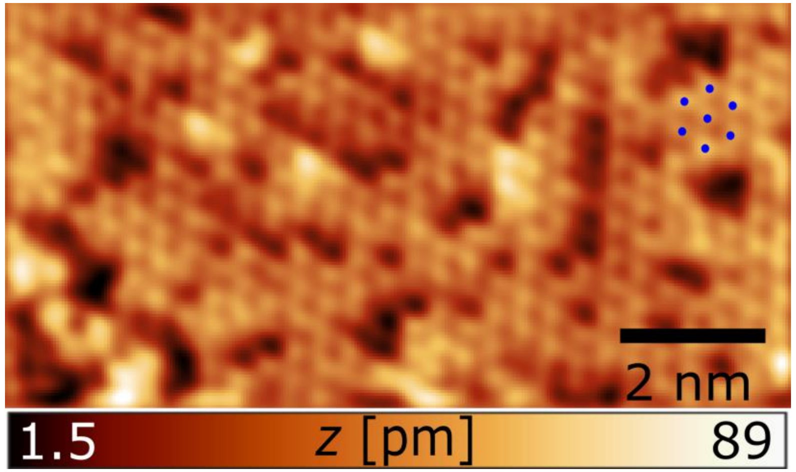

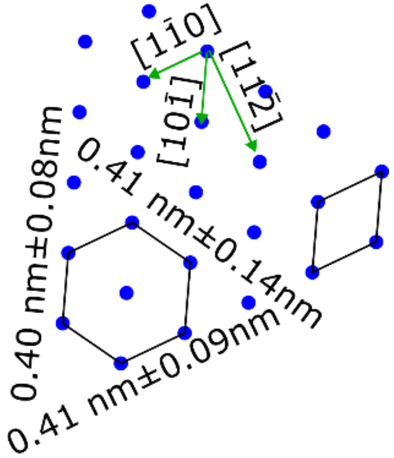

J. Goedecke et al. Phys. Rev. Materials 7, 084803, 2023

Evaporation of magnetic material on Nb(111)

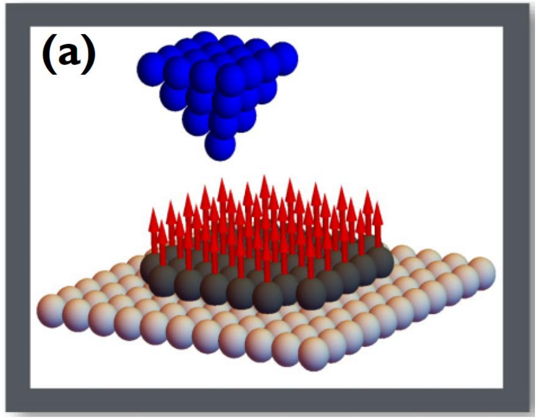

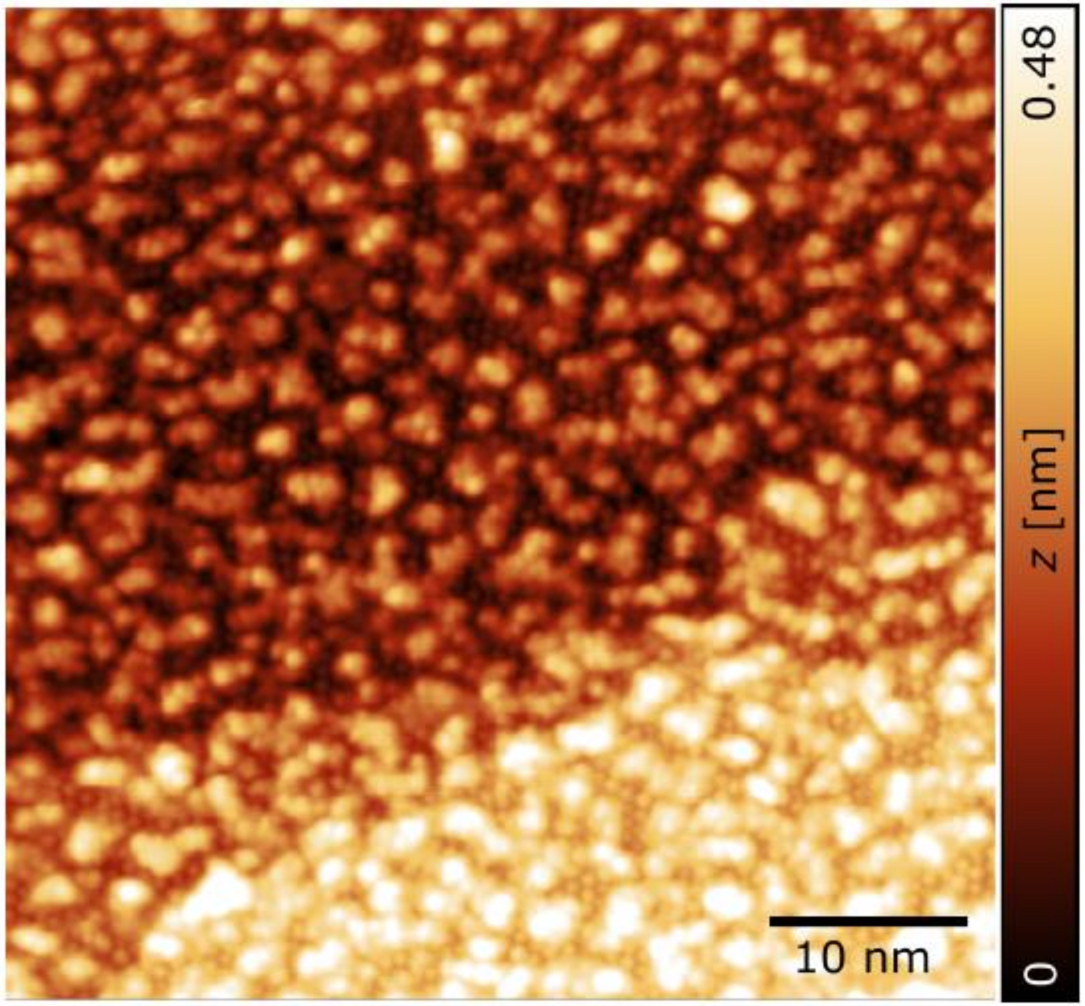

- Fe deposition leads to clustering
- presumably due to the open surface of the Kagome lattice
- growth of Fe ML on Nb(111) was not possible

Monolayer growth of Fe on Nb(110)

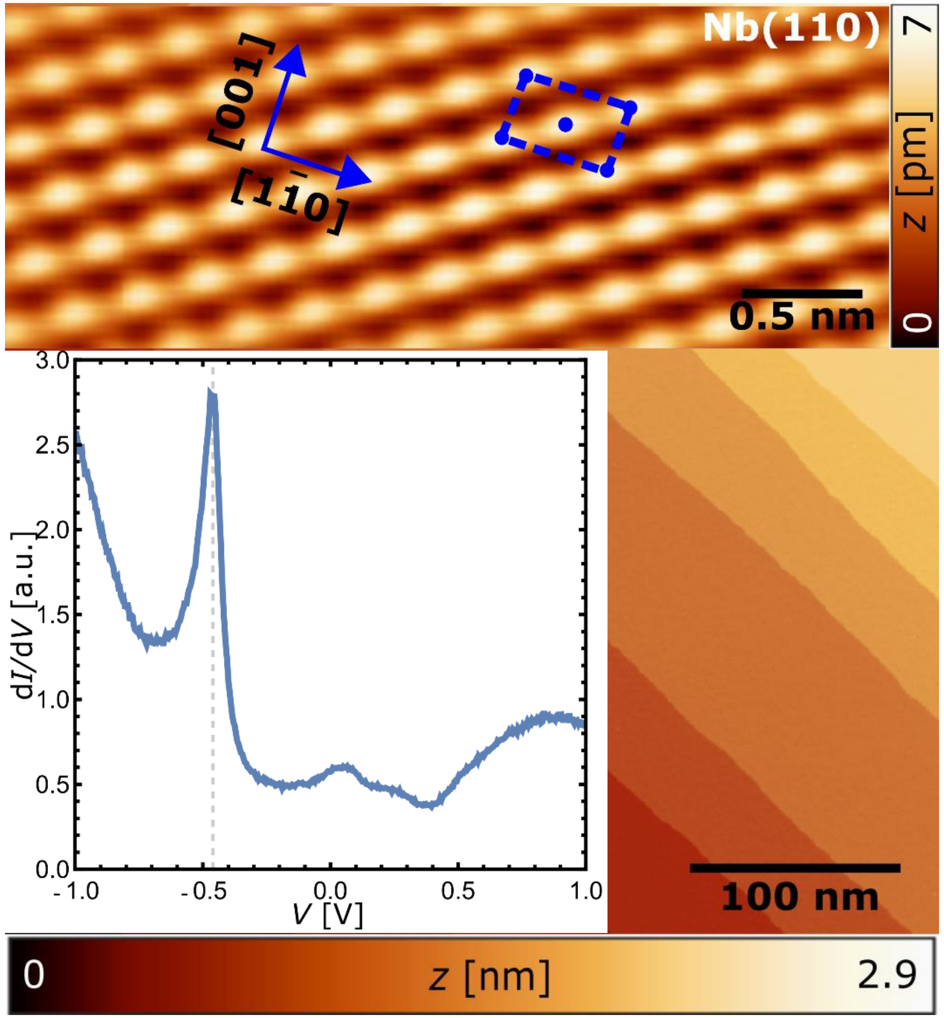

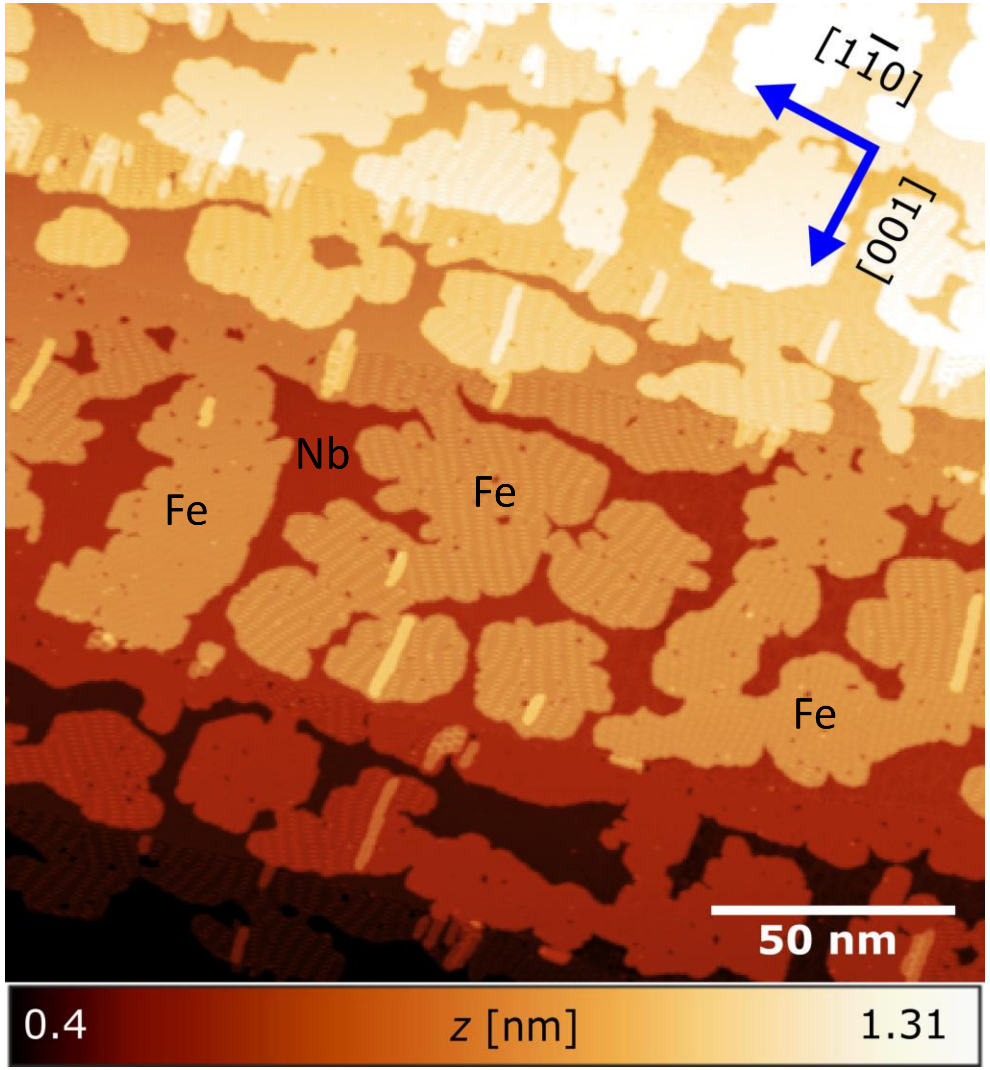

A. Odobesko *et al.*, PRB **99,** 115437 (2019)

J. Goedecke *et al.*, ACS Nano **2022** *16* (9), 14066-14074

Reconstructions of Fe ML on Nb(110)

- **disorder** in the structure
- three different reconstructions of Fe: type I, type II and type III

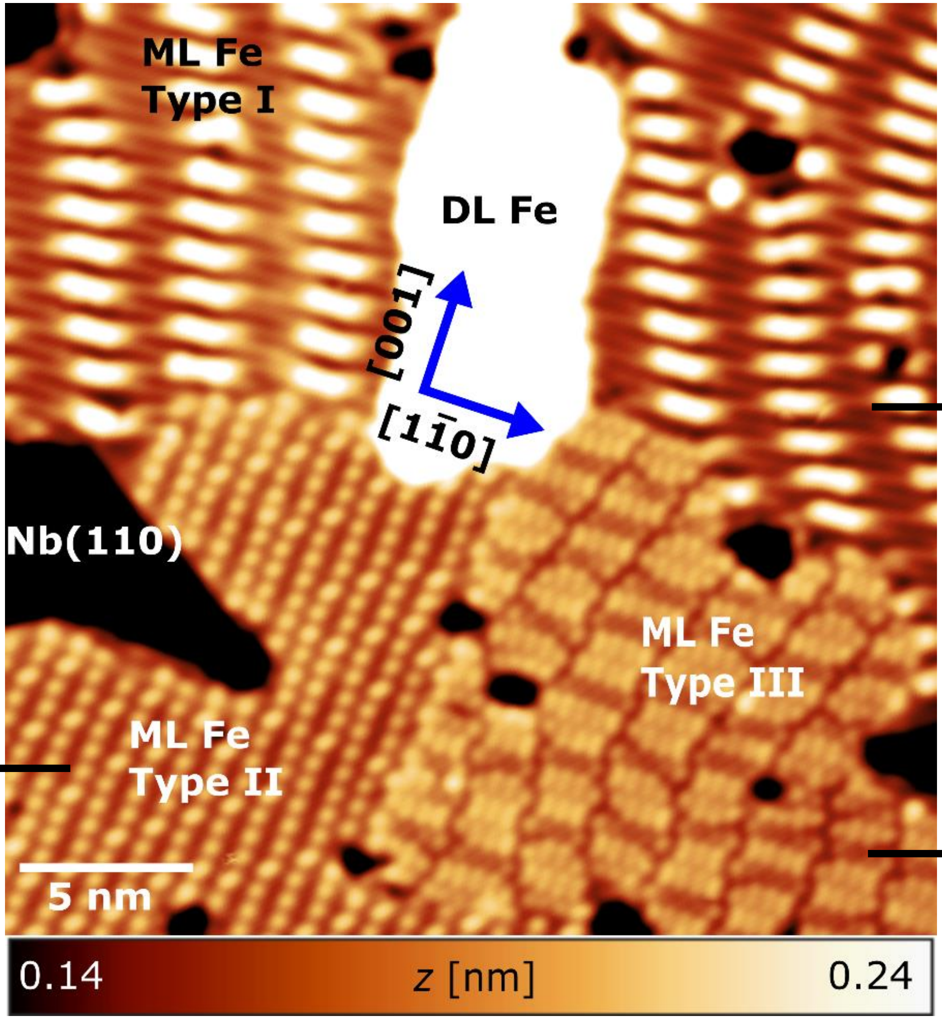

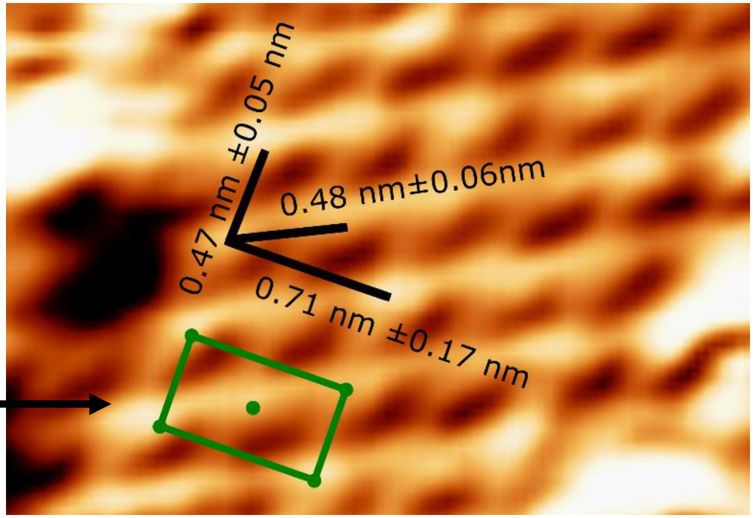

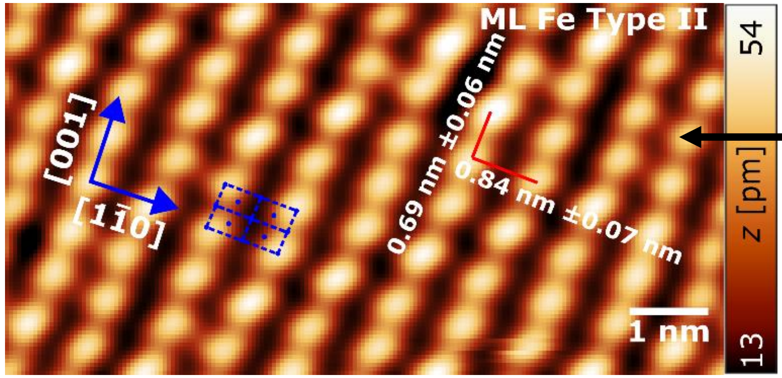

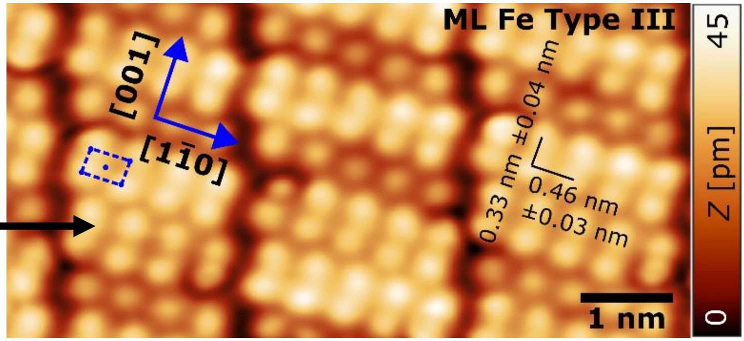

J. Goedecke *et al.*, ACS Nano **2022** *16* (9), 14066-14074

Investigating the magnetic properties via SP-STM

- spin-polarized scanning tunneling microscopy (SP-STM)
  - magnetic materials -> spin splitting of the DOS
  - parallel alignment -> high current
  - antiparallel alignment -> low current

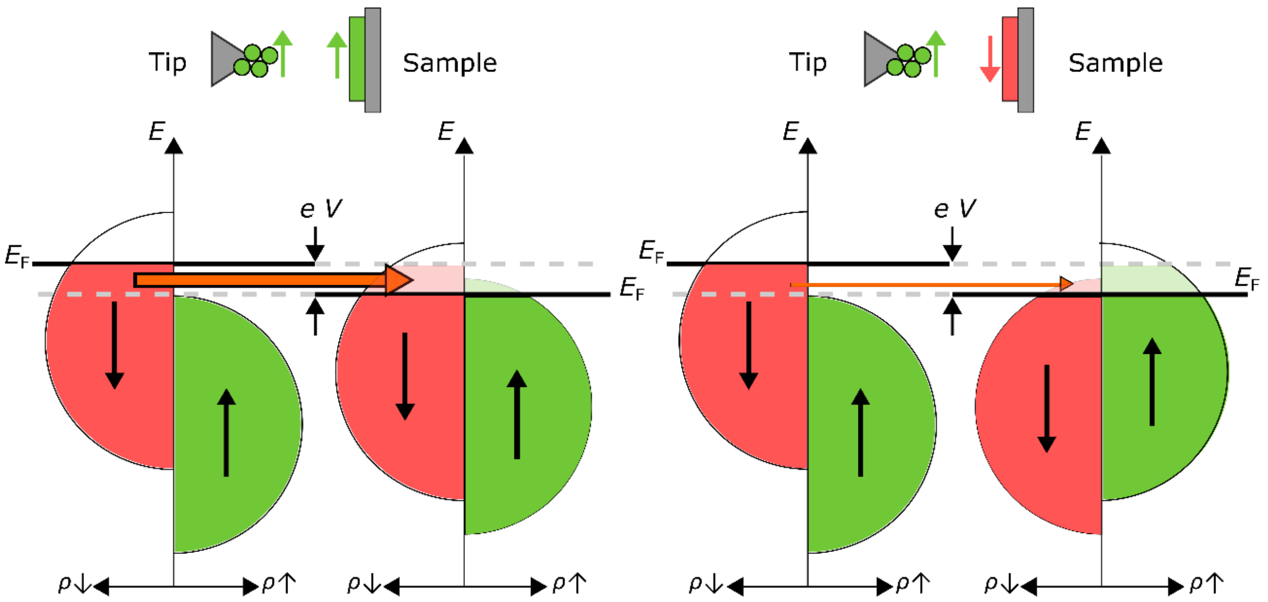

Characterization of magnetic tip 1

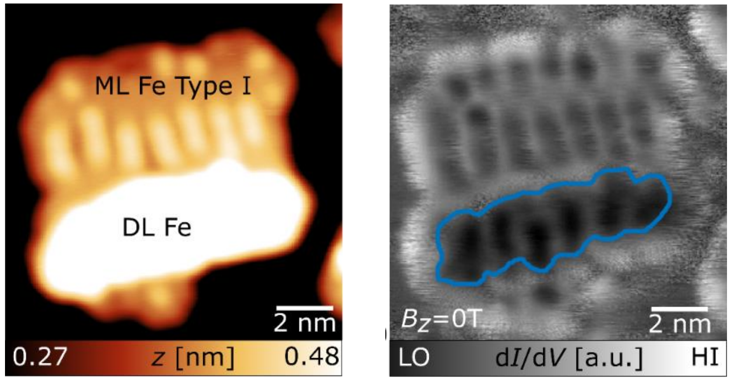

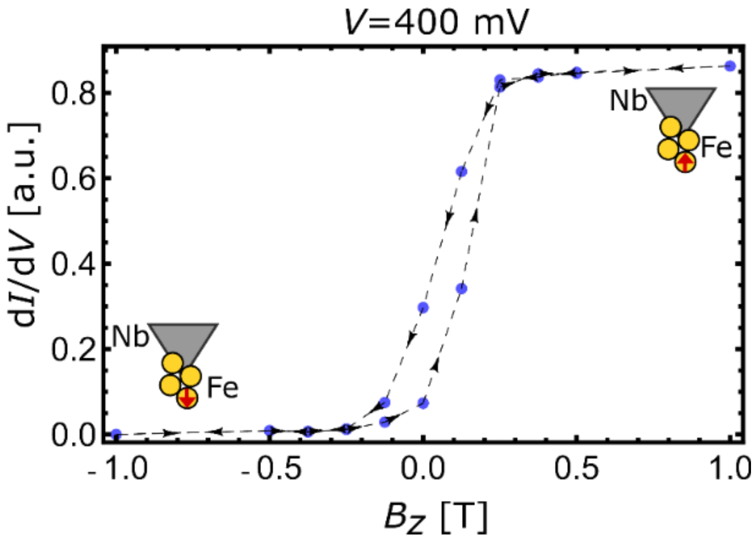

Magnetic properties of type I

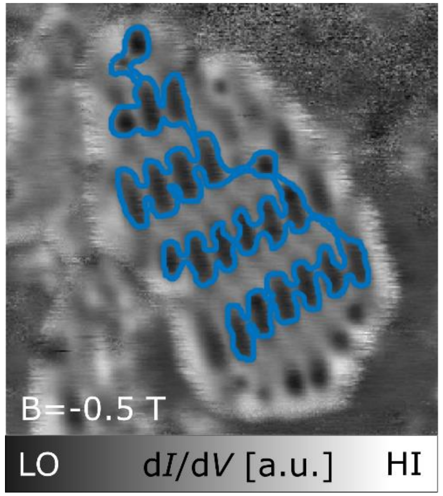

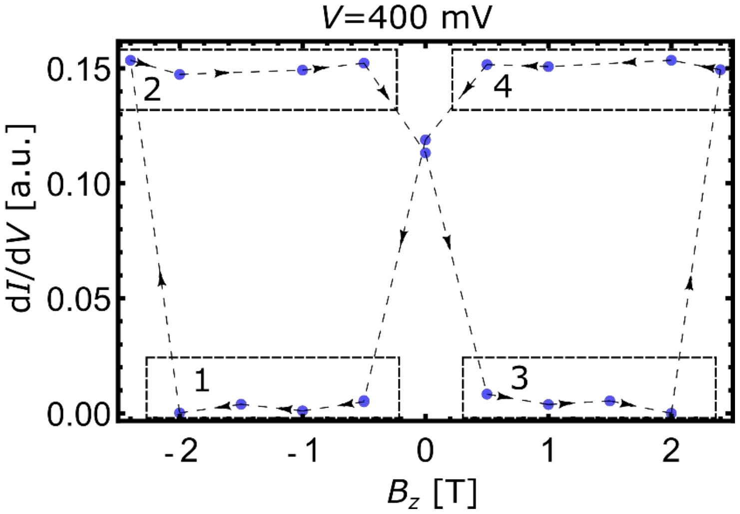

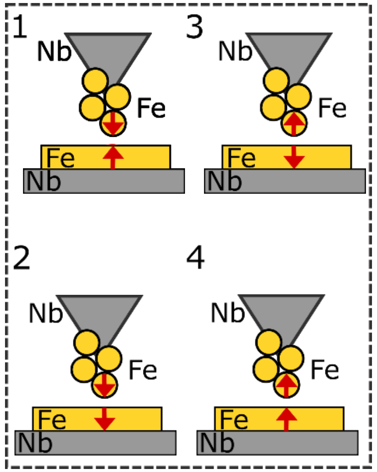

MONTECRYSTAL[1]

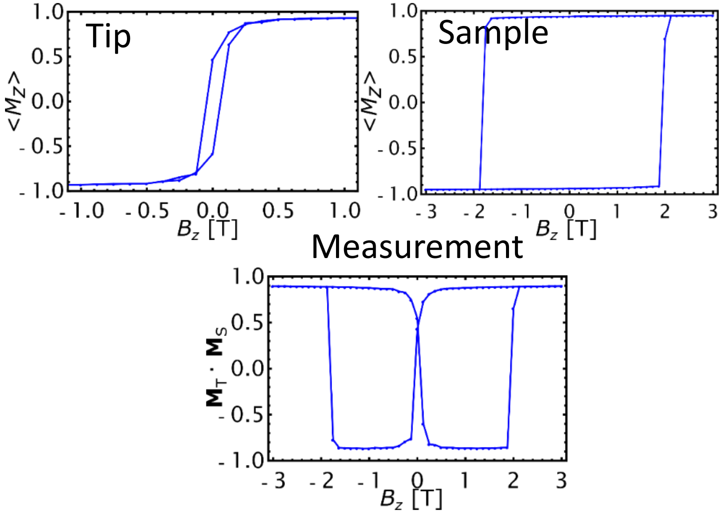

$$\frac{\mathrm{d}I}{\mathrm{d}V}(\mathbf{r}_0, V) \propto \rho_{\mathrm{t}}\rho_{\mathrm{s}}(\mathbf{r}_0, E_{\mathrm{F}} + eV) + \mathbf{M}_{\mathrm{t}}\mathbf{M}_{\mathrm{s}}(\mathbf{r}_0, E_{\mathrm{F}} + eV)$$

[1] J. Hagemeister, https://github.com/JHagemeister/MonteCrystal

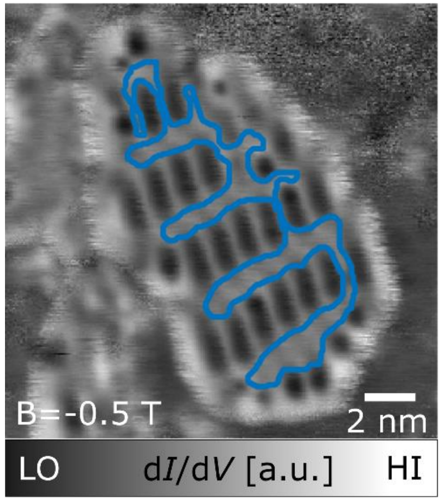

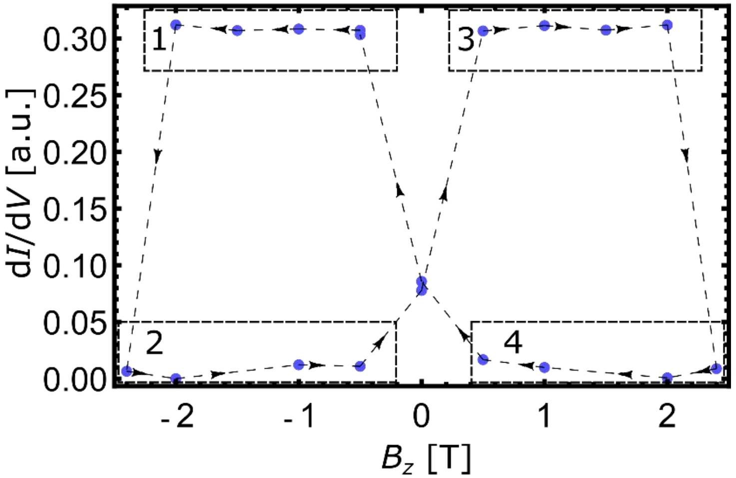

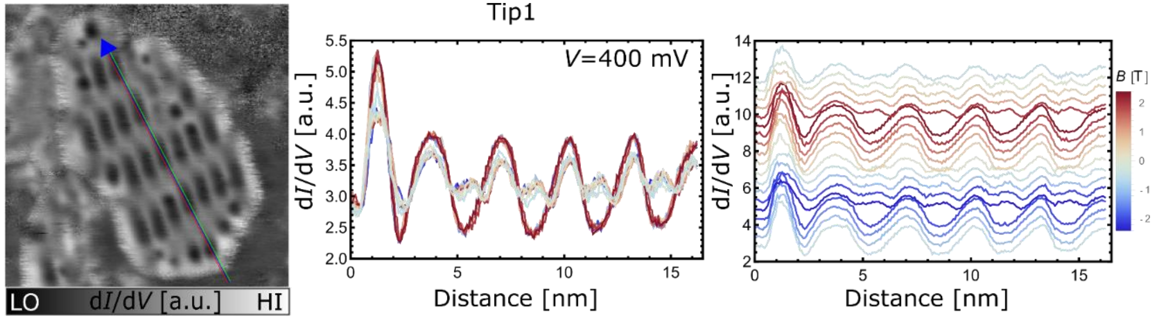

- ➢ out-of-plane ferromagnetic monodomain

Magnetic properties of type II & type III

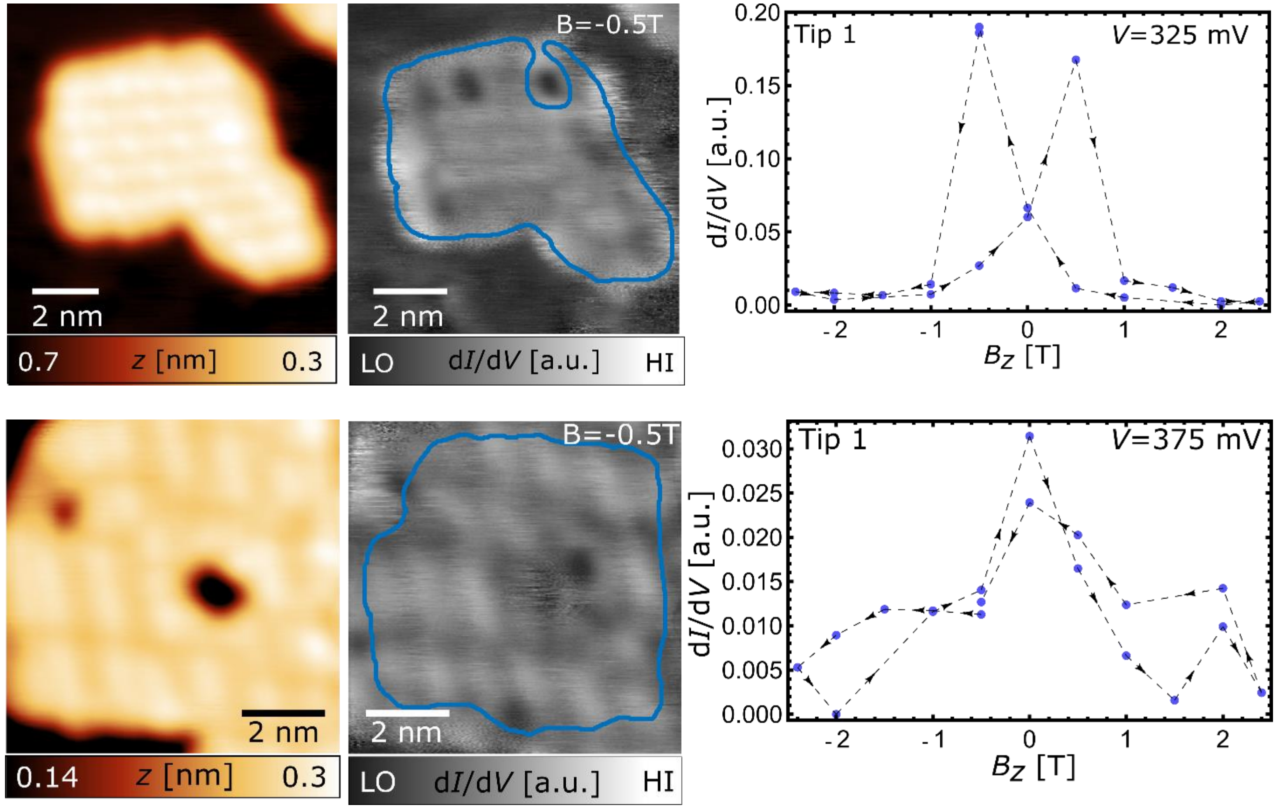

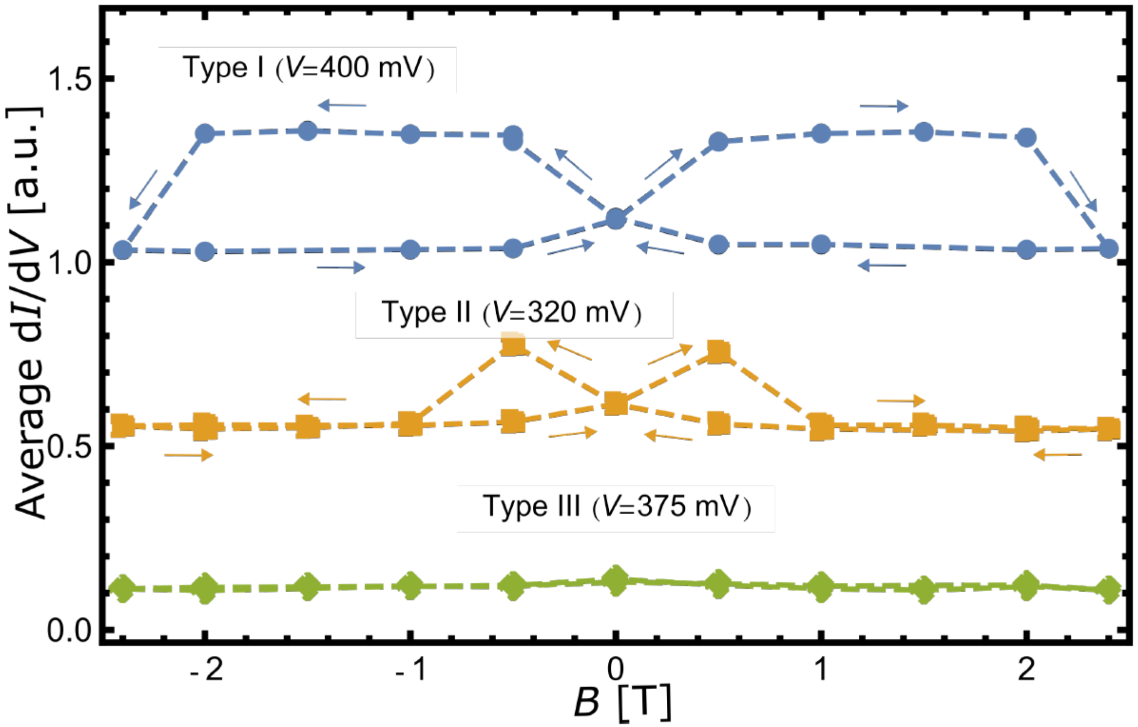

J. Goedecke *et al.*, ACS Nano **2022** *16* (9), 14066-14074 c

Fe type	B_c [T]
I	2.2 ± 0.2
II	0.75 ± 0.2
III	< 0.4

Monte Carlo simulations show:

- with increasing coercivity, increasing values for *J* and *K*

- All islands:

ferromagnetic monodomains out of plane with different coercive field strengths

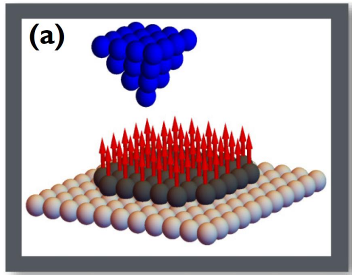

Rachel *et al*. Phys. Rev. B 96, 205131 (2017)

Tunneling processes between two superconductors

$T \neq 0\ \mathrm{K}$

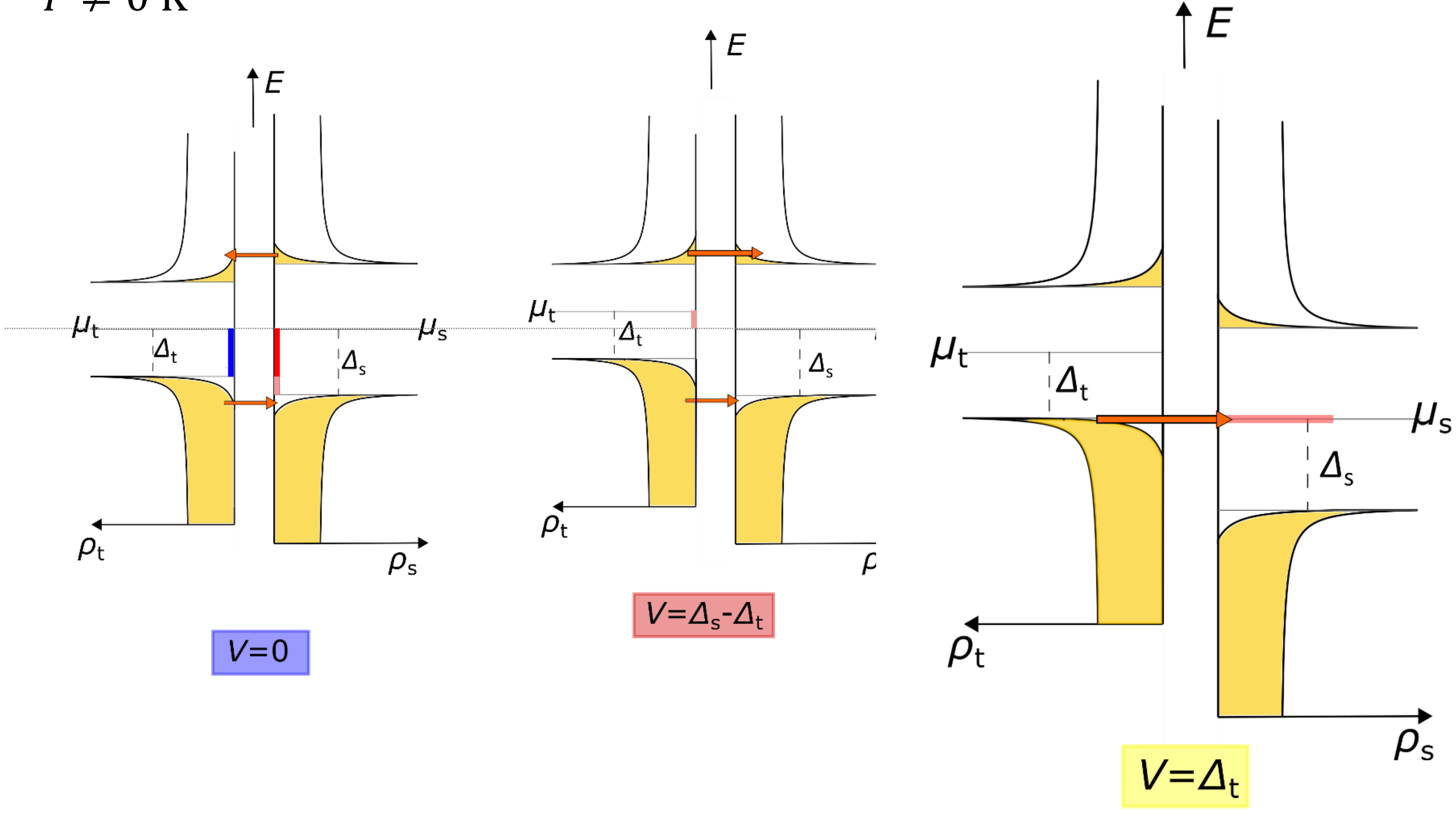

$T = 4.5\ \mathrm{K}$

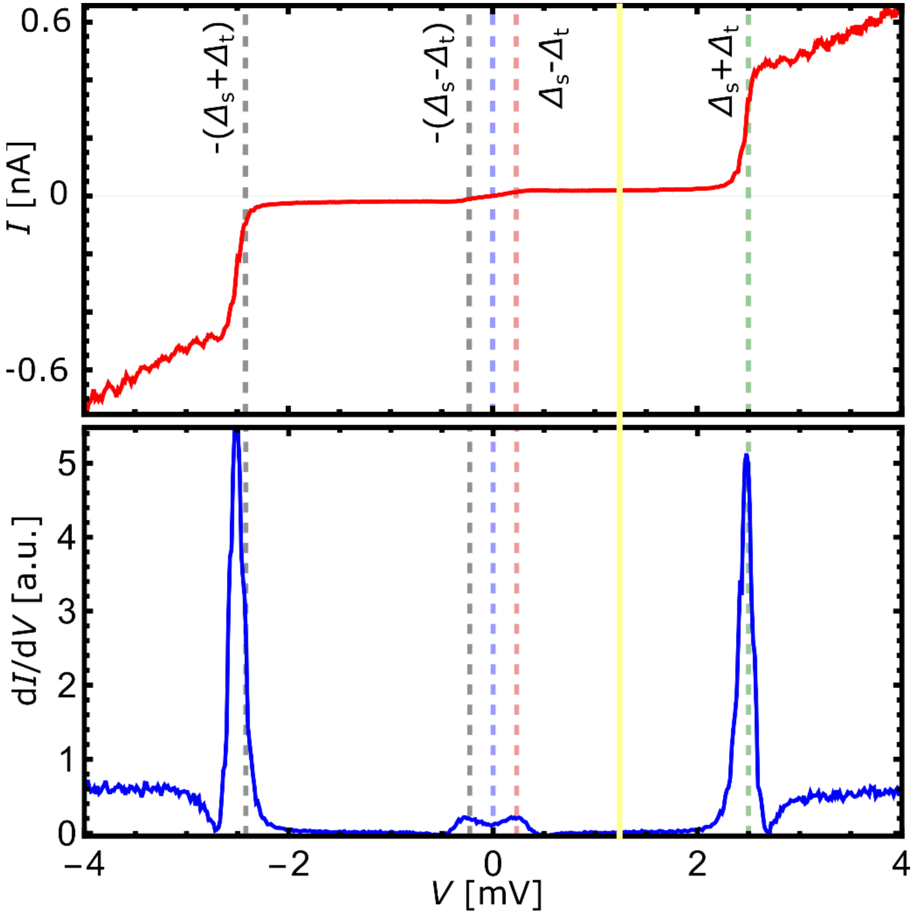

Sketch inspired by Gross, Marx, Festkörperphysik 3 Auflage, De Gruyer

Spectroscopy measurement inside the gap of Fe/Nb(110) type I

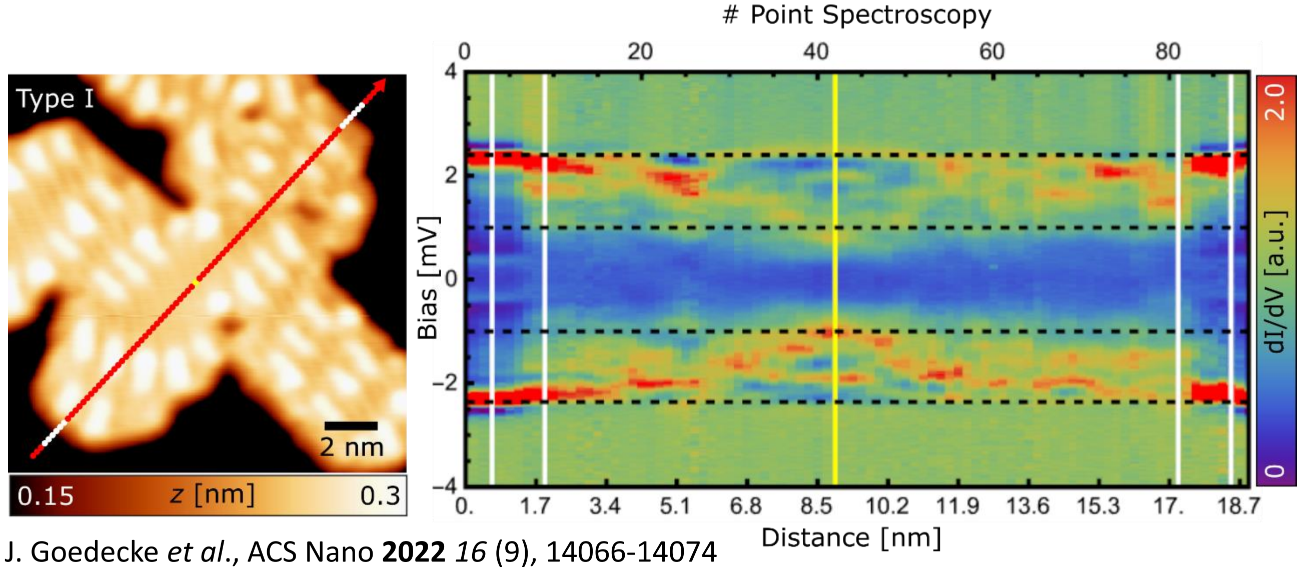

J. Goedecke *et al.*, ACS Nano **2022** *16* (9), 14066-14074

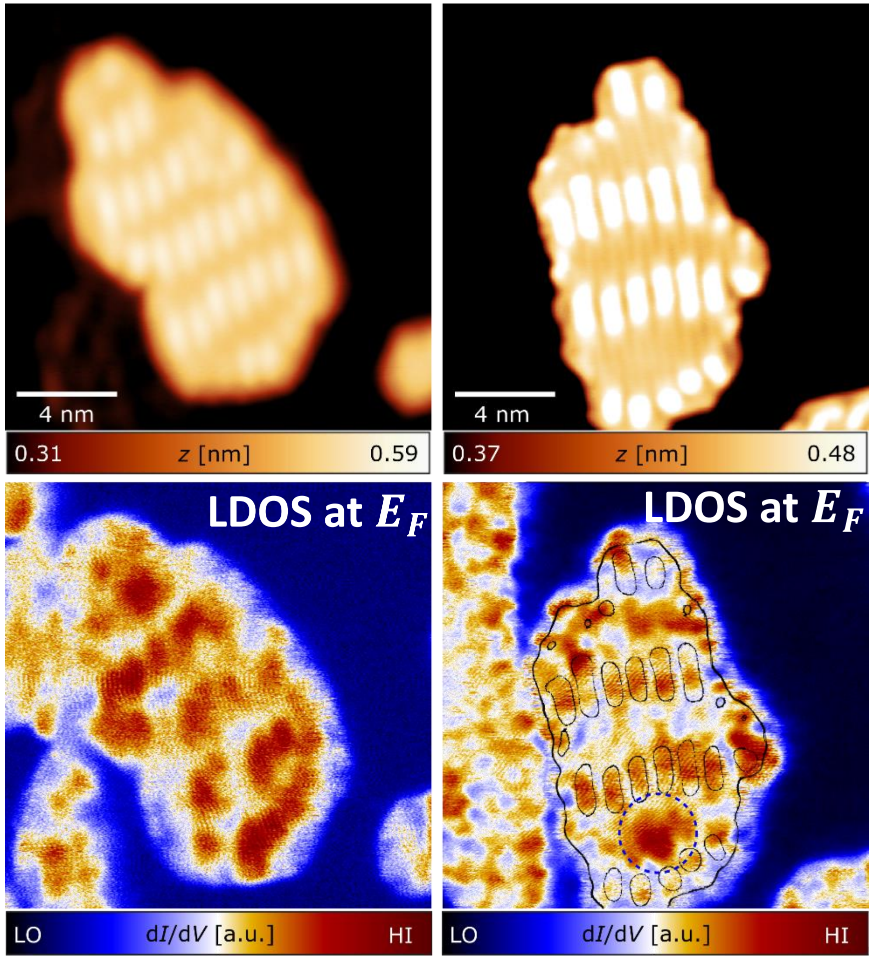

- gap filled completely with Shiba bands
- strong variation of Shiba bands
  - locally with the underlying topographic structure
  - with the intensity
- significant intensities at E_F
  - bandwidths are large enough to overlap with E_F
  - no gap reopening
  - no edge modes
- the coherence peaks are strongly suppressed

Inside the gap of Fe/Nb(110) type II & type III

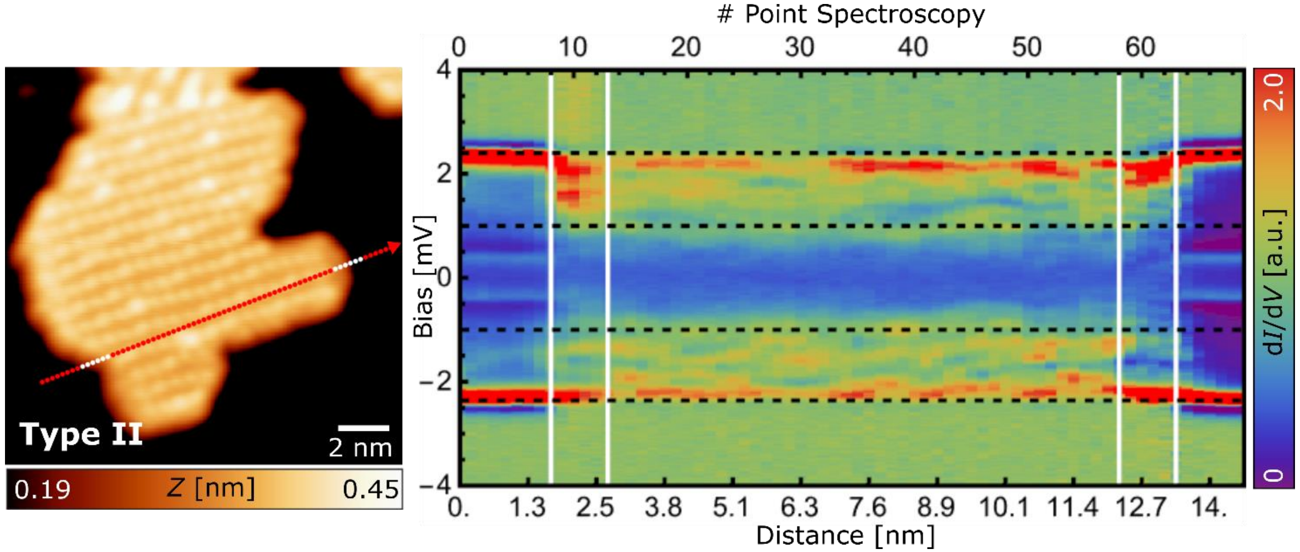

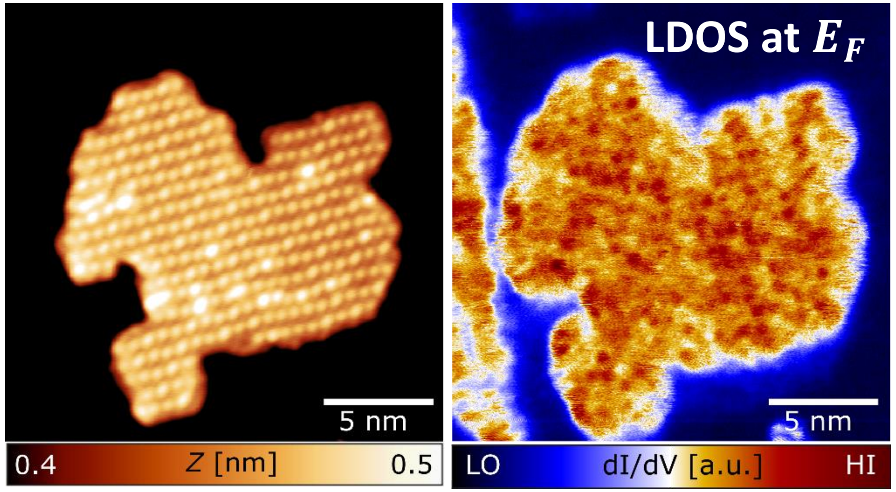

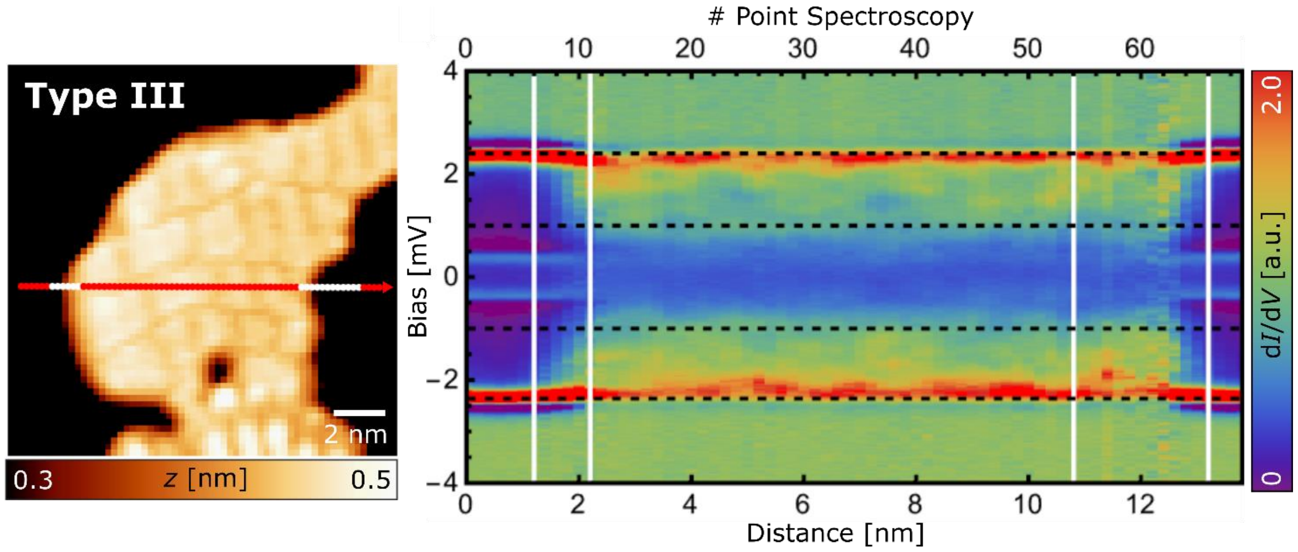

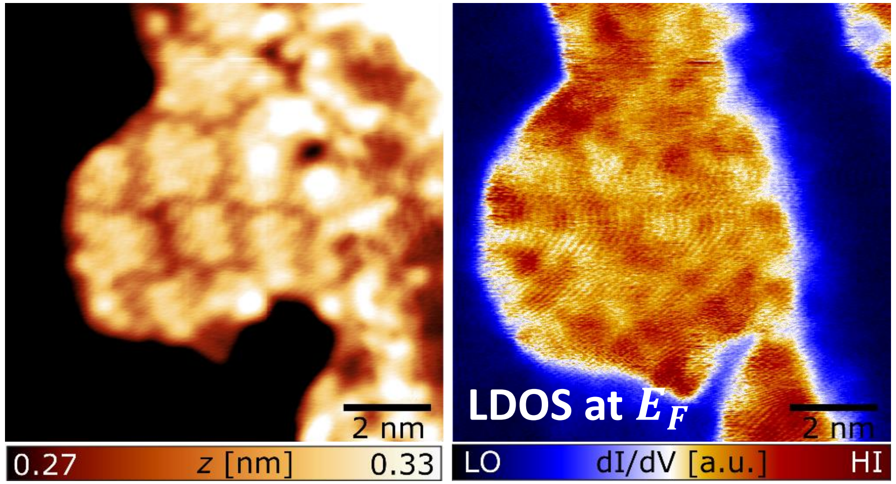

Shiba bands comparison of the different Fe types

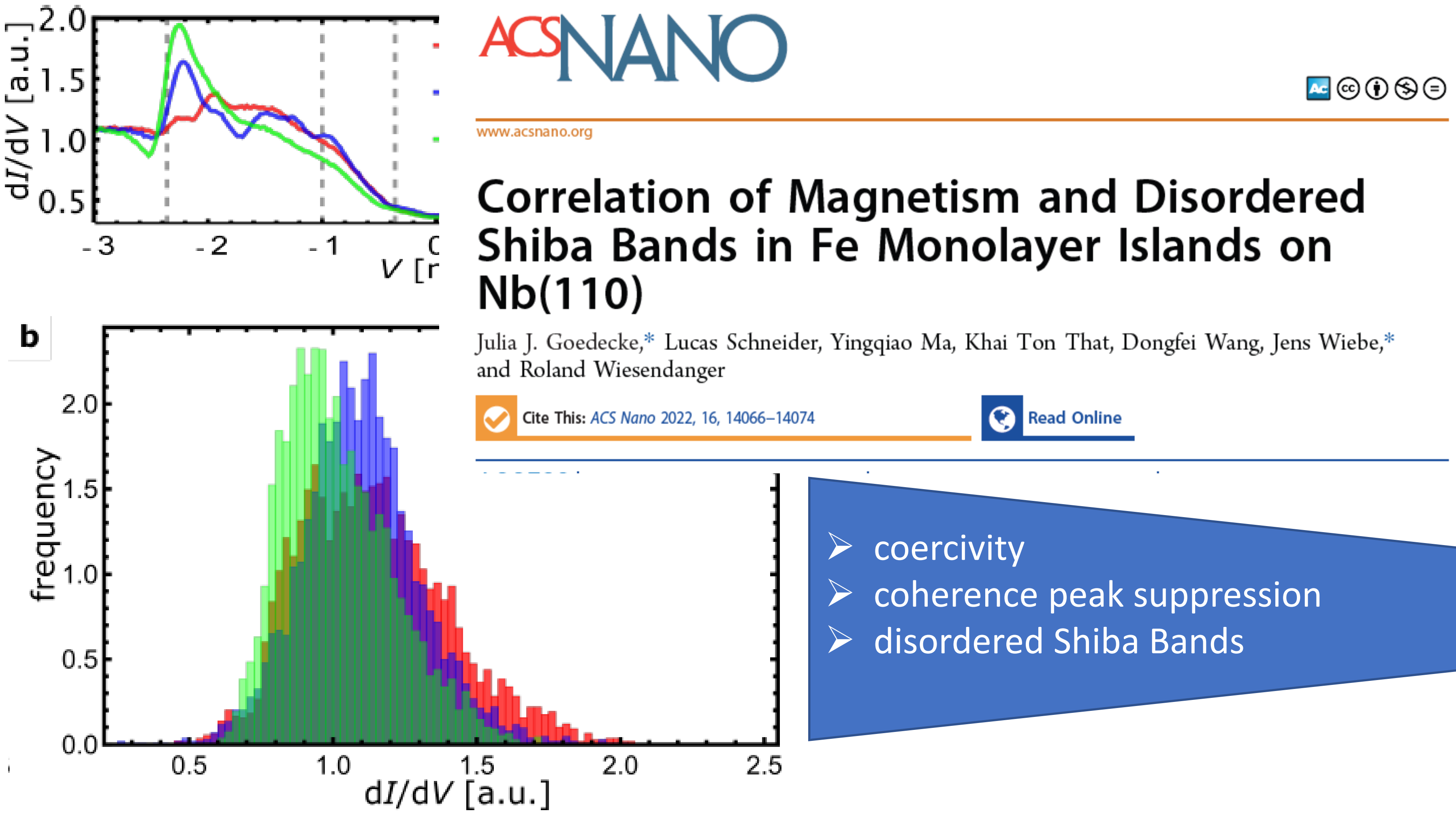

www.acsnano.org

Correlation of Magnetism and Disordered Shiba Bands in Fe Monolayer Islands on Nb(110)

Julia J. Goedecke,* Lucas Schneider, Yingqiao Ma, Khai Ton That, Dongfei Wang, Jens Wiebe,* and Roland Wiesendanger

Cite This: *ACS Nano* 2022, 16, 14066−14074

Read Online

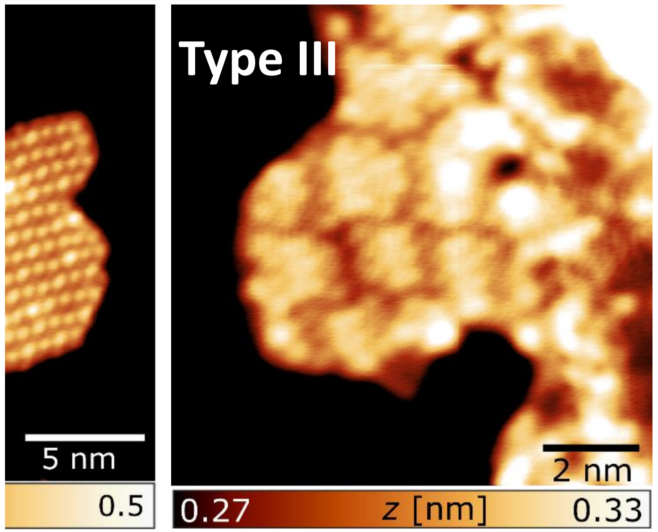

- coercivity
- coherence peak suppression
- disordered Shiba Bands

Summary

Nb(111)

- a procedure was developed to produce a clean Nb(111) surface
- the atomic structure of the clean Nb(111) surface showed a reconstruction
- deposition of iron onto the cleaned Nb(111) surface showed formation of iron clusters

Fe/Nb(110)

- the atomic resolution of the three different reconstructions of ML Fe/Nb(110) was found
- magnetic properties
  - out-of-plane ferromagnetic monodomain for all three types of reconstructions
  - different coercivities: $B_c^I > B_c^{II} > B_c^{III}$
- Shiba bands
  - gap is completely filled with Shiba bands
  - Shiba bands at E_F
  - no gap opening, no evidences for Majorana modes
    - most likely because of the disorder
- outlook

Outlook: Fe double layer

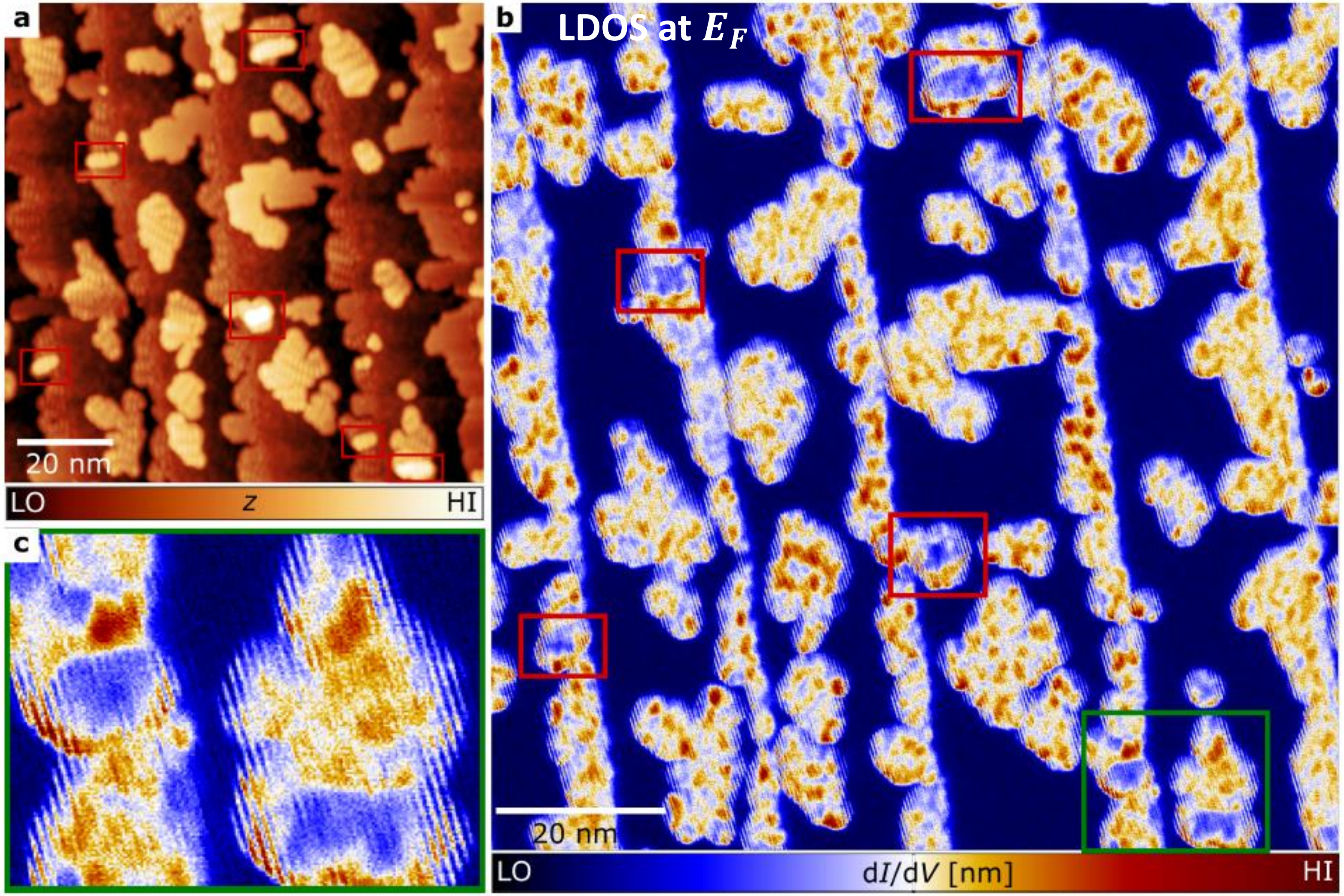

Prof. Dr. Wiesendanger

PD Dr. Jens Wiebe

Dr. Maciej Bazarnik

Dr. Lucas Schneider

Khai That Ton

Technischer Support
Dipl.-Ing. Michael Langer
Michael Brandt
Hans Jürgen Schröder

Mechanische Werkstatt

Gruppe R!

Dr. Jonas Spethman, PD Dr. Kirsten von Bergmann, Dr. Andre Kubetzka, Arturo Rodriguez, Dr. Cody Friesen, Reiner Brüning, …

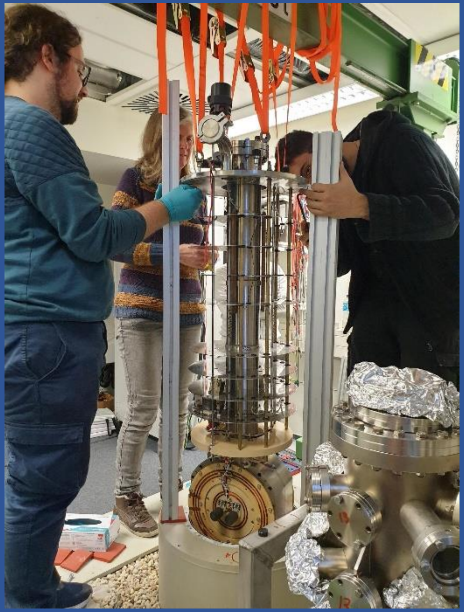

Thank you for your attention!

Disorder

- Can strongly effects topological properties of a 2D Shiba lattice
  - **Potential disorder**
  - **Magnetic disorder**

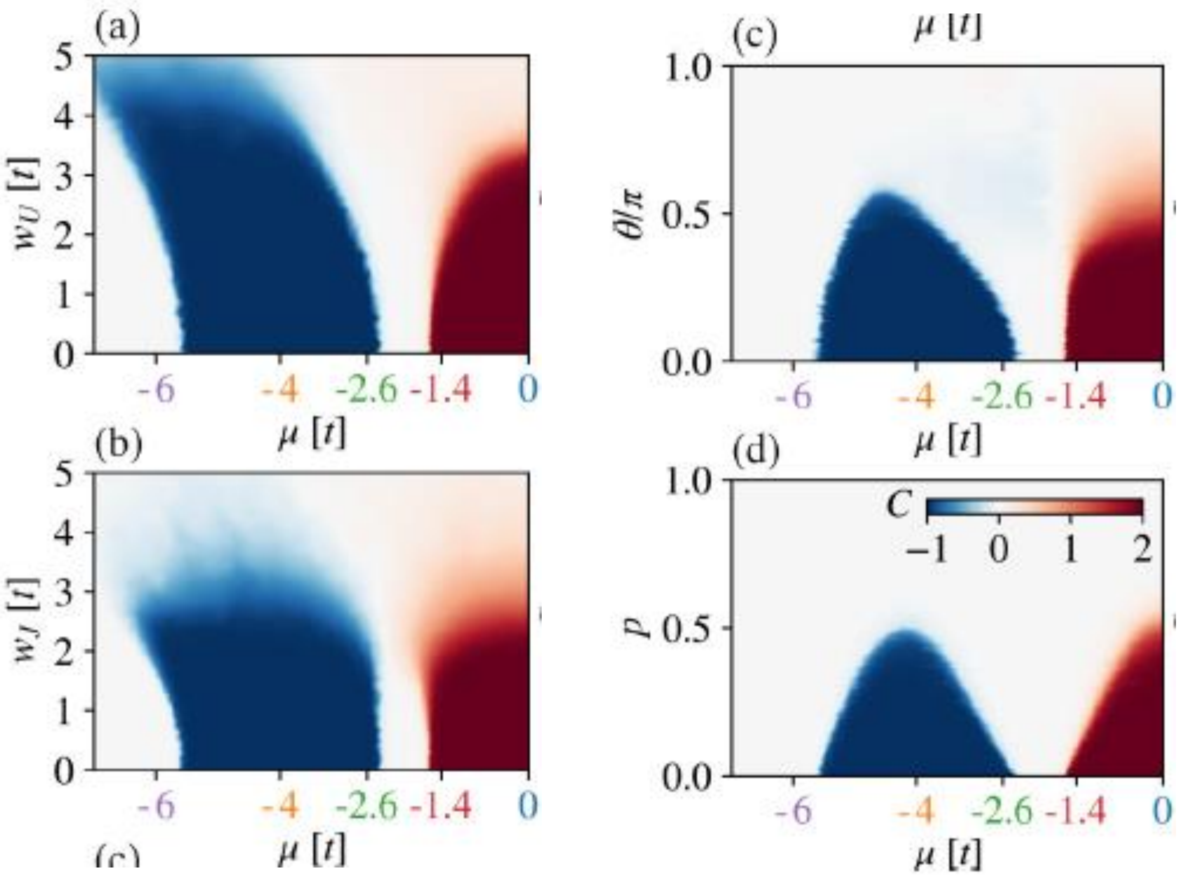

potential disorder

deviation of magnetic moment orientation

strength of J is disordered

missing magnetic moment

Mascot *et al.*, PRB 100, 235102 (2019)

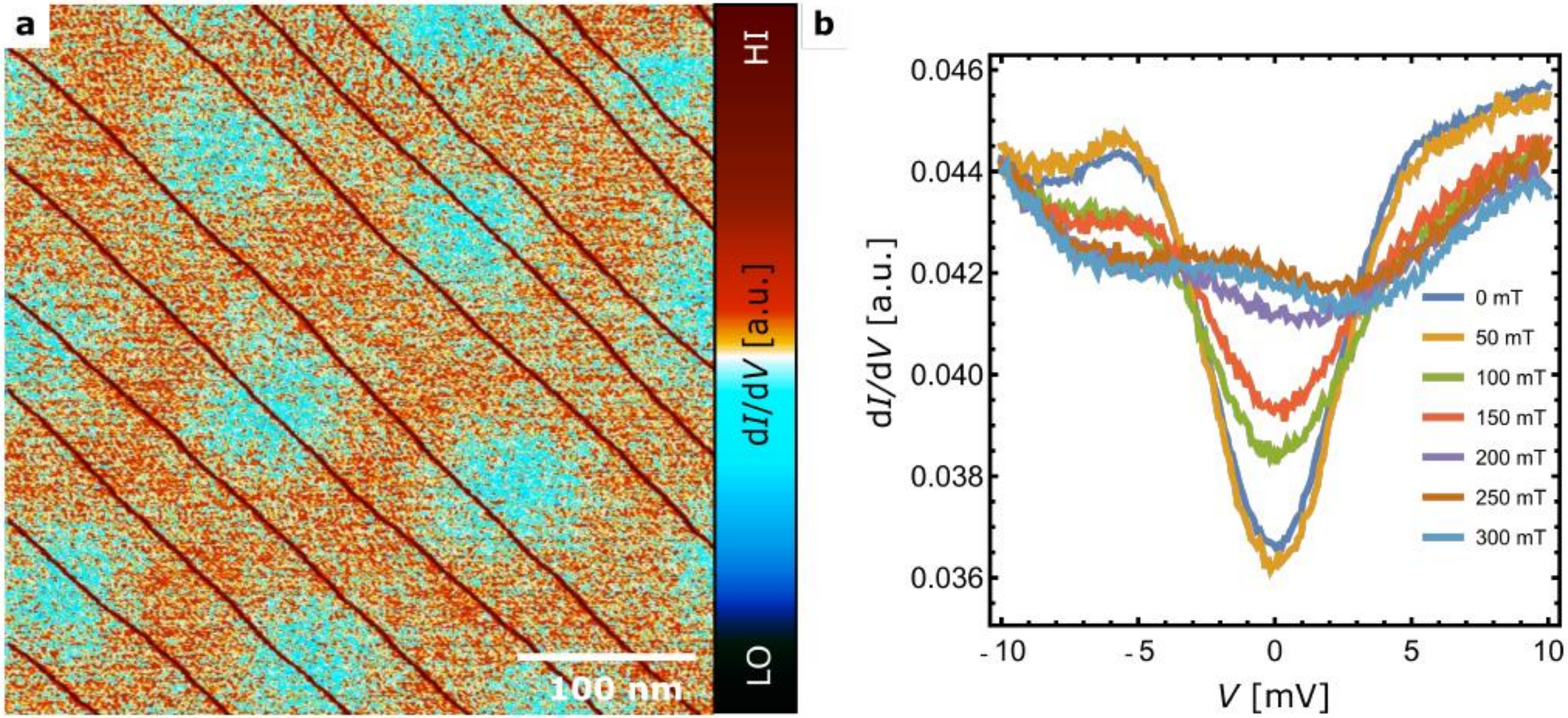

Figure 3.5: In **a** the simultaneously recorded dI/dV image of Fig. 3.4 **a** at $T = 100\,\mathrm{mT}$ is shown, which clearly shows the typical flux tubes of a type II superconductor arranged in a hexagonal lattice ($V = -1\,\mathrm{mV}$, $V_{\mathrm{mod}} = 0.5\,\mathrm{mV}$, $f = 977\,\mathrm{Hz}$, $I = 30\,\mathrm{pA}$, $T = 6.5\,\mathrm{K}$). **b** Point spectra taken on clean Nb(110) at different B-fields as indicated and shown in different colors in the plot ($V_{\mathrm{stab}} = -10\,\mathrm{mV}$, $V_{\mathrm{mod}} = 0.5\,\mathrm{mV}$, $I_{\mathrm{stab}} = 0.5\,\mathrm{nA}$, $T = 6.5\,\mathrm{K}$)

Beispiel: magnetische Momente der 3d Übergangsmetall-Ionen

aus Festkörperphysik, Gross und Marx

$$\widehat{\vec{m}}_J = \frac{1}{\hbar} g \cdot \mu_B \cdot \hat{\vec{J}}$$

Ion	**Konfiguration**	**Schema** m_ℓ = +2, +1, 0, -1, -2	**S**	**L =** $\lvert\Sigma m_\ell\rvert$	**J**	**Term**	Gesamtmoment $m_J/\mu_B = g_J[J(J+1)]^{1/2}$	Spinmoment $m_S/\mu_B = g_S[S(S+1)]^{1/2}$	m_J (μ_B) **(Exp.)**
Ti^{3+} V^{4+}	[Ar]$3d^1$	↑	1/2	2	3/2	$^2D_{3/2}$	1.55	1.73	1.8
V^{3+}	[Ar]$3d^2$	↑ ↑	1	3	2	$^3F_2$	1,63	2.83	2.8
Cr^{3+} V^{2+} Mn^{4+}	[Ar]$3d^3$	↑ ↑ ↑	3/2	3	3/2	$^4F_{3/2}$	0.77	3.87	3.8
Mn^{3+} Cr^{2+}	[Ar]$3d^4$	↑ ↑ ↑ ↑	2	2	0	$^5D_0$	0	4.90	4.9
Fe^{3+} Mn^{2+}	[Ar]$3d^5$	↑ ↑ ↑ ↑ ↑	5/2	0	5/2	$^6S_{5/2}$	5.92	5.92	5.9
Fe^{2+}	[Ar]$3d^6$	↑↓ ↑ ↑ ↑ ↑	2	2	4	$^5D_4$	6.70	4.90	5.4
Co^{2+}	[Ar]$3d^7$	↑↓ ↑↓ ↑ ↑ ↑	3/2	3	9/2	$^4F_{9/2}$	6.63	3.87	4.8
Ni^{2+}	[Ar]$3d^8$	↑↓ ↑↓ ↑↓ ↑ ↑	1	3	4	$^3F_4$	5.59	2.83	3.2
Cu^{2+}	[Ar]$3d^9$	↑↓ ↑↓ ↑↓ ↑↓ ↑	1/2	2	5/2	$^2D_{5/2}$	3.55	1.73	1.9
Zn^{2+}	[Ar]$3d^{10}$	↑↓ ↑↓ ↑↓ ↑↓ ↑↓	0	0	0	$^1S_0$	0	0	0

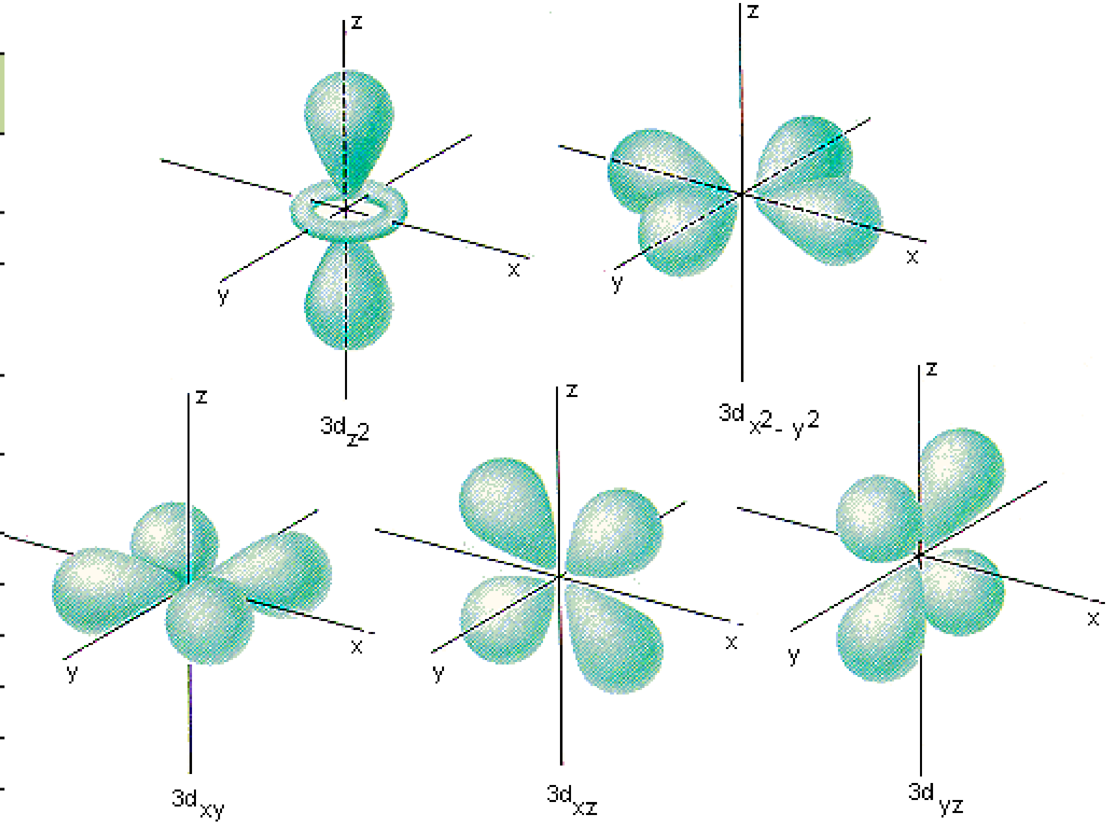

1K=90 mu eV

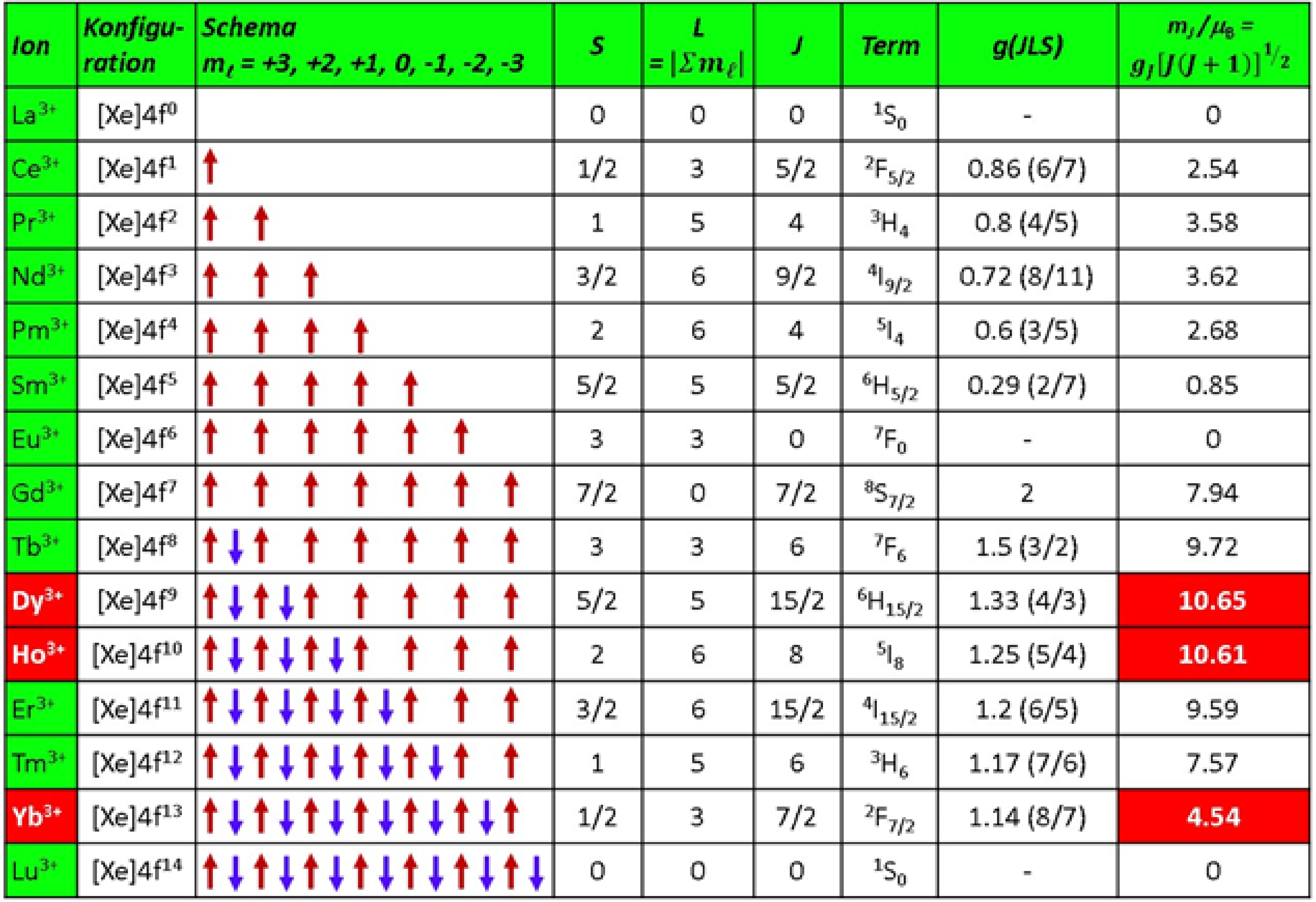

Ion	**Konfigu-ration**	**Schema** **m_ℓ = +3, +2, +1, 0, -1, -2, -3**	**S**	**L** **$= \lvert\Sigma m_\ell\rvert$**	**J**	**Term**	**g(JLS)**	**$m_J/\mu_B = g_J[J(J+1)]^{1/2}$**
La^{3+}	[Xe]$4f^0$		0	0	0	$^1S_0$	-	0
Ce^{3+}	[Xe]$4f^1$	↑	1/2	3	5/2	$^2F_{5/2}$	0.86 (6/7)	2.54
Pr^{3+}	[Xe]$4f^2$	↑ ↑	1	5	4	$^3H_4$	0.8 (4/5)	3.58
Nd^{3+}	[Xe]$4f^3$	↑ ↑ ↑	3/2	6	9/2	$^4I_{9/2}$	0.72 (8/11)	3.62
Pm^{3+}	[Xe]$4f^4$	↑ ↑ ↑ ↑	2	6	4	$^5I_4$	0.6 (3/5)	2.68
Sm^{3+}	[Xe]$4f^5$	↑ ↑ ↑ ↑ ↑	5/2	5	5/2	$^6H_{5/2}$	0.29 (2/7)	0.85
Eu^{3+}	[Xe]$4f^6$	↑ ↑ ↑ ↑ ↑ ↑	3	3	0	$^7F_0$	-	0
Gd^{3+}	[Xe]$4f^7$	↑ ↑ ↑ ↑ ↑ ↑ ↑	7/2	0	7/2	$^8S_{7/2}$	2	7.94
Tb^{3+}	[Xe]$4f^8$	↑↓ ↑ ↑ ↑ ↑ ↑ ↑	3	3	6	$^7F_6$	1.5 (3/2)	9.72
Dy^{3+}	[Xe]$4f^9$	↑↓ ↑↓ ↑ ↑ ↑ ↑ ↑	5/2	5	15/2	$^6H_{15/2}$	1.33 (4/3)	**10.65**
Ho^{3+}	[Xe]$4f^{10}$	↑↓ ↑↓ ↑↓ ↑ ↑ ↑ ↑	2	6	8	$^5I_8$	1.25 (5/4)	**10.61**
Er^{3+}	[Xe]$4f^{11}$	↑↓ ↑↓ ↑↓ ↑↓ ↑ ↑ ↑	3/2	6	15/2	$^4I_{15/2}$	1.2 (6/5)	9.59
Tm^{3+}	[Xe]$4f^{12}$	↑↓ ↑↓ ↑↓ ↑↓ ↑↓ ↑ ↑	1	5	6	$^3H_6$	1.17 (7/6)	7.57
Yb^{3+}	[Xe]$4f^{13}$	↑↓ ↑↓ ↑↓ ↑↓ ↑↓ ↑↓ ↑	1/2	3	7/2	$^2F_{7/2}$	1.14 (8/7)	**4.54**
Lu^{3+}	[Xe]$4f^{14}$	↑↓ ↑↓ ↑↓ ↑↓ ↑↓ ↑↓ ↑↓	0	0	0	$^1S_0$	-	0

Rekonstruktion Fe/Nb(110)

- lattice constant
  - $a_{Fe} = 287\text{pm}$
  - $a_{Nb} = 330\text{pm}$
- mismatch $\eta = \frac{a_{\mathrm{Fe}} - a_{\mathrm{Nb}}}{a_{\mathrm{Nb}}} = -13.33\%$

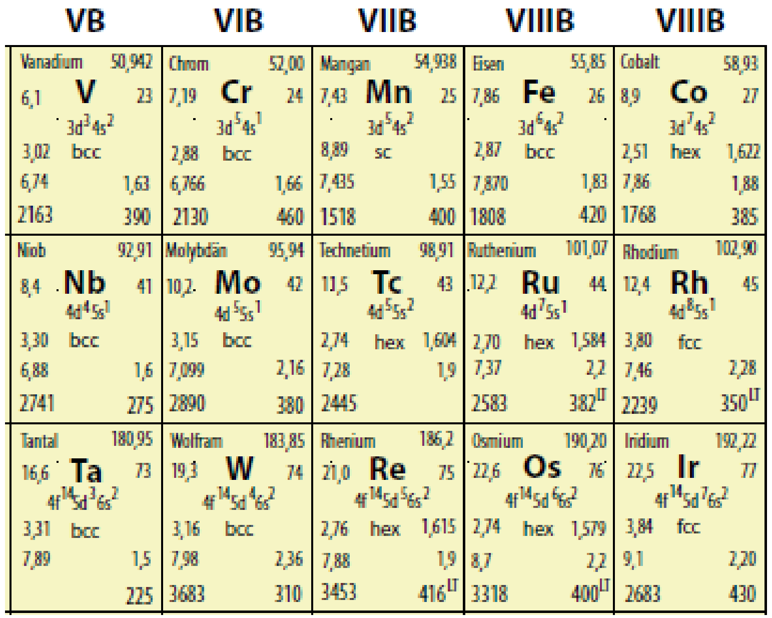

VB	VIB	VIIB	VIIIB	VIIIB
Vanadium 50,942 6,1 **V** 23 $3d^3 4s^2$ 3,02 bcc 6,74 1,63 2163 390	Chrom 52,00 7,19 **Cr** 24 $3d^5 4s^1$ 2,88 bcc 6,766 1,66 2130 460	Mangan 54,938 7,43 **Mn** 25 $3d^5 4s^2$ 8,89 sc 7,435 1,55 1518 400	Eisen 55,85 7,86 **Fe** 26 $3d^6 4s^2$ 2,87 bcc 7,870 1,83 1808 420	Cobalt 58,93 8,9 **Co** 27 $3d^7 4s^2$ 2,51 hex 1,622 7,86 1,88 1768 385
Niob 92,91 8,4 **Nb** 41 $4d^4 5s^1$ 3,30 bcc 6,88 1,6 2741 275	Molybdän 95,94 10,2 **Mo** 42 $4d^5 5s^1$ 3,15 bcc 7,099 2,16 2890 380	Technetium 98,91 11,5 **Tc** 43 $4d^5 5s^2$ 2,74 hex 1,604 7,28 1,9 2445	Ruthenium 101,07 12,2 **Ru** 44 $4d^7 5s^1$ 2,70 hex 1,584 7,37 2,2 2583 382^{LT}	Rhodium 102,90 12,4 **Rh** 45 $4d^8 5s^1$ 3,80 fcc 7,46 2,28 2239 350^{LT}
Tantal 180,95 16,6 **Ta** 73 $4f^{14} 5d^3 6s^2$ 3,31 bcc 7,89 1,5 225	Wolfram 183,85 19,3 **W** 74 $4f^{14} 5d^4 6s^2$ 3,16 bcc 7,98 2,36 3683 310	Rhenium 186,2 21,0 **Re** 75 $4f^{14} 5d^5 6s^2$ 2,76 hex 1,615 7,88 1,9 3453 416^{LT}	Osmium 190,20 22,6 **Os** 76 $4f^{14} 5d^6 6s^2$ 2,74 hex 1,579 8,7 2,2 3318 400^{LT}	Iridium 192,22 22,5 **Ir** 77 $4f^{14} 5d^7 6s^2$ 3,84 fcc 9,1 2,20 2683 430

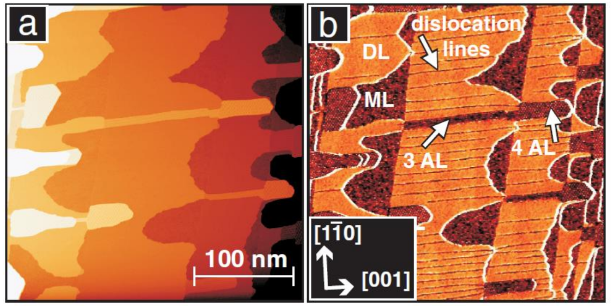

FIG. 1 (color online). 1.7 atomic layers Fe on W(110) with local Fe coverages of 1–4 atomic layers. (a) Constant-currrent STM image showing the topography. (b) dI/dU map showing the details of the varying local coverage with dislocation lines in the double layer areas. Tunneling parameters: $I = 500$ pA, $U_{\mathrm{bias}} = 550$ mV.

pseudomorphic
With annealing at 500K
Mismatch 9,4%

Fe/W(110) (9,4%),
Fe/Mo(110) (8,6%),
Fe/V(110) (5%)

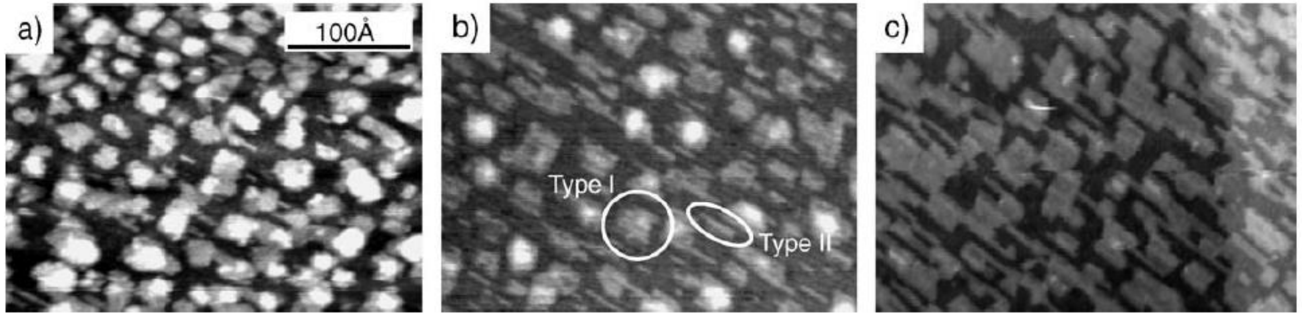

Fig. 7. Annealing series of 0.25 ML Fe grown at RT on Nb(110). Annealing processes lasted 5 min each. Temperatures: (a) 800 K, (b) 900 K, (c) 1000 K.

Fe/NbOx

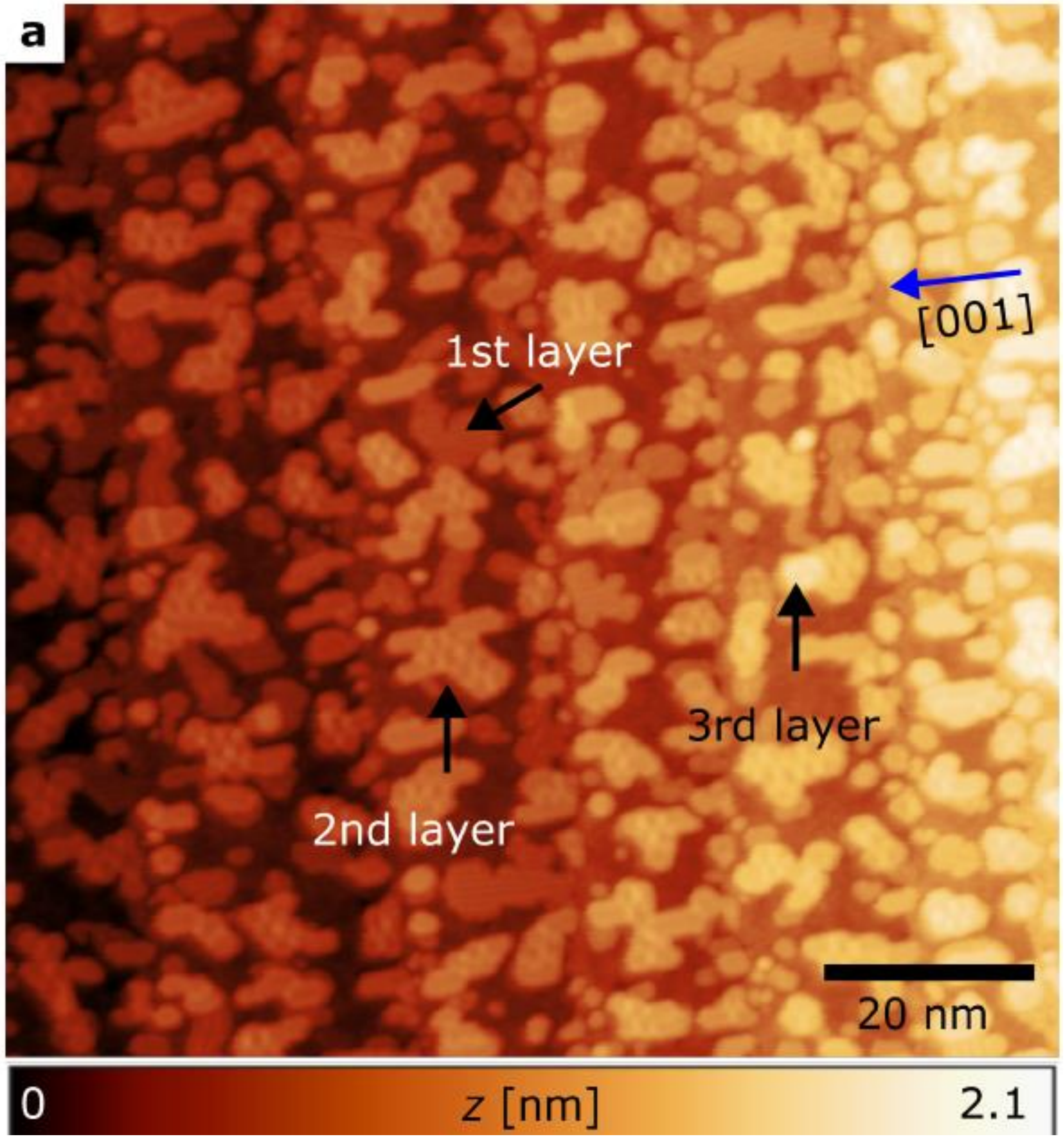

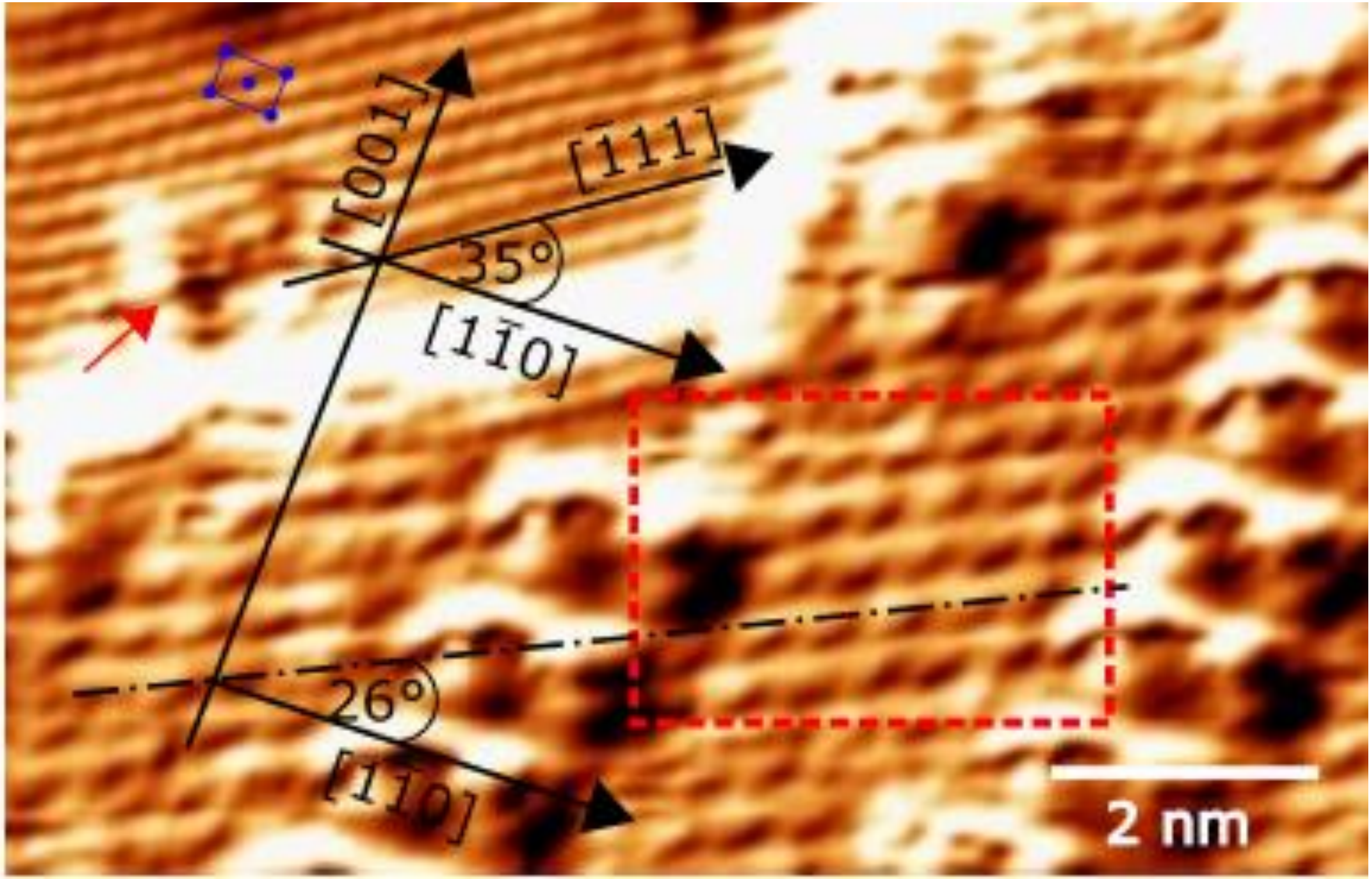
[001]
[$\bar{1}$11]
35°
[1$\bar{1}$0]
26°
[1$\bar{1}$0]
2 nm

Distance measurement

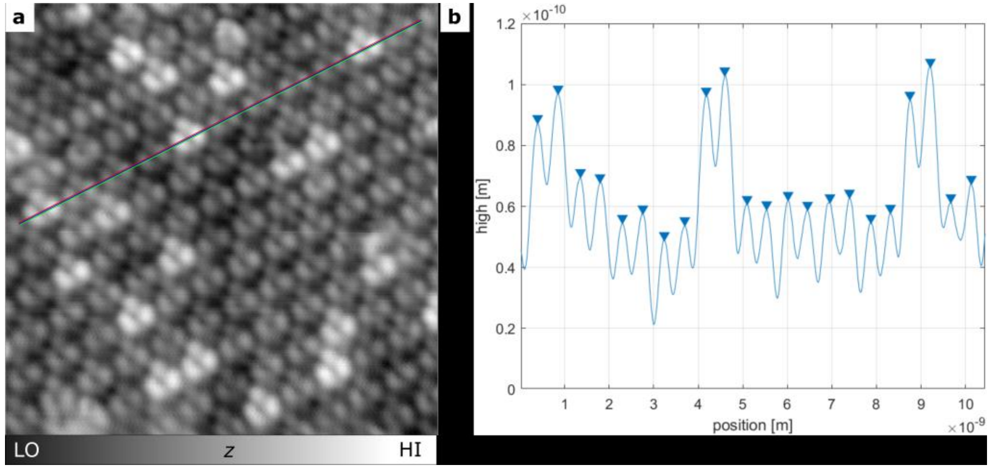

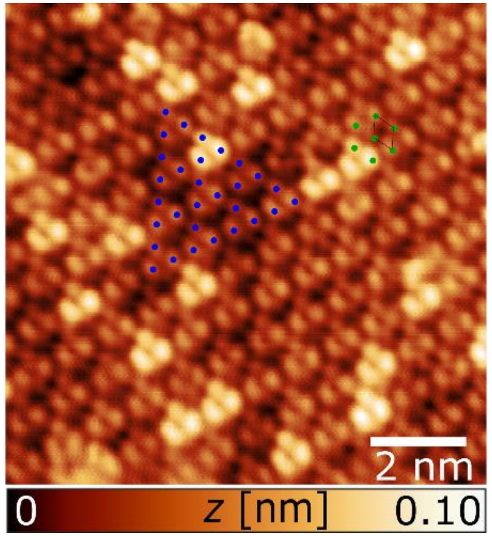

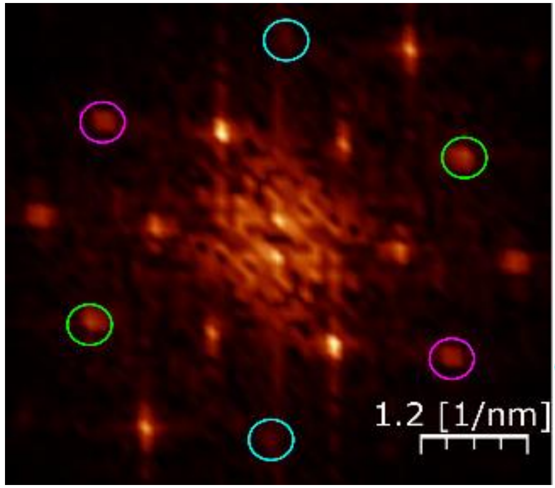

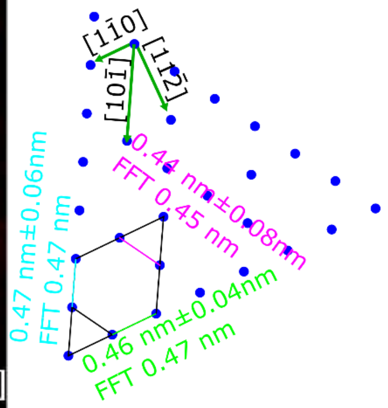

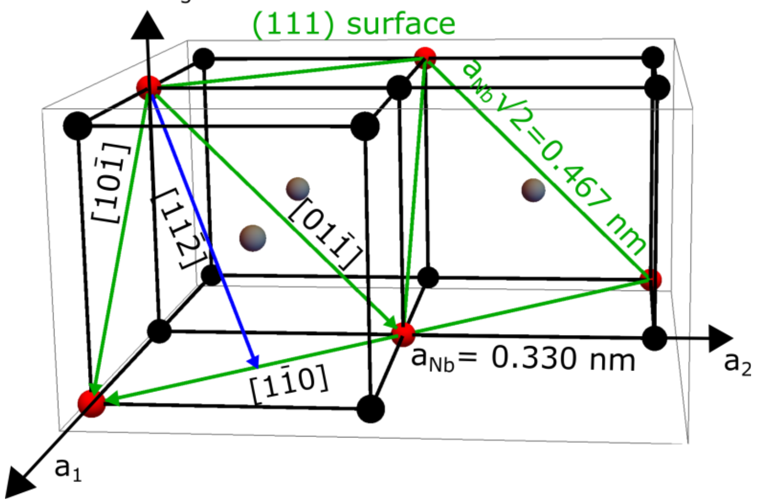

Local spin-resolved SP-STS on Fe/Nb(110) to determine the bias

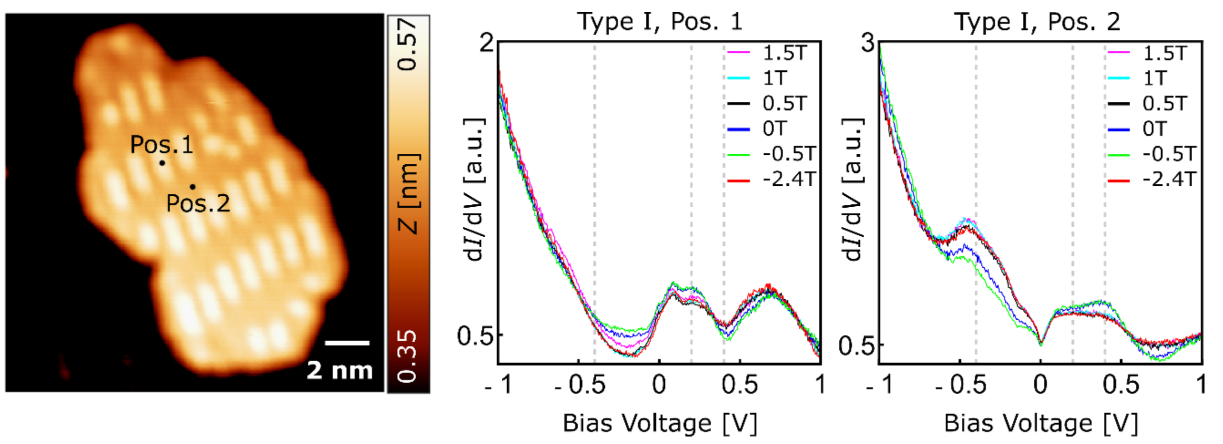

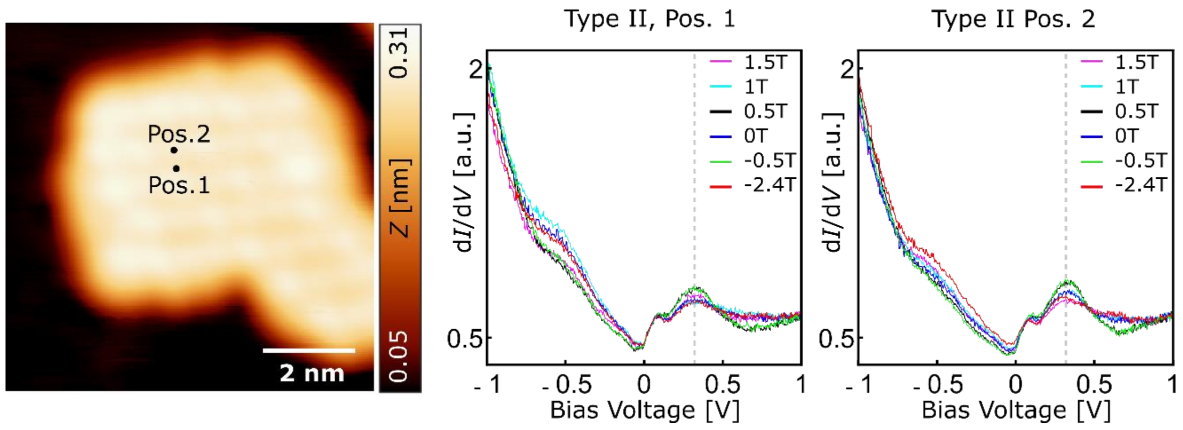

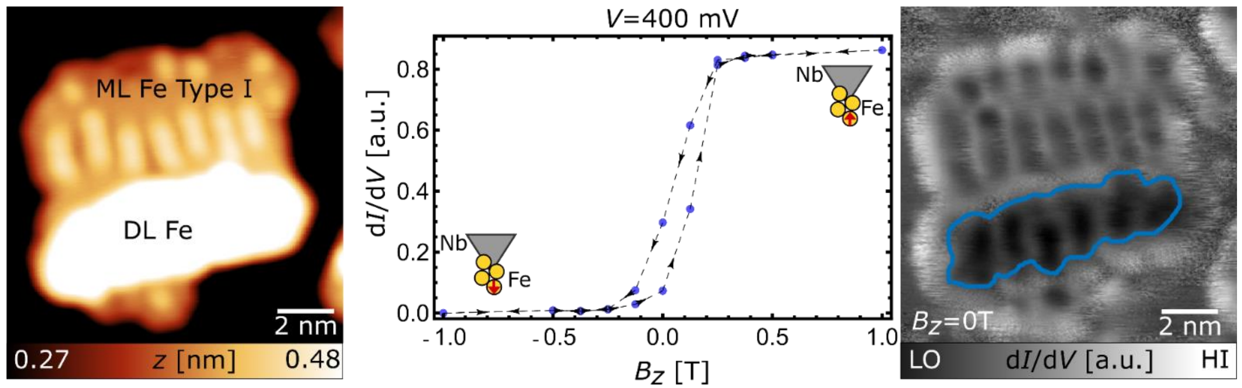

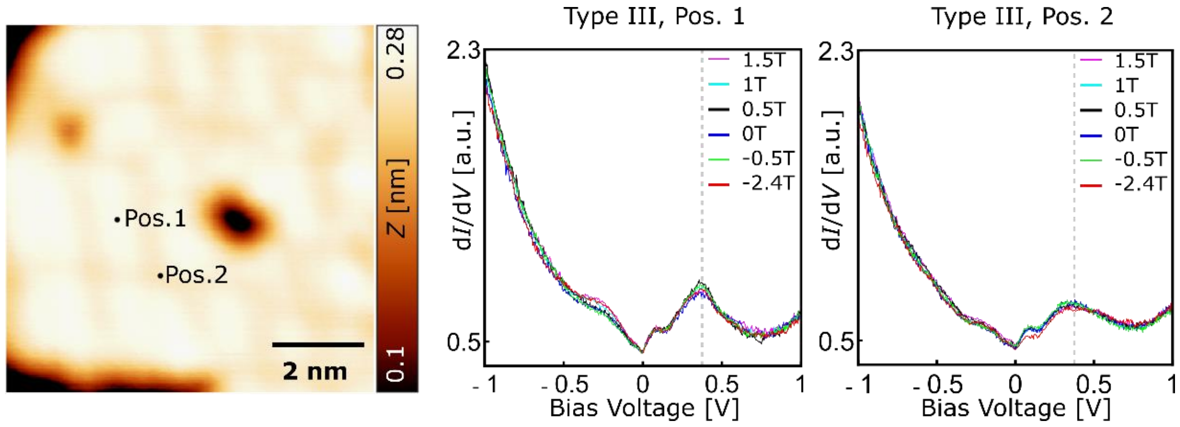

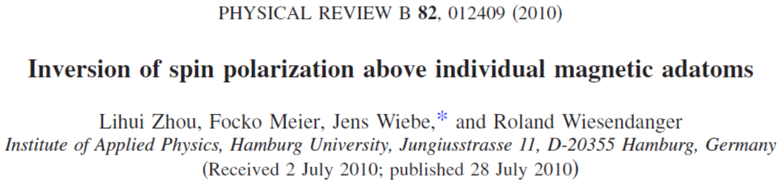

PHYSICAL REVIEW B **82**, 012409 (2010)

Inversion of spin polarization above individual magnetic adatoms

Lihui Zhou, Focko Meier, Jens Wiebe,* and Roland Wiesendanger
Institute of Applied Physics, Hamburg University, Jungiusstrasse 11, D-20355 Hamburg, Germany
(Received 2 July 2010; published 28 July 2010)

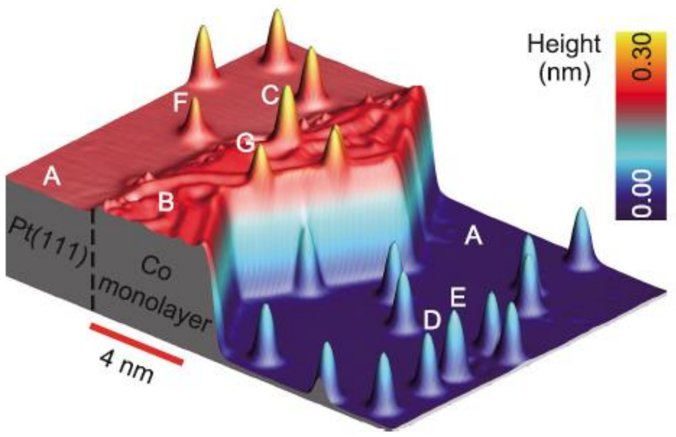

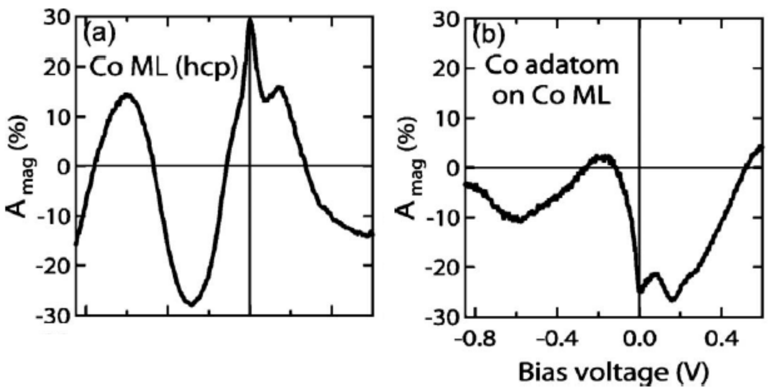

$$dI/dV(x,y,V) \propto \rho_T(E_F)\cdot\rho_S(E_F+eV,\vec{R}_T) \times[1+P_T(E_F)\cdot P_S(E_F+eV,\vec{R}_T)\cdot\cos\theta].$$

$$P=(\rho^{\uparrow}-\rho^{\downarrow})/(\rho^{\uparrow}+\rho^{\downarrow})$$

$$A_{mag}(V)\equiv(dI^{\uparrow\uparrow}/dV-dI^{\uparrow\downarrow}/dV)/(dI^{\uparrow\uparrow}/dV+dI^{\uparrow\downarrow}/dV) = P_T(E_F)\cdot P_S(E_F+eV,\vec{R}_T).$$

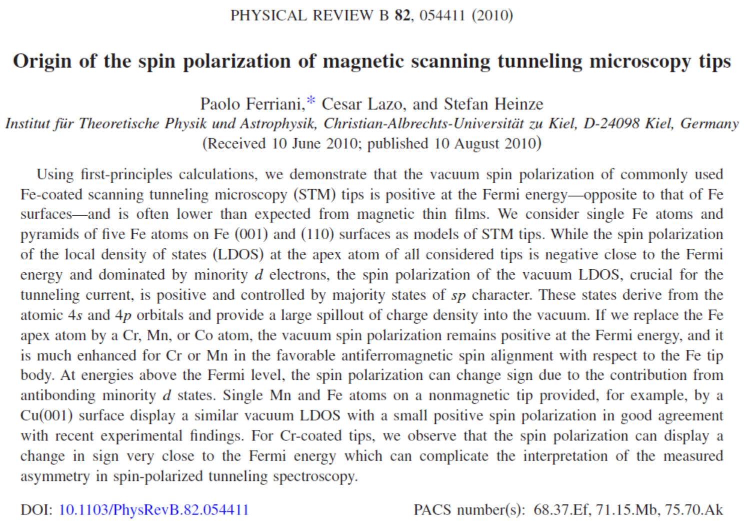

PHYSICAL REVIEW B **82**, 054411 (2010)

Origin of the spin polarization of magnetic scanning tunneling microscopy tips

Paolo Ferriani,* Cesar Lazo, and Stefan Heinze
Institut für Theoretische Physik und Astrophysik, Christian-Albrechts-Universität zu Kiel, D-24098 Kiel, Germany
(Received 10 June 2010; published 10 August 2010)

Using first-principles calculations, we demonstrate that the vacuum spin polarization of commonly used Fe-coated scanning tunneling microscopy (STM) tips is positive at the Fermi energy—opposite to that of Fe surfaces—and is often lower than expected from magnetic thin films. We consider single Fe atoms and pyramids of five Fe atoms on Fe (001) and (110) surfaces as models of STM tips. While the spin polarization of the local density of states (LDOS) at the apex atom of all considered tips is negative close to the Fermi energy and dominated by minority *d* electrons, the spin polarization of the vacuum LDOS, crucial for the tunneling current, is positive and controlled by majority states of *sp* character. These states derive from the atomic 4*s* and 4*p* orbitals and provide a large spillout of charge density into the vacuum. If we replace the Fe apex atom by a Cr, Mn, or Co atom, the vacuum spin polarization remains positive at the Fermi energy, and it is much enhanced for Cr or Mn in the favorable antiferromagnetic spin alignment with respect to the Fe tip body. At energies above the Fermi level, the spin polarization can change sign due to the contribution from antibonding minority *d* states. Single Mn and Fe atoms on a nonmagnetic tip provided, for example, by a Cu(001) surface display a similar vacuum LDOS with a small positive spin polarization in good agreement with recent experimental findings. For Cr-coated tips, we observe that the spin polarization can display a change in sign very close to the Fermi energy which can complicate the interpretation of the measured asymmetry in spin-polarized tunneling spectroscopy.

DOI: 10.1103/PhysRevB.82.054411 PACS number(s): 68.37.Ef, 71.15.Mb, 75.70.Ak

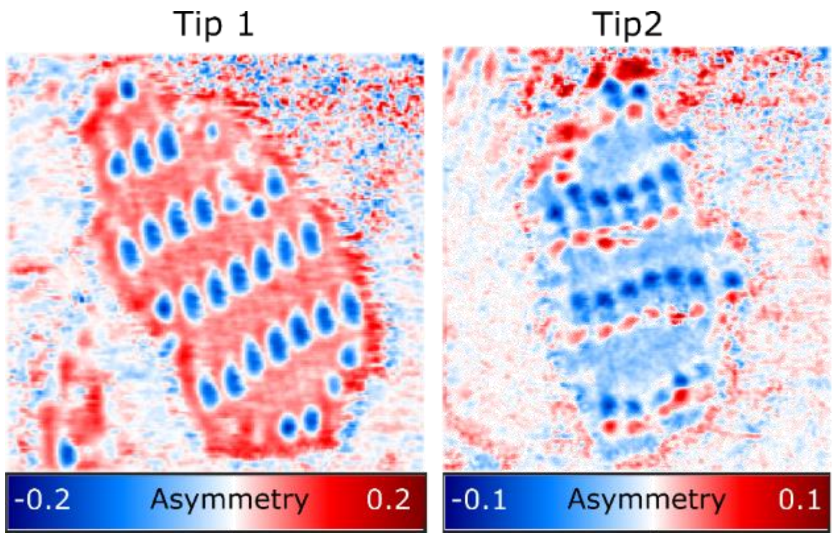

Asym map

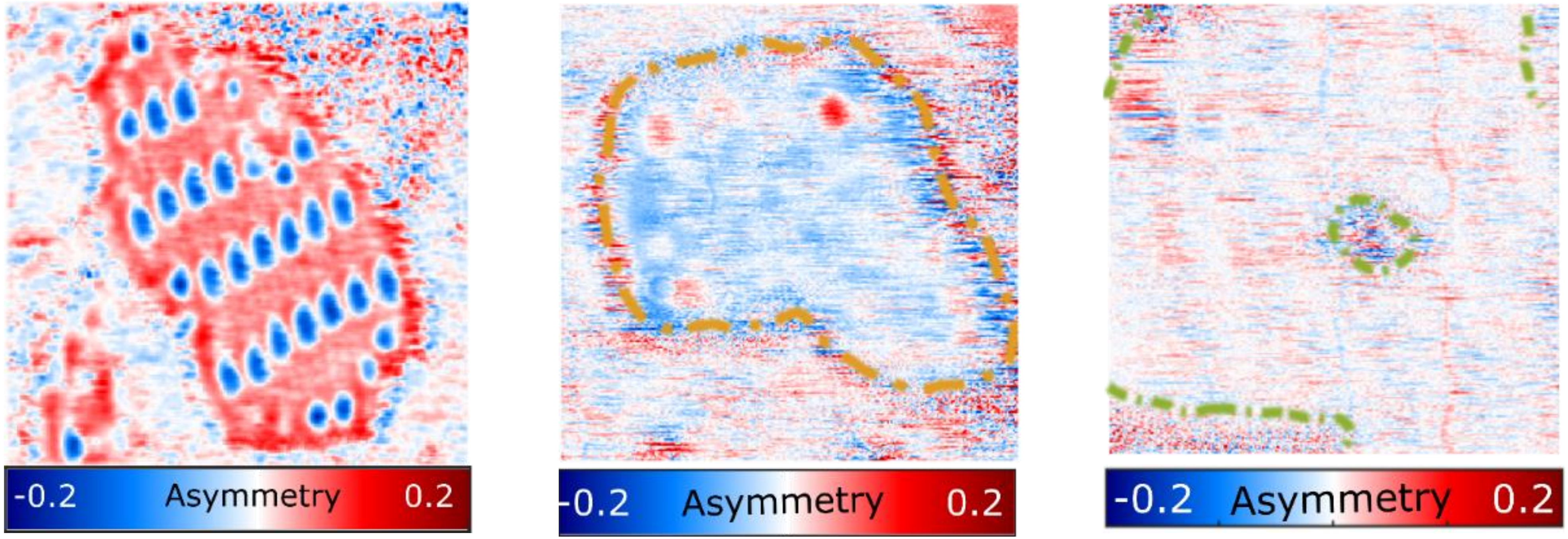

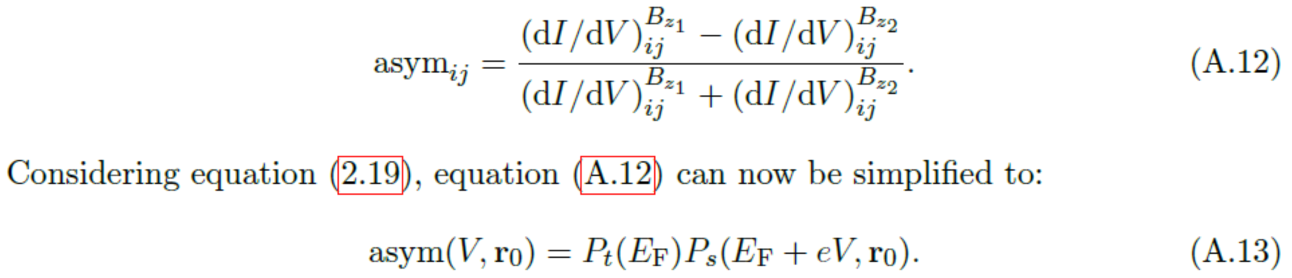

$$\mathrm{asym}_{ij} = \frac{(\mathrm{d}I/\mathrm{d}V)_{ij}^{B_{z1}} - (\mathrm{d}I/\mathrm{d}V)_{ij}^{B_{z2}}}{(\mathrm{d}I/\mathrm{d}V)_{ij}^{B_{z1}} + (\mathrm{d}I/\mathrm{d}V)_{ij}^{B_{z2}}}. \qquad (A.12)$$

Considering equation (2.19), equation (A.12) can now be simplified to:

$$\mathrm{asym}(V, \mathbf{r}_0) = P_t(E_\mathrm{F})P_s(E_\mathrm{F} + eV, \mathbf{r}_0). \qquad (A.13)$$

Simulations with MonteCrystal[1]

$$H = -\sum_{i,j} J_{i,j}\left(\mathbf{S}_i \cdot \mathbf{S}_j\right) + \sum_i K_z \left(S_i^z\right)^2 + \sum_i K_x \left(S_i^x\right)^2 - \mu_B \sum_i S_i^z \cdot B_z$$

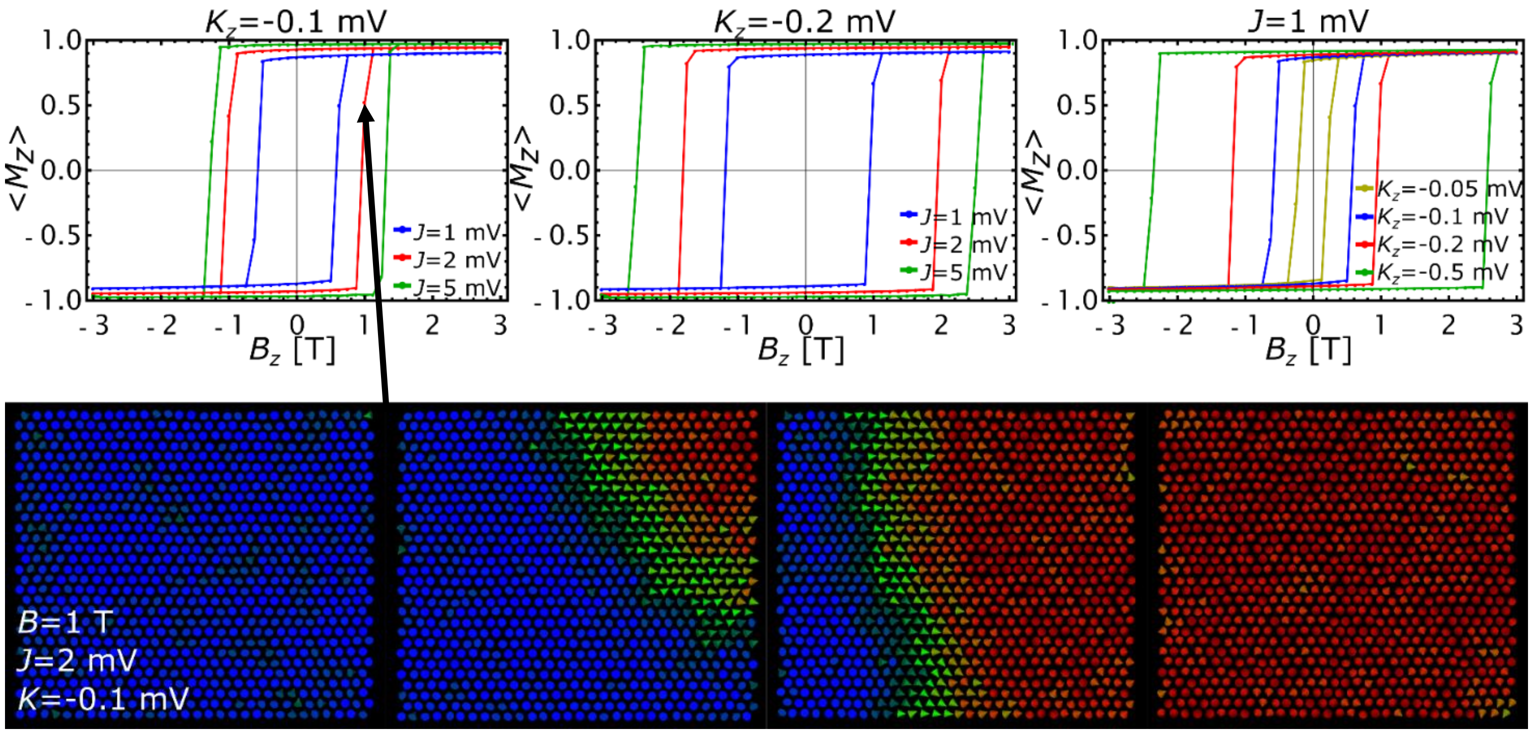

- ➢ coercivity increases with J and Kz
- ➢ switching is most often initiated by a nucleation at the edge or corner of the island
- ➢ to a good approximation the switching behaviour is size-independent
- ➢ extraction of J and K for the different Fe types

Fe Type	B_c[T]	J_1[meV]	K_z[meV]
I	2.5	5	-0.2
	2.5	1	-0.5
II	1	2	-0.1
	0.62	1	-0.1
III	0.25	1	-0.05

[1] J. Hagemeister, https://github.com/JHagemeister/MonteCrystal

Magnetic Measurements

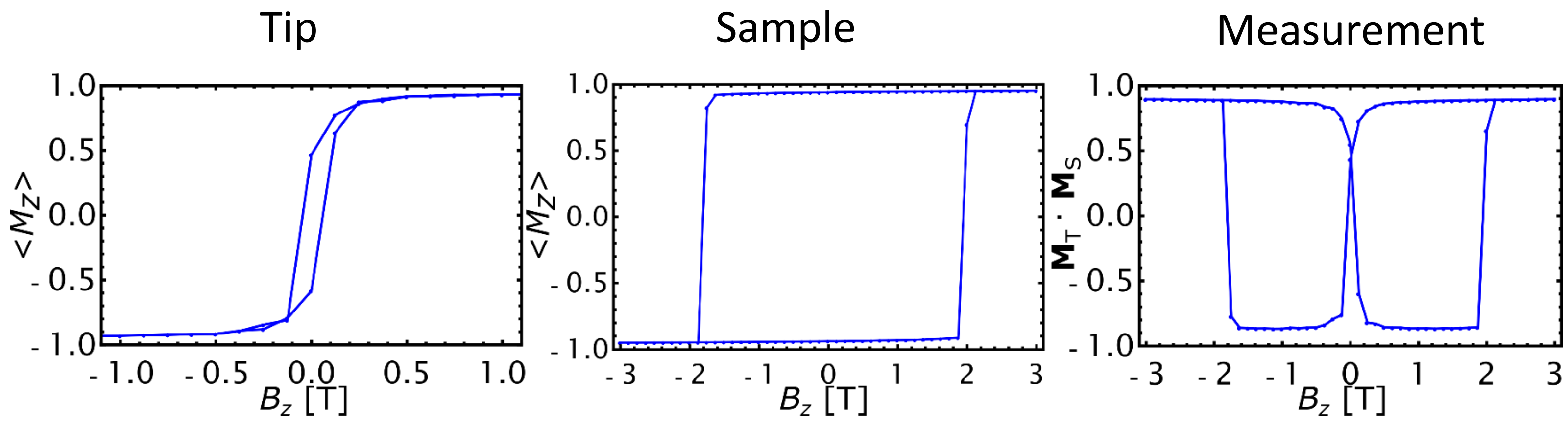
Tip

Sample

Measurement

$$\frac{\mathrm{d}I}{\mathrm{d}V}(\mathbf{r}_0, V) \propto \rho_\mathrm{t}\rho_\mathrm{s}(\mathbf{r}_0, E_\mathrm{F} + eV) + \mathbf{M}_\mathrm{t}\mathbf{M}_\mathrm{s}(\mathbf{r}_0, E_\mathrm{F} + eV)$$

$$\mathbf{M} = (\rho_\uparrow - \rho_\downarrow)\,\mathbf{e}_\mathrm{M}$$

$$P = \frac{\rho_\uparrow - \rho_\downarrow}{\rho_\uparrow + \rho_\downarrow}$$

$$\frac{\mathrm{d}I}{\mathrm{d}V} \propto \rho_\mathrm{t}(E_\mathrm{F})\rho_\mathrm{s}(E_\mathrm{F} + eV, \mathbf{r}_0)(1 + P_\mathrm{t}(E_\mathrm{F})P_\mathrm{s}(E_\mathrm{F} + eV, \mathbf{r}_0)\cos(\theta))$$

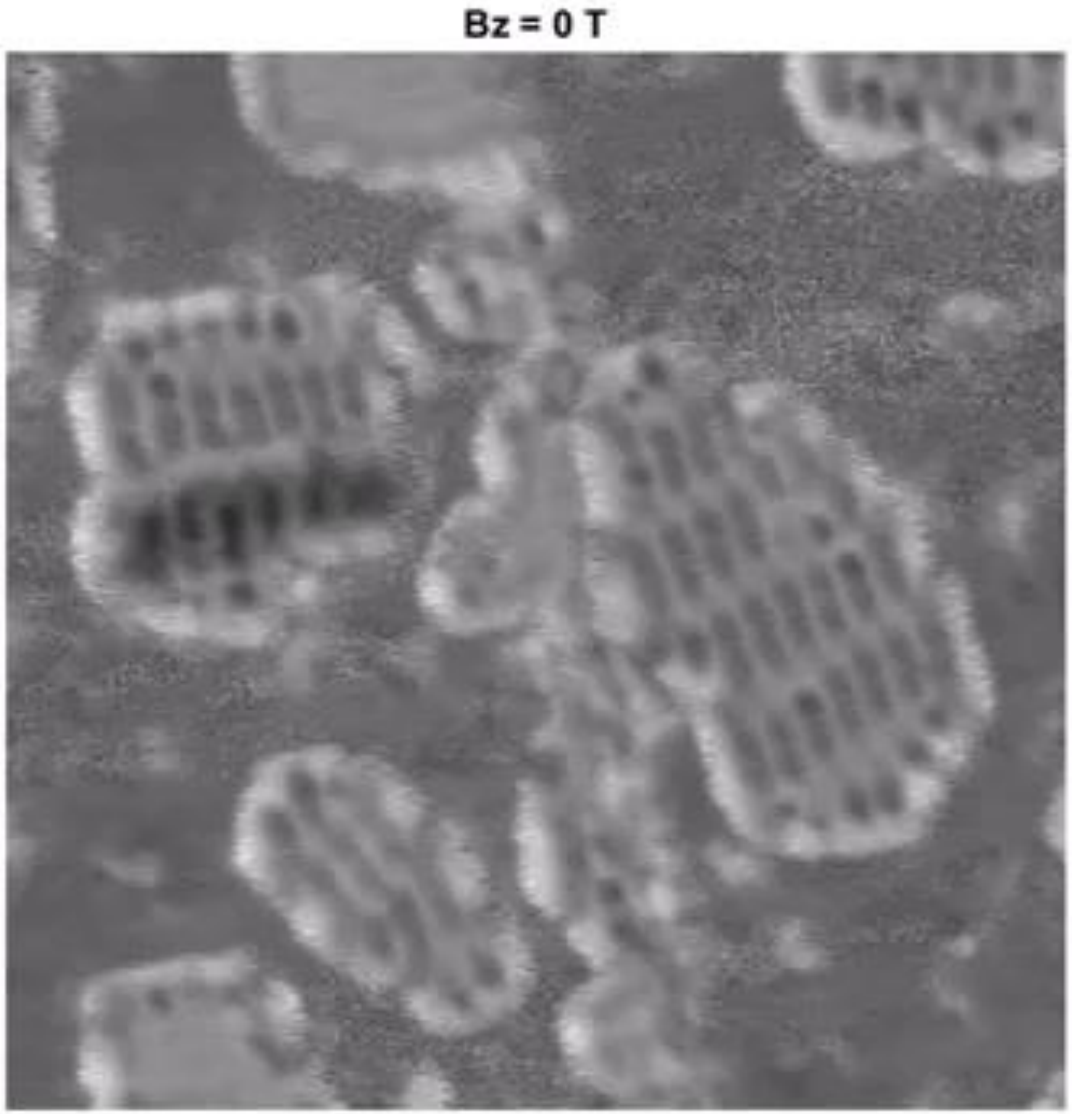
Bz = 0 T

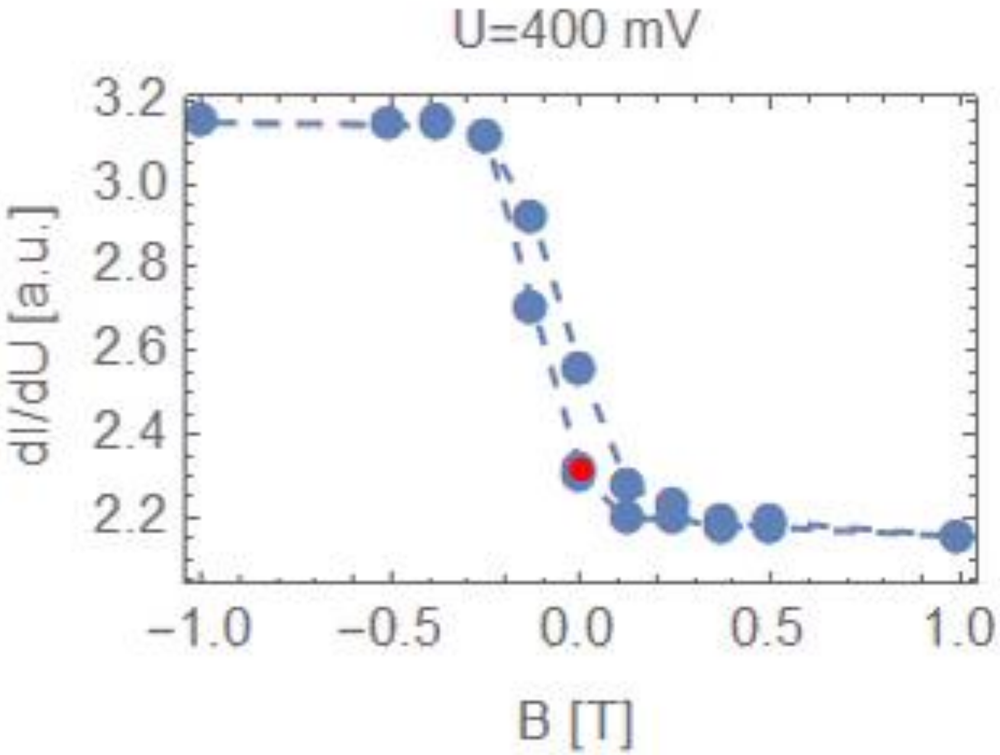
U=400 mV
3.2
3.0
2.8
2.6
2.4
2.2
dI/dU [a.u.]
−1.0
−0.5
0.0
0.5
1.0
B [T]

Simulations of the total magnetization <M>

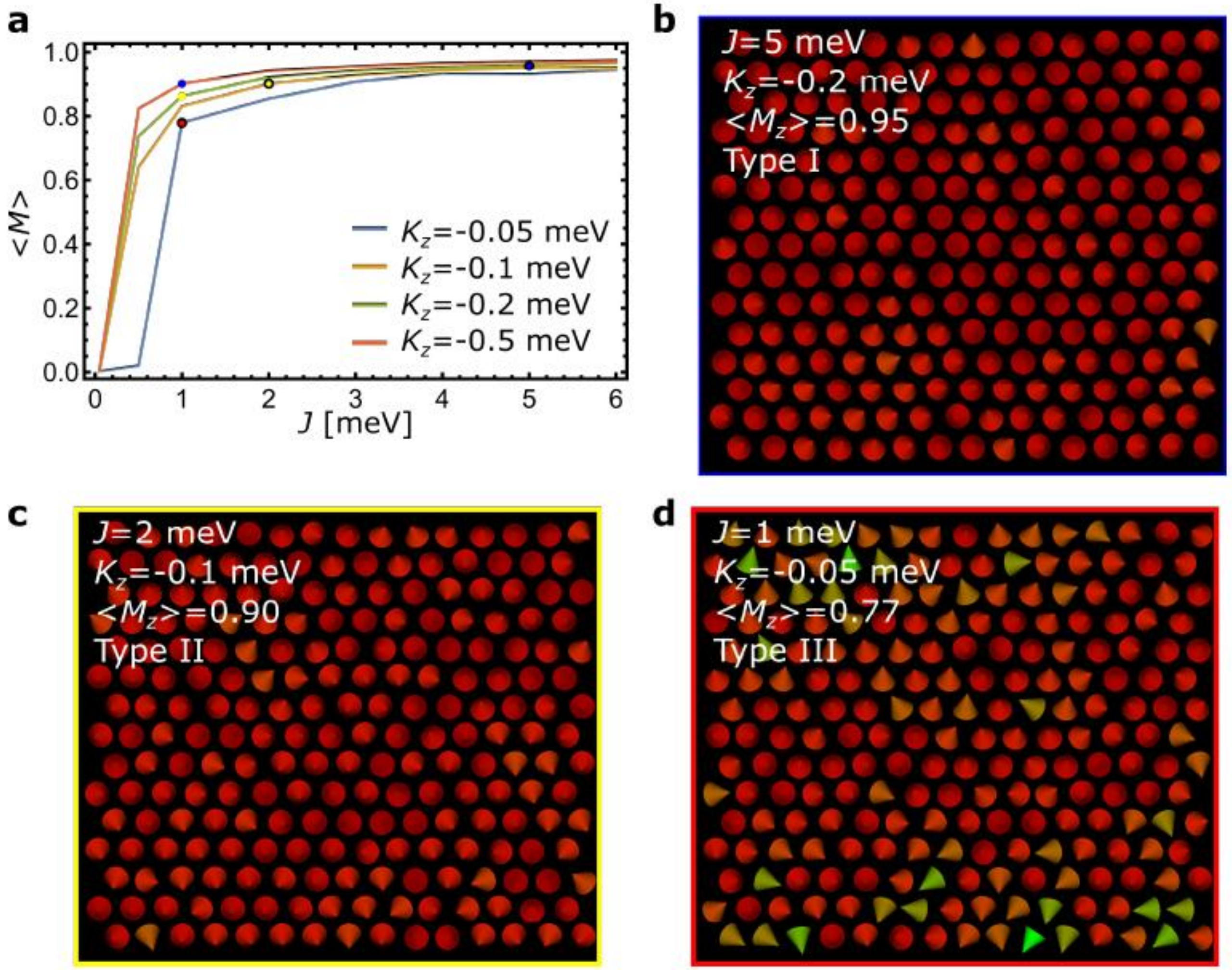

- ➢ dots here representing the possible combination of J and K for each type
- ➢ total magnetization:
    - ➢ type I 95%,
    - ➢ type II 90%
    - ➢ type III 77%

Shiba state

$$H_{\mathrm{YSR}} = \left(\frac{p^2}{2m} - \mu\right) \boldsymbol{\tau}_z + [V\boldsymbol{\tau}_z - J\,\mathbf{S}\,\boldsymbol{\sigma}]\;\delta(\mathbf{r}) + \Delta\boldsymbol{\tau}_x.$$

$$E_{\mathrm{YSR}} = \pm\Delta\frac{1-\alpha^2+\beta^2}{\sqrt{(1-\alpha^2+\beta^2)^2+4\alpha^2}}, \qquad \begin{aligned}\alpha &= \pi\rho S J\\ \beta &= \pi\rho V\end{aligned}$$

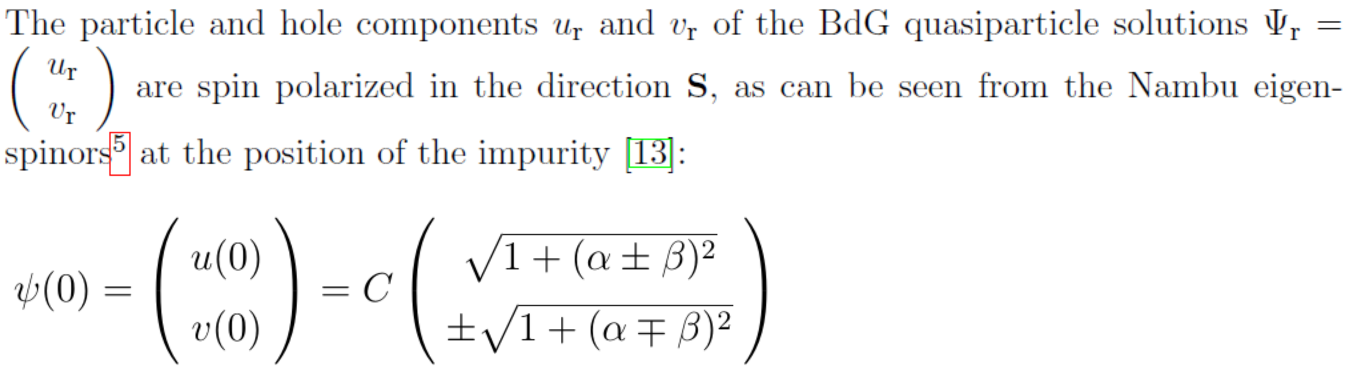

The particle and hole components u_{r} and v_{r} of the BdG quasiparticle solutions $\Psi_{\mathrm{r}} = \begin{pmatrix} u_{\mathrm{r}} \\ v_{\mathrm{r}} \end{pmatrix}$ are spin polarized in the direction $\mathbf{S}$, as can be seen from the Nambu eigenspinors[5] at the position of the impurity [13]:

$$\psi(0) = \begin{pmatrix} u(0) \\ v(0) \end{pmatrix} = C \begin{pmatrix} \sqrt{1+(\alpha\pm\beta)^2} \\ \pm\sqrt{1+(\alpha\mp\beta)^2} \end{pmatrix}$$

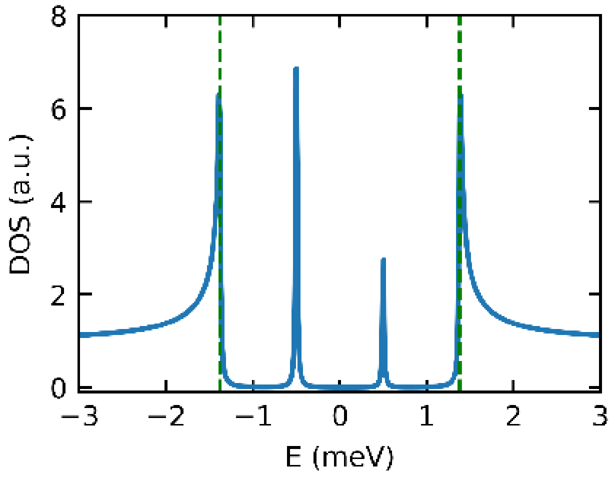

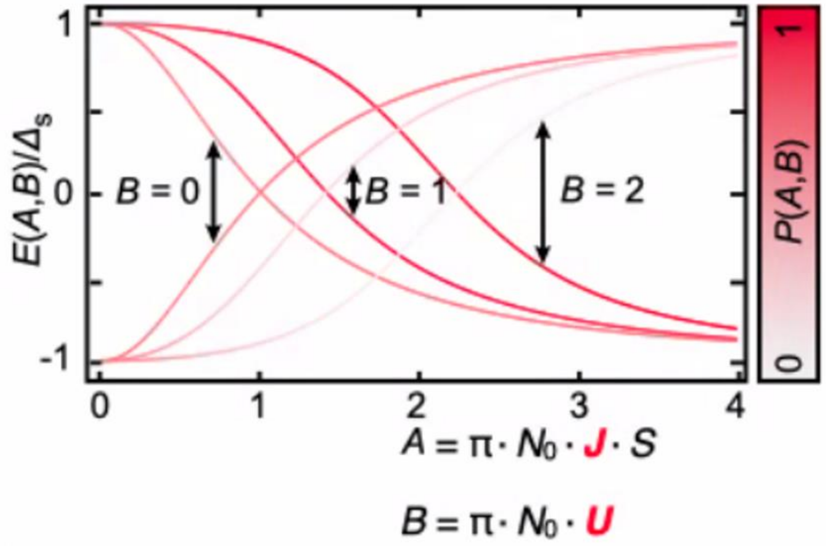

Dissertation Lucas Schneider

Shiba Type II + III

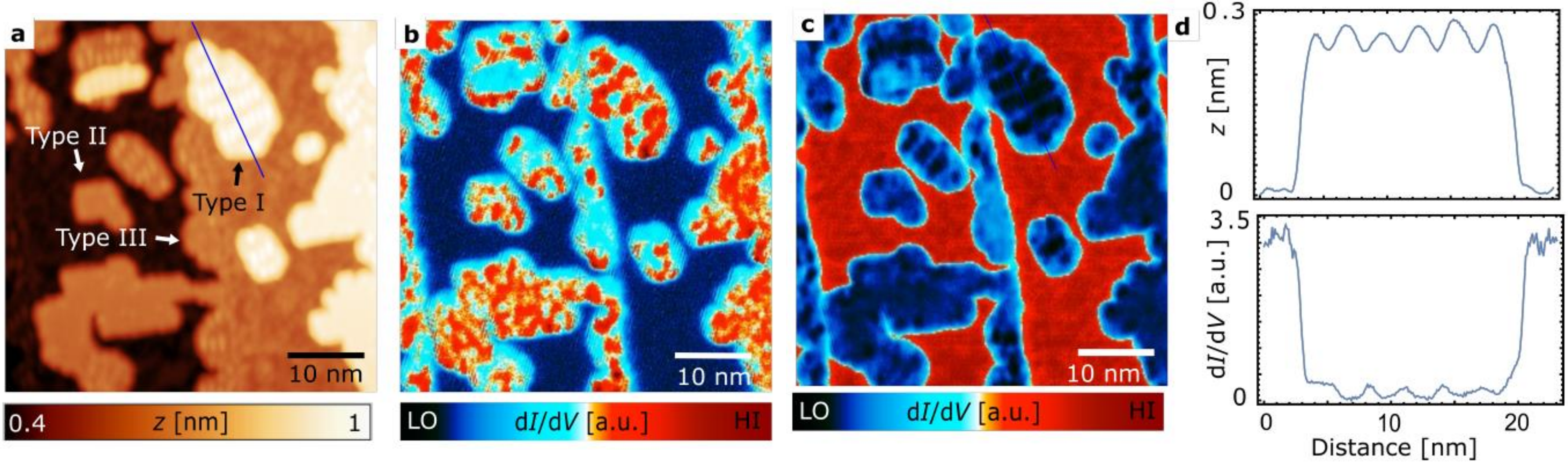

Iron double layer and the Shiba bands

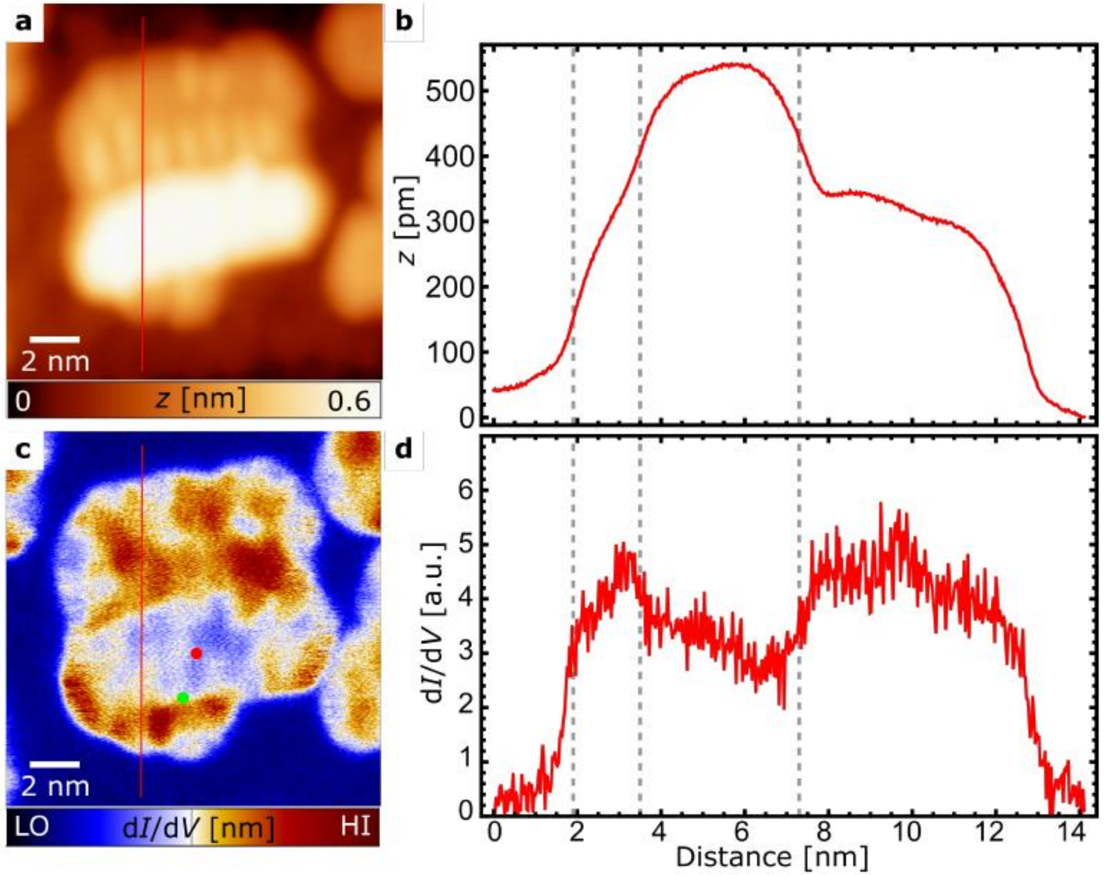

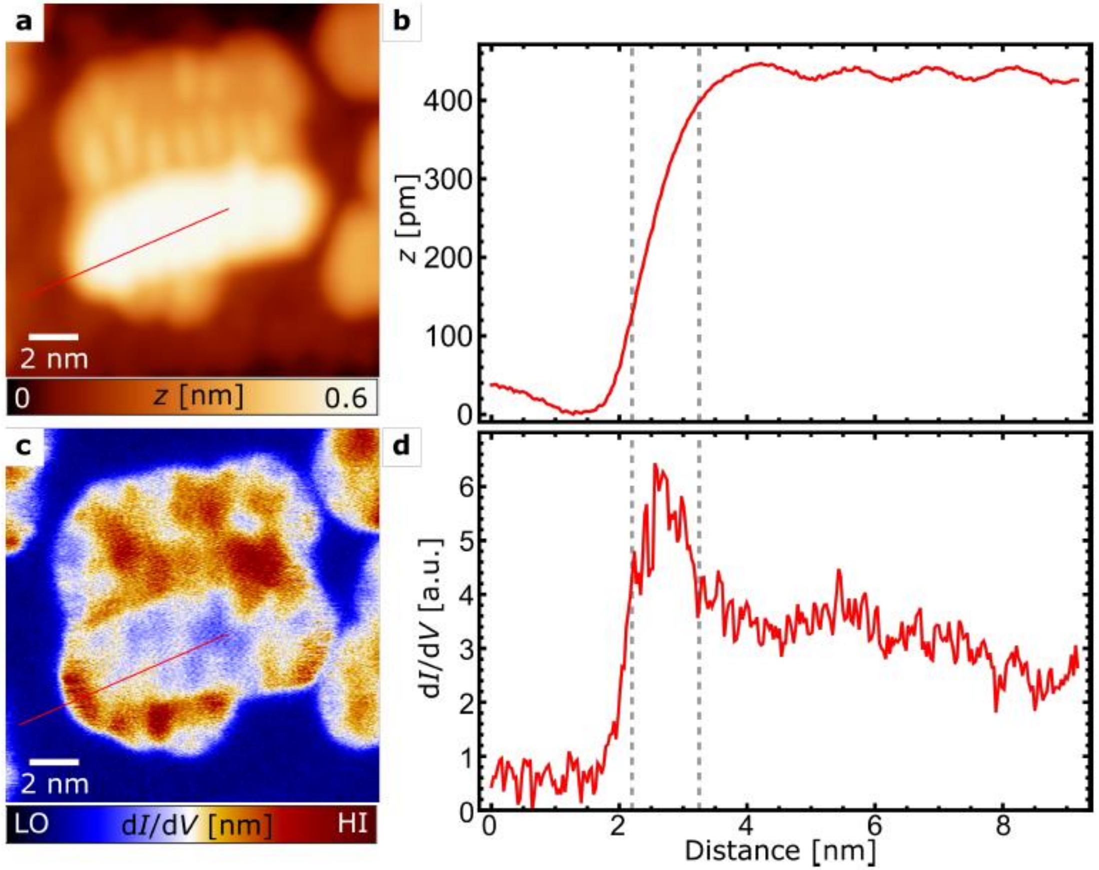

Iron double layer and the Shiba bands

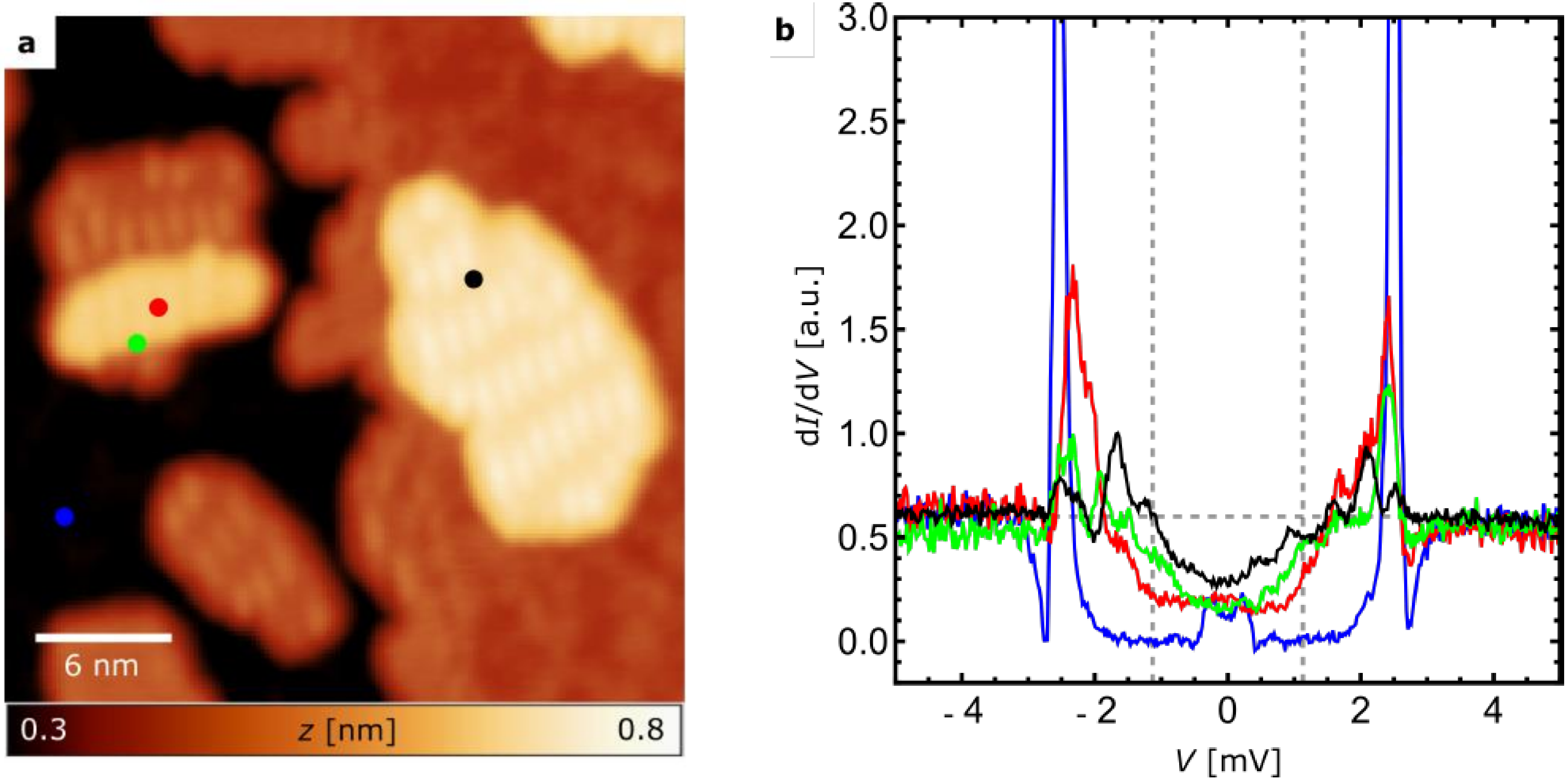

Magnetic properties of the DL

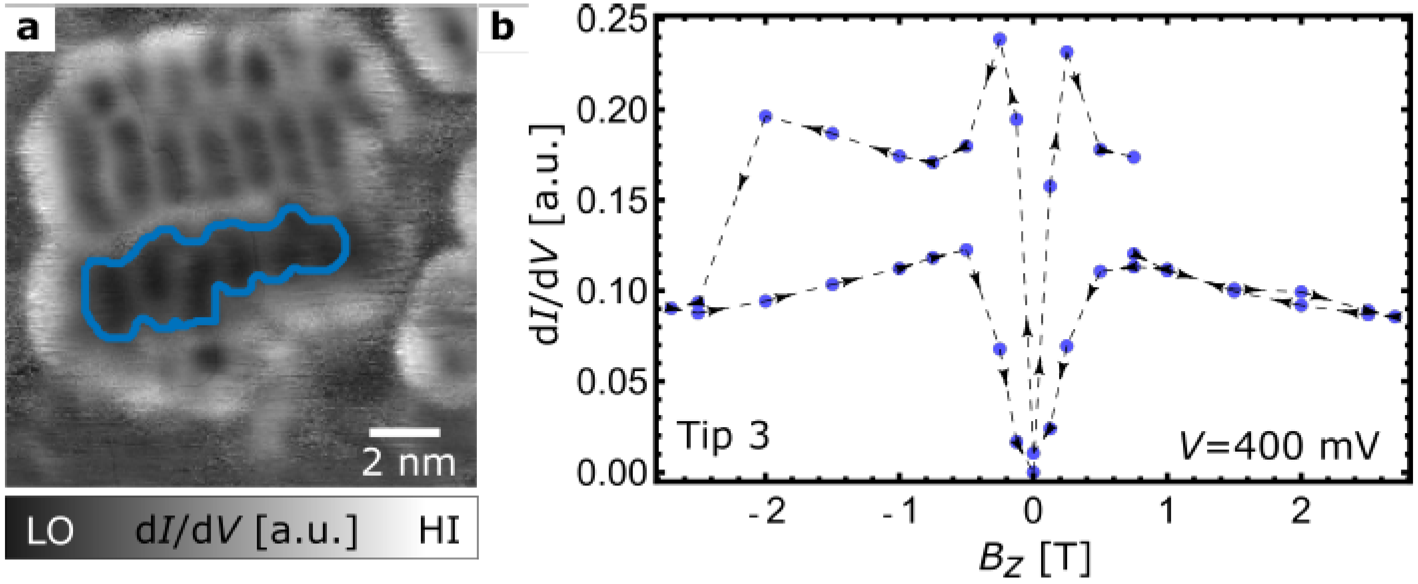

Figure 4.31: a First dI/dV map of the loop with the extracted data (blue outlined area) averaged and plotted as a function of the B-field with the resulting hysteresis loop b. A similar magnetic behavior is found as for type I ML islands. Note that compared to Fig. 4.18 b, the magnetic loop here was recorded at up to ±2.7 T. For tip 3 it must be added that the loops were not measured correctly to the end. For a complete loop one can imagine the measuring points mirrored around $B = 0\,\mathrm{T}$. Measurement parameters: $I = 1\,\mathrm{nA}$, $V_{\mathrm{mod}} = 10\,\mathrm{mV}$, $V = 400\,\mathrm{mV}$, $f = 1197\,\mathrm{Hz}$ and $T = 4.5\,\mathrm{K}$.

Practical realization of Majoranas via Yu-Shiba-Rusinov states

Single magnetic impurity

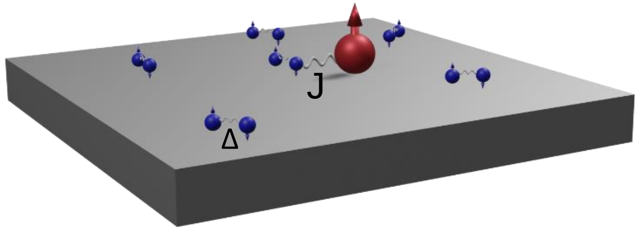

$$H_{\mathrm{YSR}} = \left(\frac{p^2}{2m} - \mu\right) \boldsymbol{\tau}_z + [V\boldsymbol{\tau}_z - J\,\mathbf{S}\,\boldsymbol{\sigma}]\ \delta(\mathbf{r}) + \Delta\boldsymbol{\tau}_x$$

$$E_{\mathrm{YSR}} = \pm\Delta\frac{1-\alpha^2+\beta^2}{\sqrt{(1-\alpha^2+\beta^2)^2+4\alpha^2}}$$

$$\alpha = \pi\rho S J \qquad \beta = \pi\rho V$$

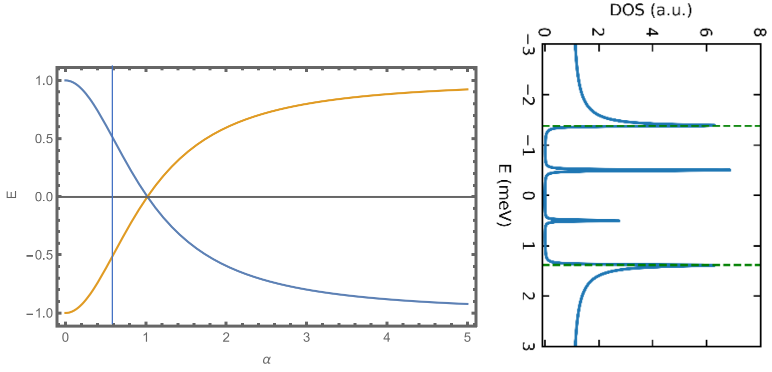

Multiple magnetic impurities

Shiba bands in 1D chain

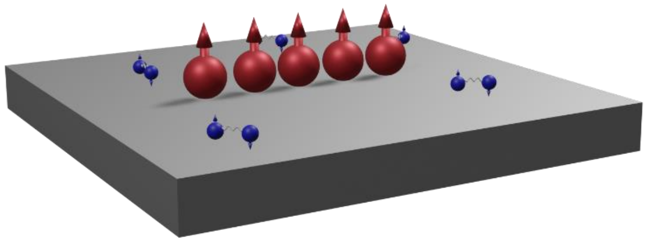

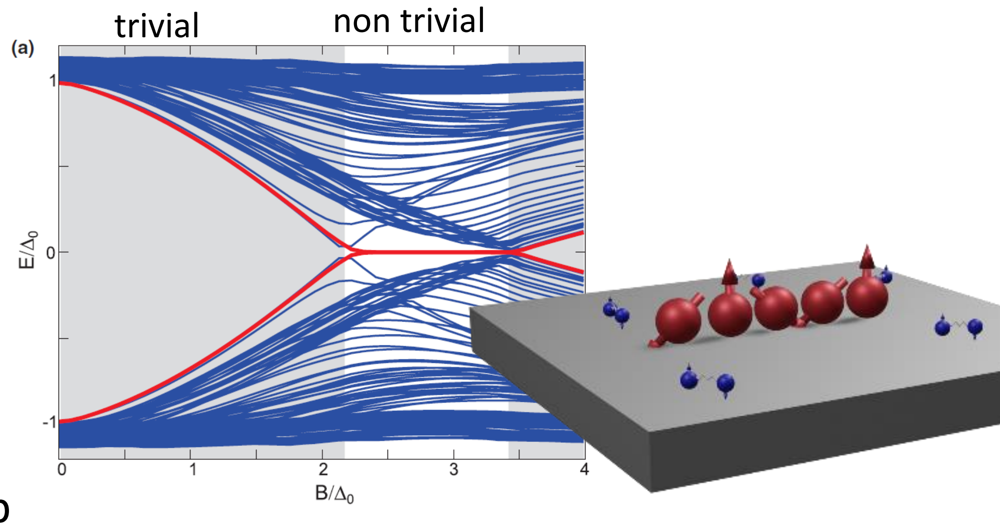

small overlap

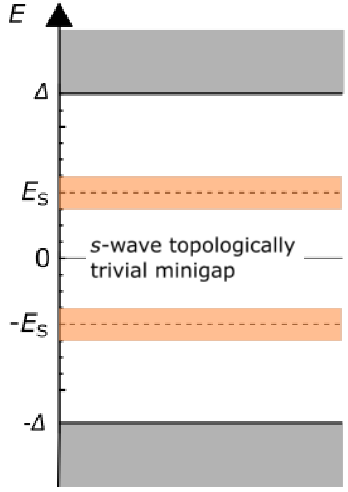

s-wave topologically trivial minigap

strong overlap

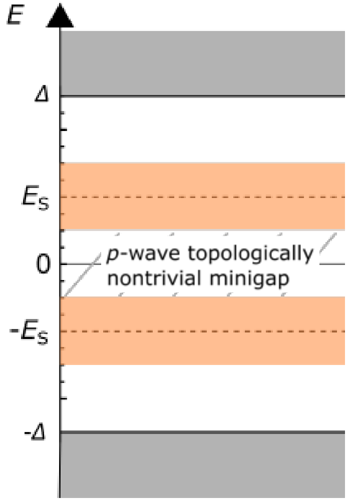

p-wave topologically nontrivial minigap

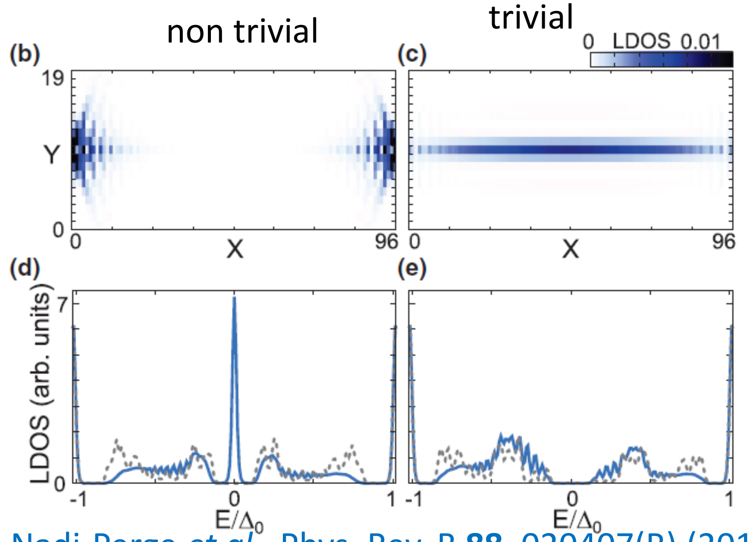

Nadj-Perge *et al.*, Phys. Rev. B **88**, 020407(R) (2013);

Practical realization of Majoranas via Yu-Shiba-Rusinov states

Single magnetic impurity

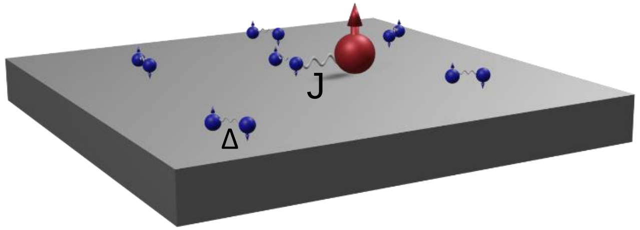

$$H_{\mathrm{YSR}} = \left(\frac{p^2}{2m} - \mu\right) \boldsymbol{\tau}_z + [V\boldsymbol{\tau}_z - J\,\mathbf{S}\,\boldsymbol{\sigma}]\ \delta(\mathbf{r}) + \Delta\boldsymbol{\tau}_x$$

$$E_{\mathrm{YSR}} = \pm\Delta\frac{1-\alpha^2+\beta^2}{\sqrt{(1-\alpha^2+\beta^2)^2+4\alpha^2}}$$

$$\alpha = \pi\rho S J \qquad \beta = \pi\rho V$$

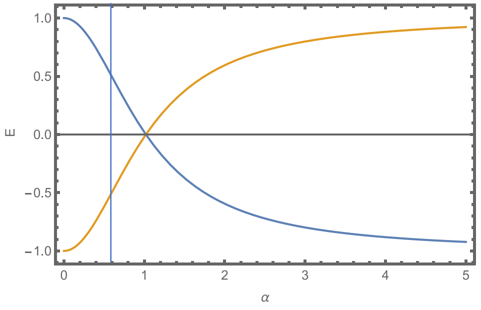

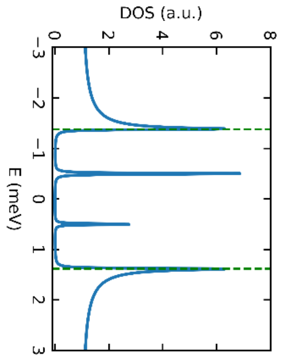

Multiple magnetic impurities

Shiba bands in 1D chain

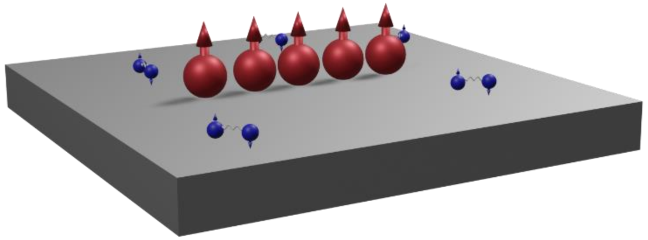

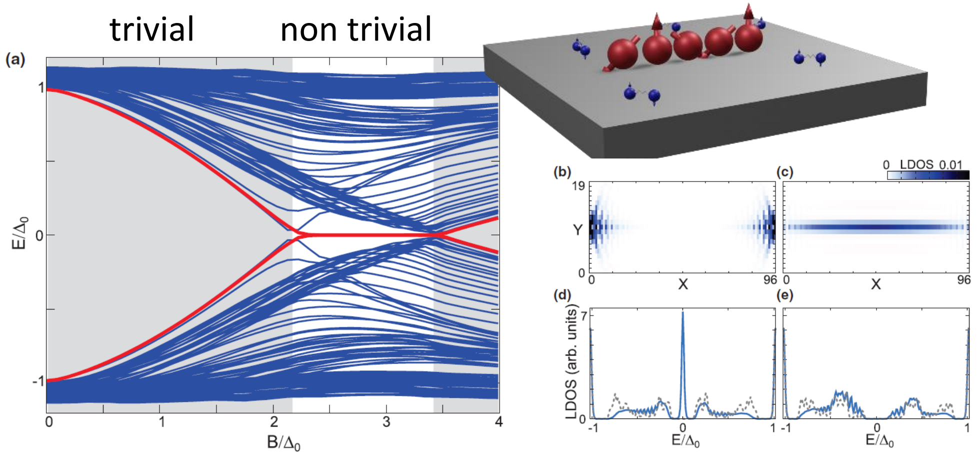

small overlap

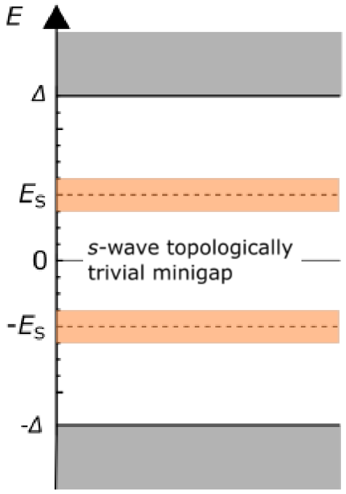

strong overlap

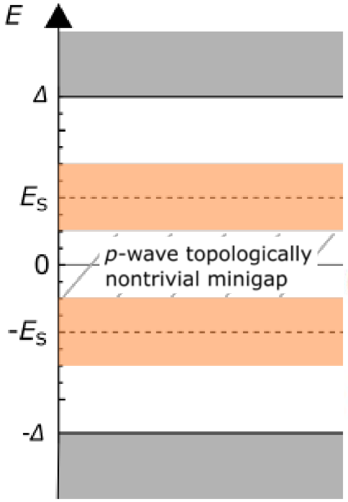

Shiba bands in 2D lattice

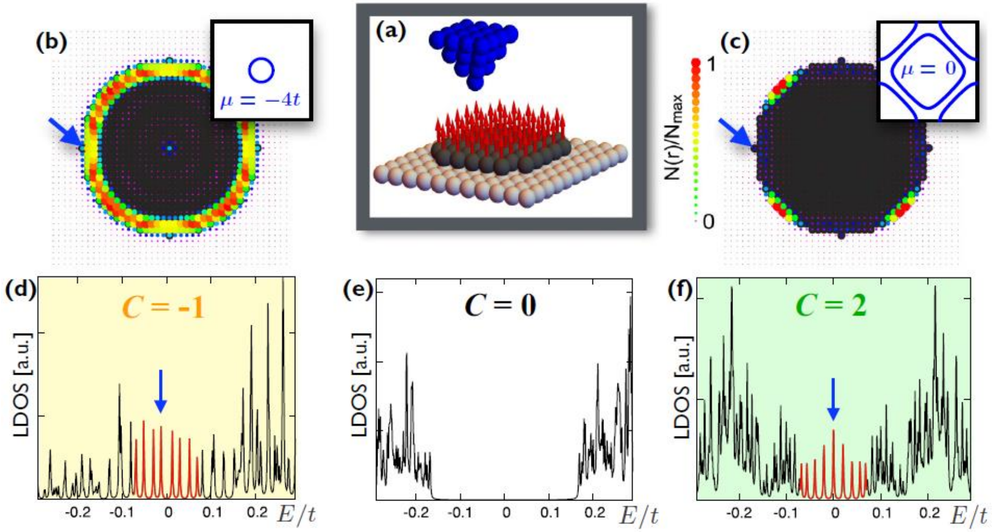

- Why niobium:
  - high Tc = 9.2K of all elemental superconductors
  - largest energy gap
  - spin-orbit coupling (even is comparatively light element)
- Nb(110) twofold surface symmetry
- Nb(111) threefold surface symmetry
  - could favor the formation of chiral spin structures which might eliminate the need for strong spin-orbit coupling. Problem with Nb: high contamination with (mostly) oxygen
  - Established process for Nb(110): cleaning by sputtering and annealing at very high temperature near to melting point [1]
  - No established process for cleaning Nb(111)

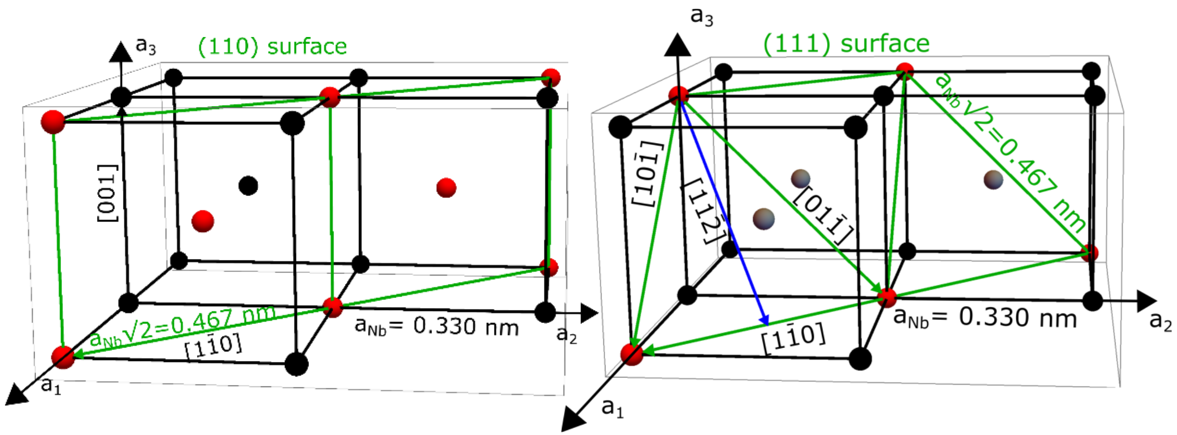

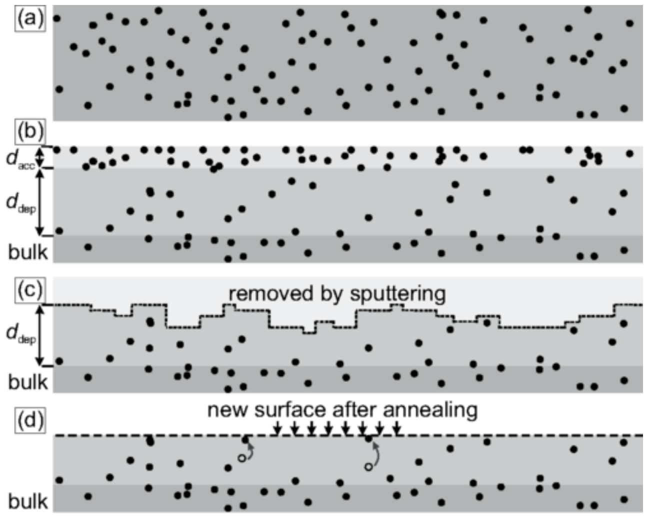

[1] A. Odobesko *et al.*, PRB **99,** 115437 (2019)

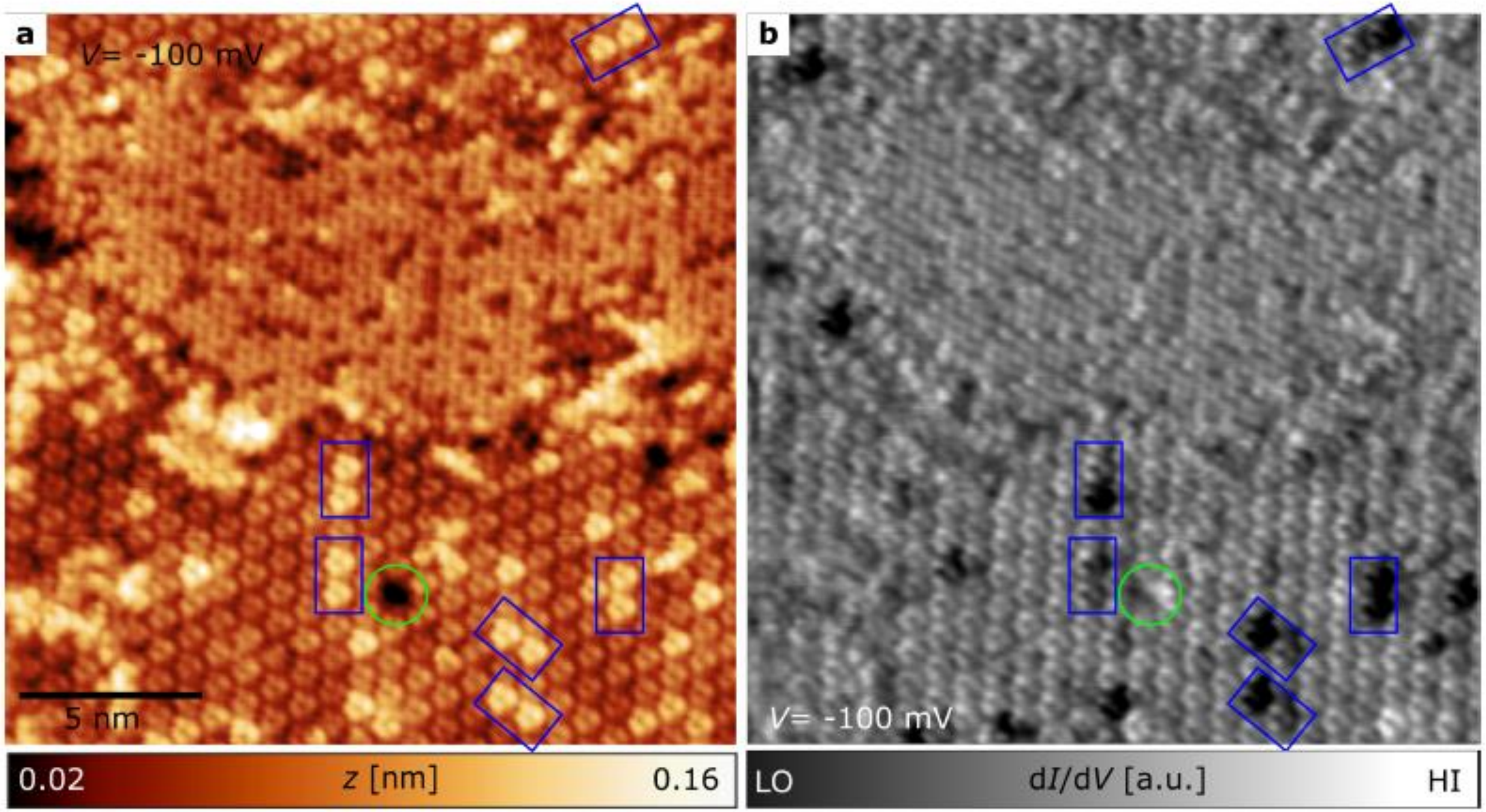

Figure 4.10: In a the Kagome-like reconstruction can be seen with the simultaneously recorded $\mathrm{d}I/\mathrm{d}V$ map in b, in which two of the bright three atom clusters (framed in blue) show a strongly reduced $\mathrm{d}I/\mathrm{d}V$ value at $V = -100\,\mathrm{mV}$ in contrast to the neighbouring atoms. In addition, there is a defect in the lattice (framed in green) where the $\mathrm{d}I/\mathrm{d}V$ values are larger at this energy. Measurement parameters for a and b: $V = -100\,\mathrm{mV}$, $I = 1\,\mathrm{nA}$, $T = 25\,\mathrm{K}$.

DMI

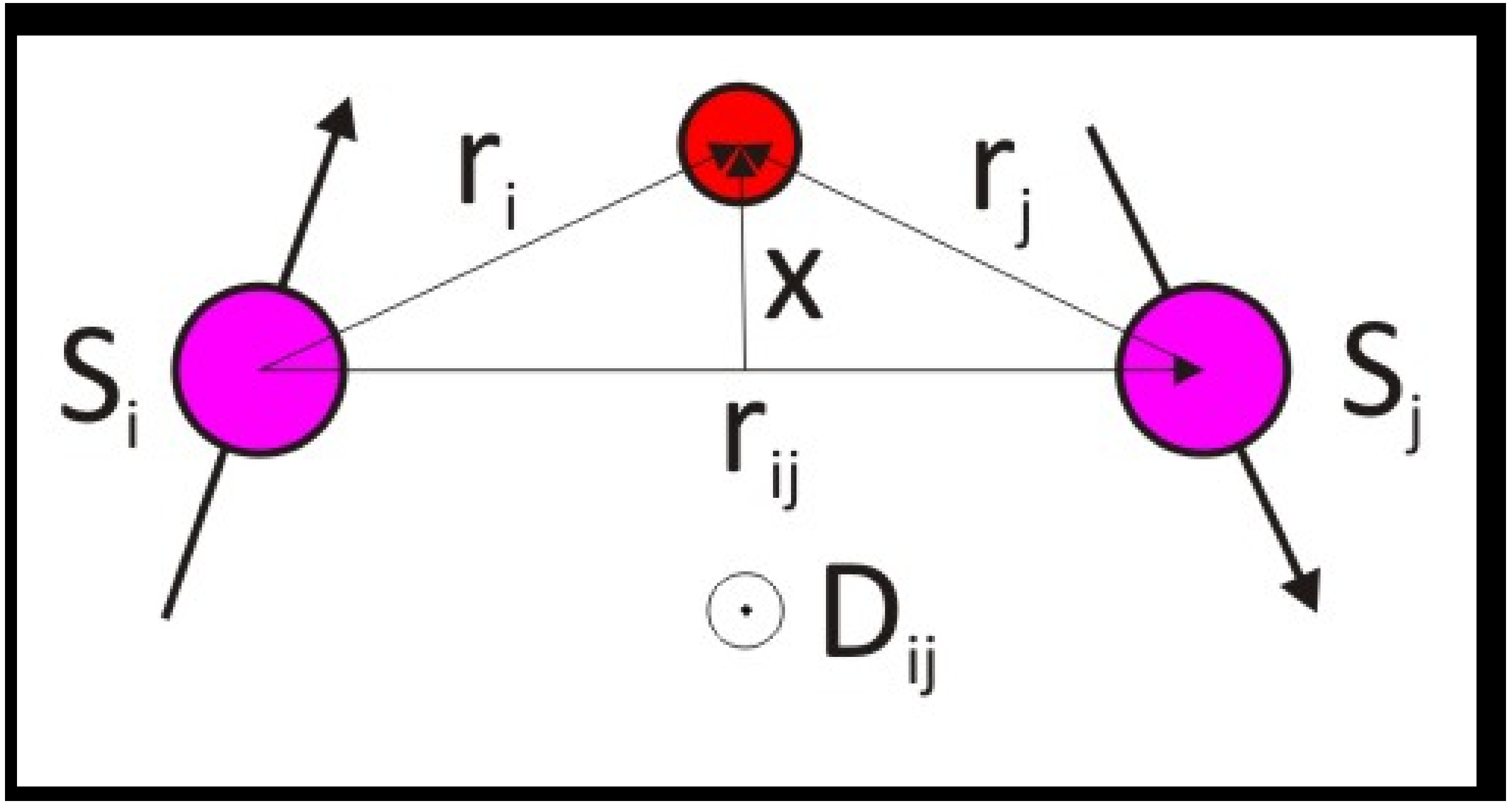

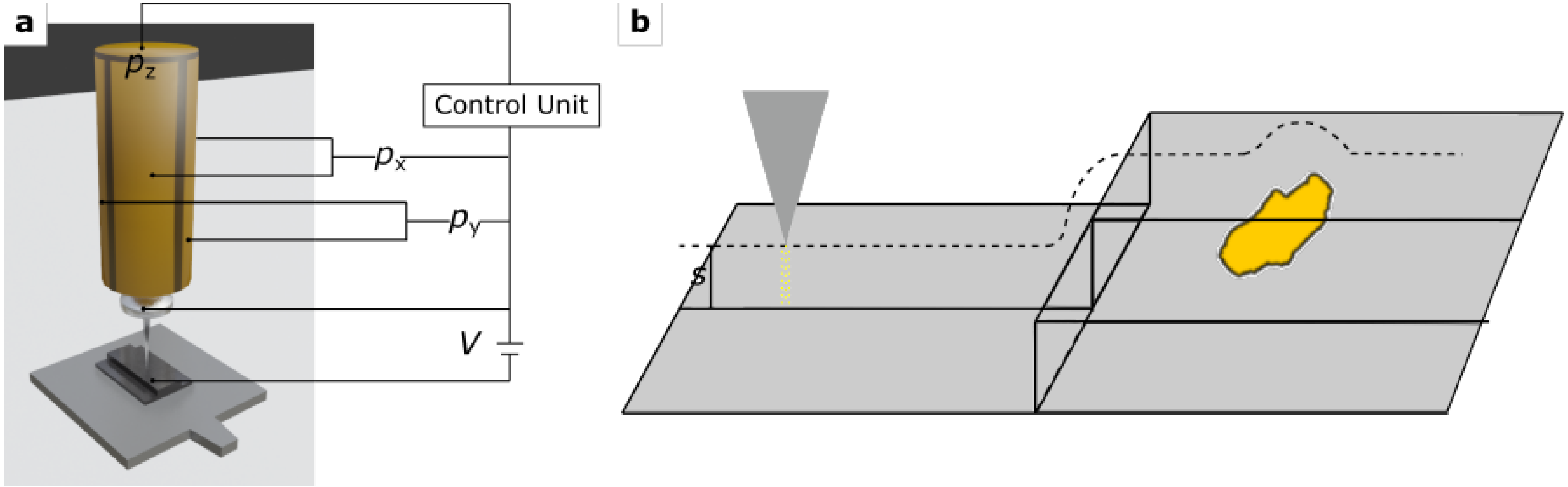

$$I \propto \int^{eV} \rho_t(\pm eV \mp E)\, \rho_s(E, r_0)\, T(E, eV)\, dE,$$

$$T(E, eV) = \exp\left\{-2(s+R)\left[\frac{2m}{\hbar^2}\left(\frac{\phi_t + \phi_s}{2} + \frac{eV}{2} - E\right)\right]^{\frac{1}{2}}\right\}$$

PHYSICAL REVIEW B **103**, 235437 (2021)

Coupling of Yu-Shiba-Rusinov states in one-dimensional chains of Fe atoms on Nb(110)

Felix Friedrich,[1,*] Robin Boshuis,[1] Matthias Bode,[1,2] and Artem Odobesko[1]

[1] *Physikalisches Institut, Experimentelle Physik II, and Würzburg-Dresden Cluster of Excellence ct.qmat, Universität Würzburg, Am Hubland, 97074 Würzburg, Germany*

[2] *Wilhelm Conrad Röntgen-Center for Complex Material Systems (RCCM), Universität Würzburg, Am Hubland, 97074 Würzburg, Germany*

(Received 11 March 2021; revised 14 June 2021; accepted 14 June 2021; published 28 June 2021)

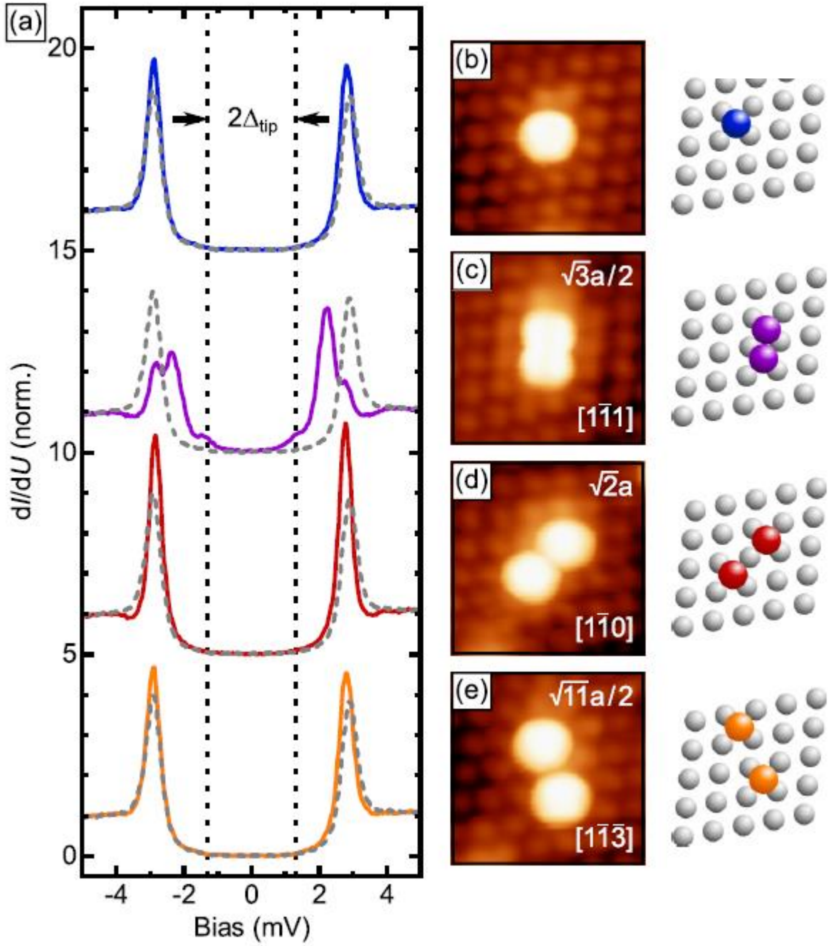

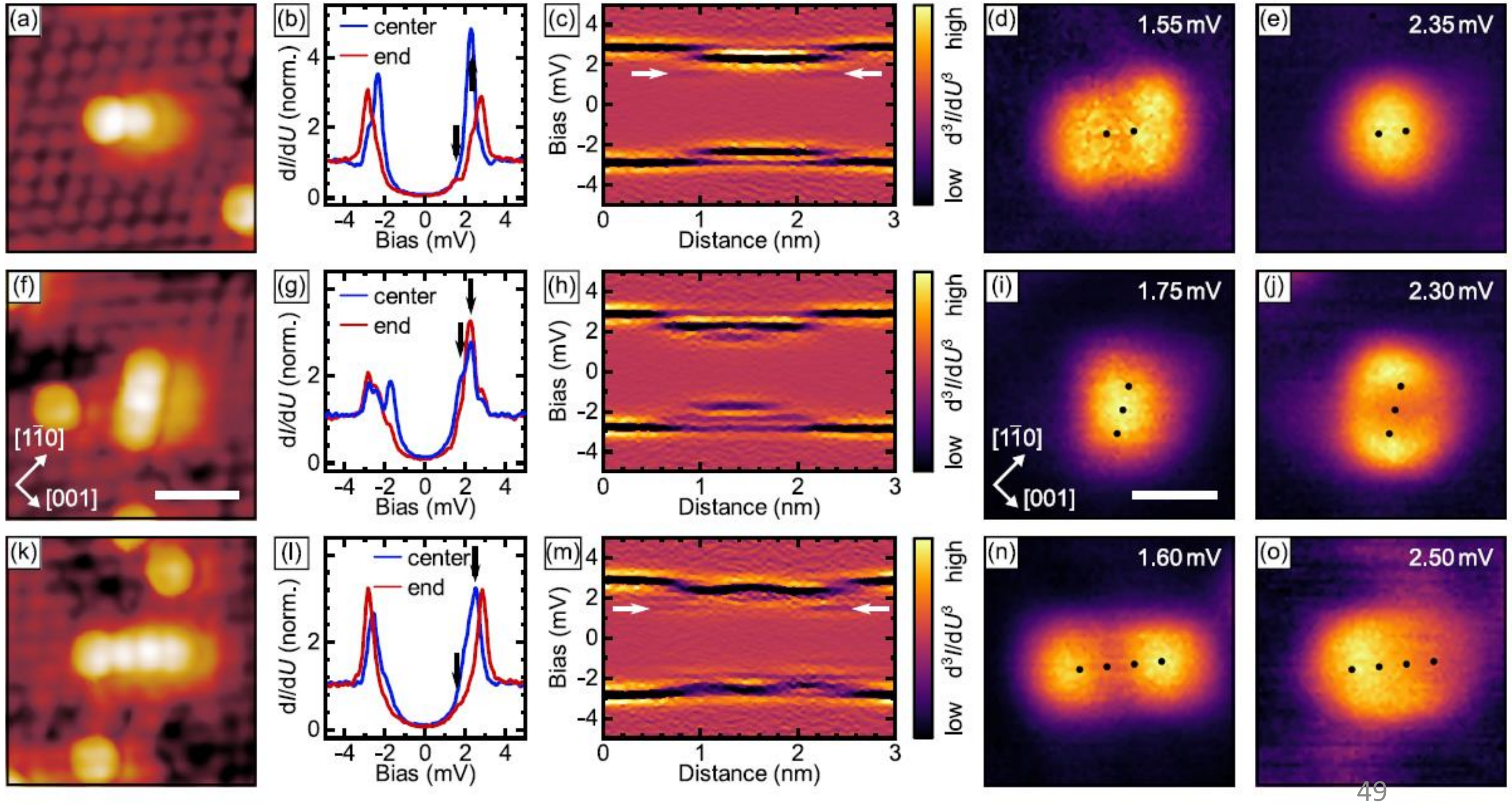

ARTICLES
https://doi.org/10.1038/s41565-022-01078-4
nature nanotechnology

OPEN

Precursors of Majorana modes and their length-dependent energy oscillations probed at both ends of atomic Shiba chains

Lucas Schneider[1], Philip Beck[1], Jannis Neuhaus-Steinmetz[1], Levente Rózsa[2], Thore Posske[3,4], Jens Wiebe[1]✉ and Roland Wiesendanger[1]

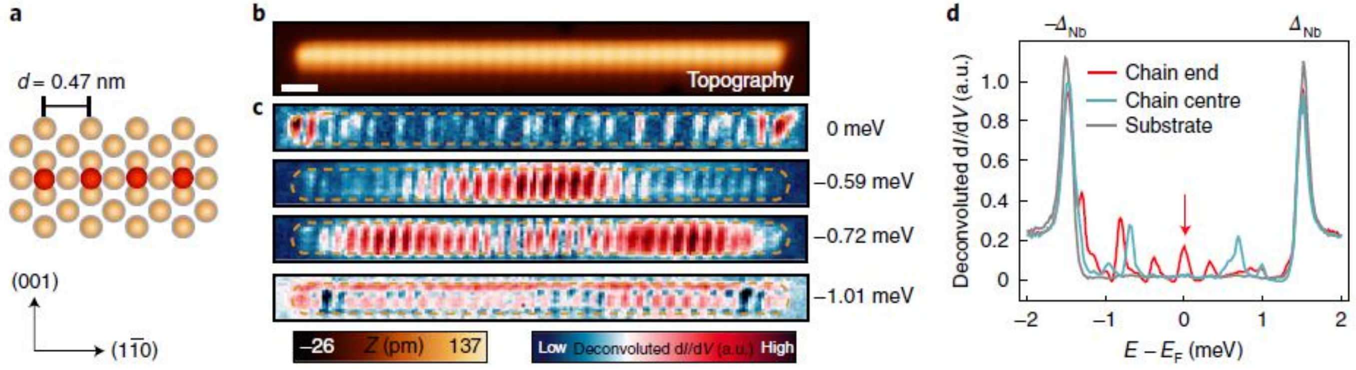

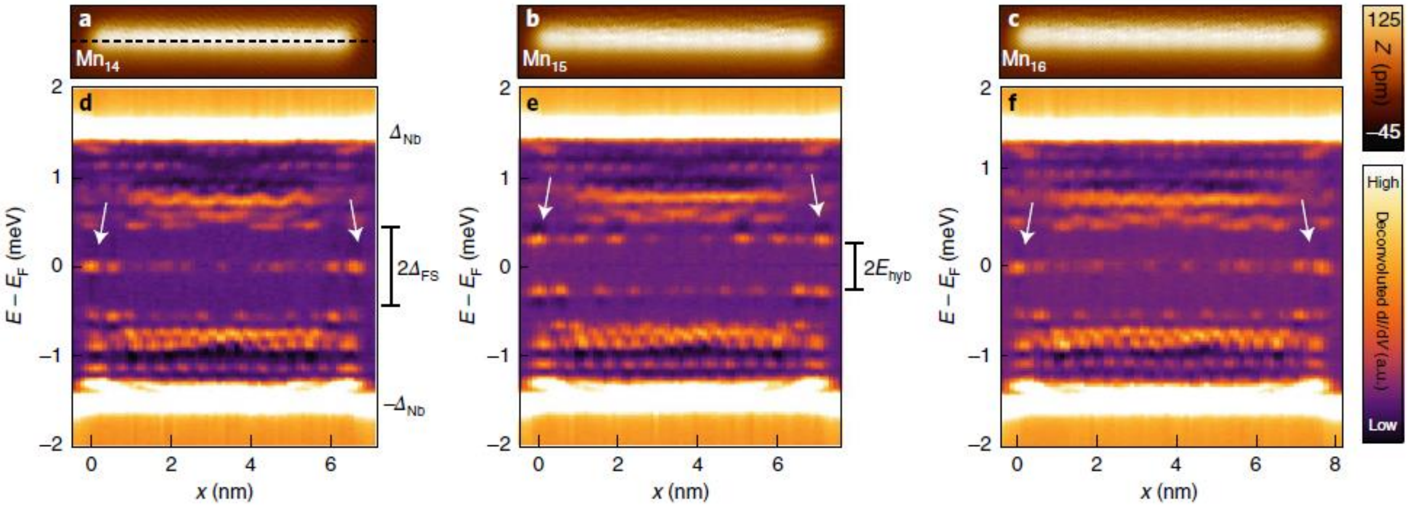

nature communications

Article
https://doi.org/10.1038/s41467-023-36201-z

Antiferromagnetism-driven two-dimensional topological nodal-point superconductivity

Received: 12 August 2022
Accepted: 17 January 2023

Maciej Bazarnik[1,2,5], Roberto Lo Conte[1,5], Eric Mascot[1,3,5],
Kirsten von Bergmann[1], Dirk K. Morr[4] & Roland Wiesendanger[1]

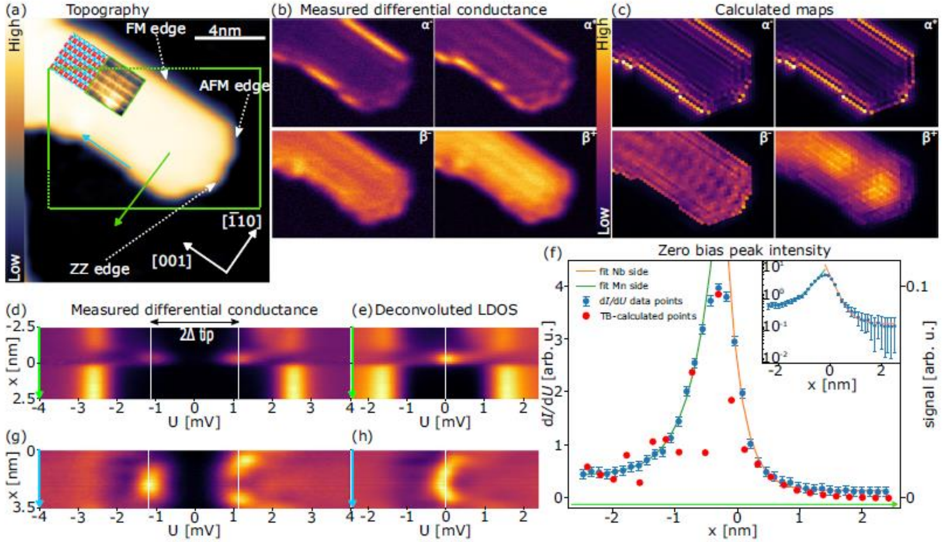

Fig. 3 | Spatial dependence of tunneling spectroscopic features. **a** A topography image of a defect-free Mn island. The insets show an SP-STM image of part of the island and a sketch of the $c(2\times 2)$ antiferromagnetic state. The green rectangle indicates the sample area of panel **b**. **b** Differential tunneling conductance maps acquired with a superconducting Nb-coated Cr tip at characteristic energies as indicated for $\alpha^{\pm}$ and $\beta^{\pm}$. **c** Tight-binding model calculated maps for the same spectroscopic features as in panel **b**. **d** Spectra along the line marked with a green arrow in panel **a** crossing one of the FM edges. **e** Deconvoluted LDOS obtained from the data in panel **d**. **f** Intensity of the zero-bias peak as a function of the distance from the edge. The green and orange curves are exponential decay fits to experimental data towards the Mn and Nb, respectively. The error bars represent measurement noise level. The inset shows a semi-log plot for experimental data and fits. **g** Spectra along the line marked with a blue arrow in panel **a** along one of the ferromagnetic edges. **h** Deconvoluted LDOS from panel **g**. Through the panels **d**–**f** the 0 on the x-axis is set to the half-height of the Mn island in the topography profile along the green arrow. Tunneling parameters: **a** $I_t = 1$ nA, $U = 50$ mV; **b** $I_{ts} = 1$ nA, $U_{stab} = 20$ mV, $U_{mod} = 100$ μV, $Z_{approach} = 80$ pm, for $\alpha^{\pm}$ $U = \pm 1.05$ mV, for $\beta^{\pm}$ $U = \pm 1.9$ mV; **d** $I_{ts} = 1$ nA, $U_{stab} = 20$ mV, $U_{mod} = 100$ μV, $Z_{approach} = 100$ pm; **g** $I_{ts} = 1$ nA, $U_{stab} = 20$ mV, $U_{mod} = 100$ μV, $Z_{approach} = 100$ pm.

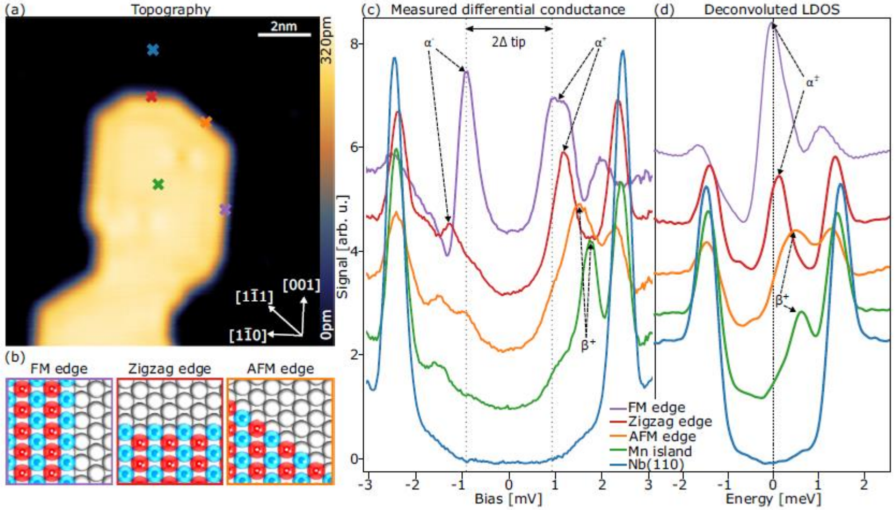

Local tunneling spectroscopy on a Mn/Nb(110) island. **a** Topography f a single Mn island with well-developed edges along the main crystal-ic directions. **b** Schematics of the atomic and spin structure of a FM, ZZ, M edge, respectively. **c** Tunneling point spectra acquired with a super-ting Nb-coated Cr tip at the positions indicated in panel **a**. **d** Deconvoluted LDOS obtained from the spectra displayed in panel **c**. α and β mark the states corresponding to calculated dispersive edge modes shown in Fig. 1. Tunneling parameters: **a** tunneling current $I_t = 1$ nA, bias $U = 20$ mV; **c** stabilization tunneling current $I_{ts} = 1$ nA, stabilization bias $U_{stab} = 20$ mV, modulation bias $U_{mod} = 100$ μV, vertical tip shift towards the sample's surface after stabilization $Z_{approach} = 80$ pm.

Spin-Bahn-Kopplung

$$H_{\mathrm{SO}} = \lambda \mathbf{L} \cdot \mathbf{S},$$

$$\lambda = \frac{1}{8\pi\epsilon_0 m^2 c^2} \cdot \frac{Ze^2}{r^3}.$$

Austauschwechselwirkung

$$H_{\mathrm{Heisenberg}} = -\sum_{i,j} J_{ij} \mathbf{S}_i \cdot \mathbf{S}_j,$$

$$J = \int \Psi_i^*(\mathbf{r}_1)\Psi_j^*(\mathbf{r}_2)\frac{e^2}{|\mathbf{r}_1 - \mathbf{r}_2|}\Psi_i(\mathbf{r}_1)\Psi_j(\mathbf{r}_2)d\mathbf{r}_1 d\mathbf{r}_2.$$

Anyonen

Bosonen $|\psi_1\psi_2> = \frac{1}{\sqrt{2}}(|\psi_1>|\psi_2> + |\psi_2>|\psi_1>)$ → $|\psi_1\psi_2> = +|\psi_2\psi_1>$

Fermionen $|\psi_1\psi_2> = \frac{1}{\sqrt{2}}(|\psi_1>|\psi_2> - |\psi_2>|\psi_1>)$ → $|\psi_1\psi_2> = -|\psi_2\psi_1>$

Anyonen $|\psi_1\psi_2> = e^{i\theta}|\psi_2\psi_1>$

Majorana returns

Frank Wilczek

In his short career, Ettore Majorana made several profound contributions. One of them, his concept of 'Majorana fermions' — particles that are their own antiparticle — is finding ever wider relevance in modern physics.

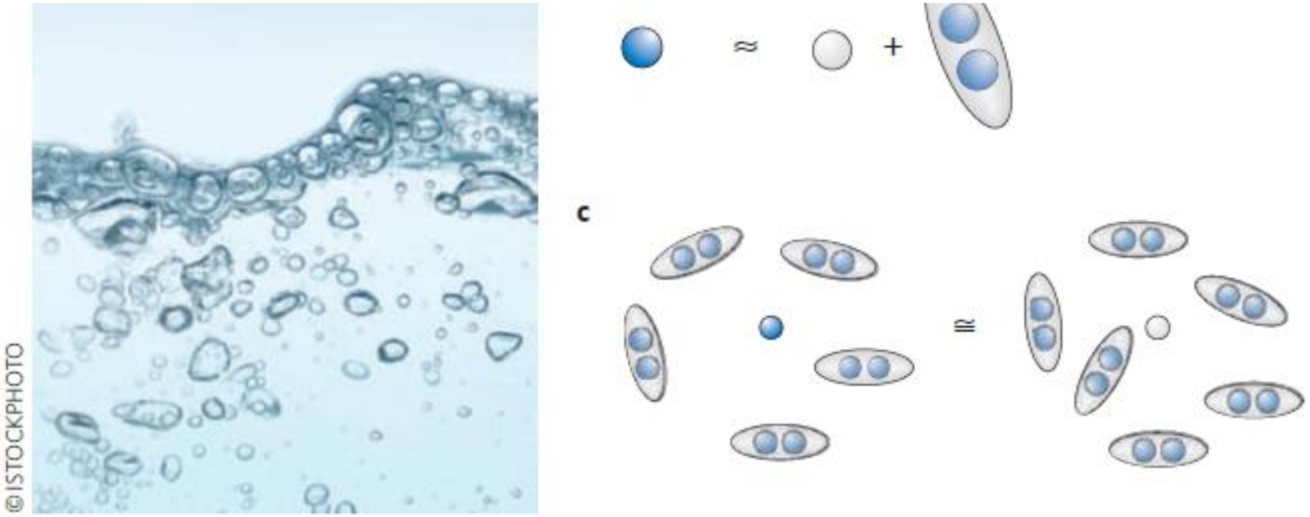

Figure 1 | Antimatter matters in the solid state. **a**, A familiar concept in solid-state physics, holes are bubbles of missing electrons in the Fermi sea of the electronic spectrum, behaving like positively charged electrons. **b**, In a superconductor, the properties of electrons (blue) and holes (grey) are drastically modified by their interaction with the surrounding sea of Cooper pairs; a hole can attract or bind to a Cooper pair, and acquire negative charge. **c**, More importantly, Cooper pairs cluster around holes and thin out around electrons, in such a way that no rigorous distinction between them remains.

Topologie

- Gebiet in der Mathematik
  - Klassifizierung von geometrischen Objekten (topologischen Räumen)
  - Wie kann man mathematisch beschreiben ob zwei geometrische Objekte topologisch äquivalent sind?
    - Zwei geometrische Objekte sind topologisch äquivalent wenn man sie kontinuierlich ineinander verformen kann (homöomorph)
  - Klassifizierung mittels topologischer Invariante
    - Chern-Nummer
  - In FK: Summe der Valenzbänder eines Materials in einer Phase weist eine topologische Eigenschaft auf

kontinuierliche Verformung

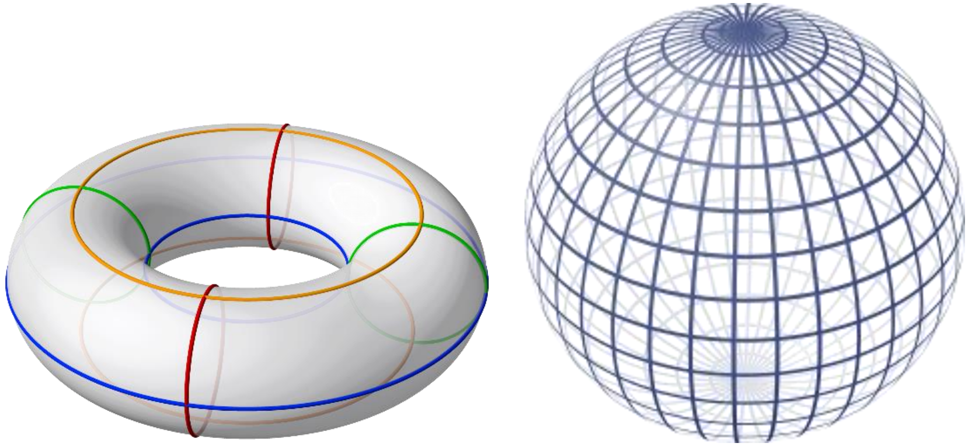

Topologisch invariante Chern-Nummer

$$\mathbf{H}(\mathbf{R}(t))$$

$$|\Psi_m(\mathbf{R}(t_0))\rangle \to e^{i(\phi_m(t)+\gamma_m(t))}\,|\Psi_m(\mathbf{R}(t_0+T))\rangle$$

$$\gamma_m = \oint_\Gamma \mathbf{A}_m(\mathbf{R})d\mathbf{R} = \int_S \mathbf{F}_m \cdot \mathbf{n}\; d^2R.$$

$$C_m = \frac{1}{2\pi}\int_S \mathbf{F}_m(\mathbf{R})\cdot \mathbf{n}d^2R.$$

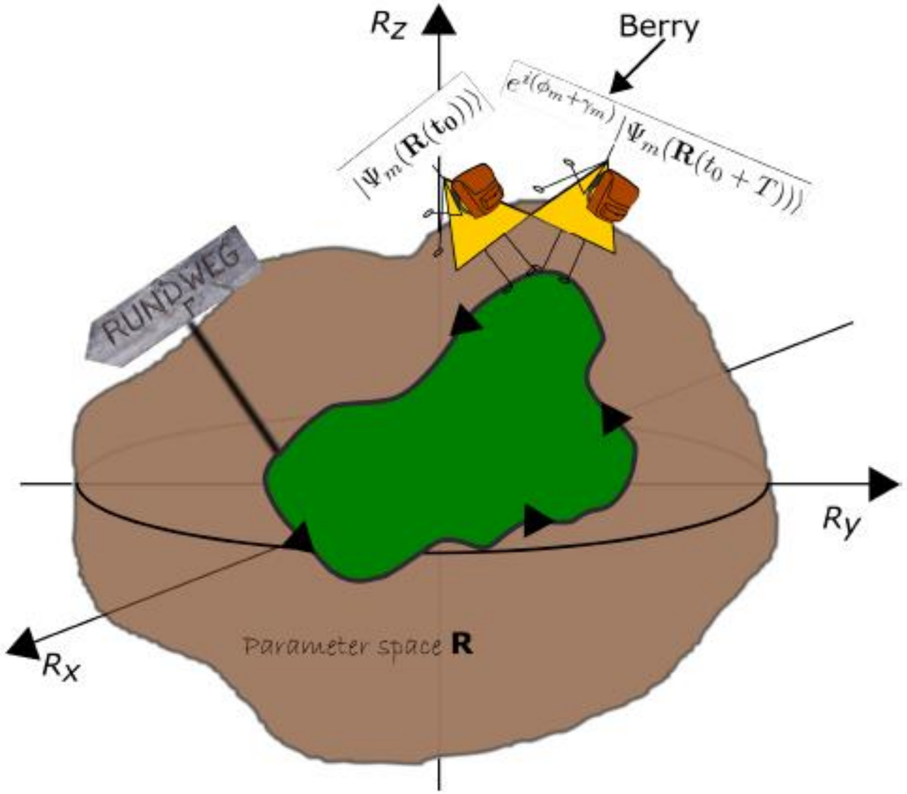

p-wave-Modell 1D

$$H_{\mathrm{BdG}} = \sum_j \left[-t\left(c_j^\dagger c_{j+1} + c_{j+1}^\dagger c_j\right) - \mu c_j^\dagger c_j + \Delta\left(c_{j+1}^\dagger c_j^\dagger + c_j c_{j+1}\right)\right].$$

$$c_j = \tfrac{1}{2}(\gamma_{2j-1} + i\gamma_{2j}) \qquad c_j^\dagger = \tfrac{1}{2}(\gamma_{2j-1} - i\gamma_{2j})$$

$$H_{BdG} = \frac{i}{2}\sum_j [-\mu\gamma_{2j-1}\gamma_{2j} + (t+\Delta)\gamma_{2j}\gamma_{2j+1} + (-t+\Delta)\gamma_{2j-1}\gamma_{2j+2}].$$

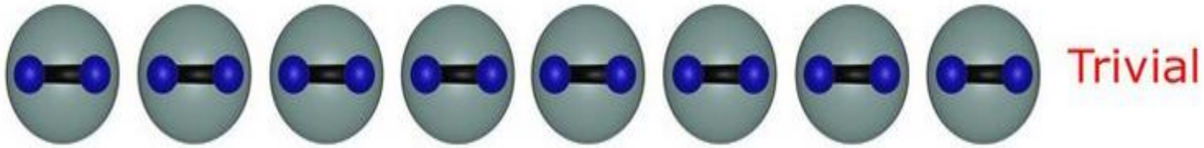

$$\mu < 0 \qquad |\Delta| = t = 0,$$

$$H = -\mu \tfrac{i}{2} \textstyle\sum_j (\gamma_{2j-1}\gamma_{2j})$$

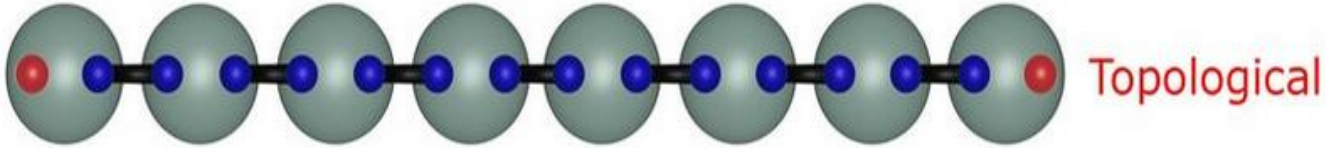

$$|\Delta| = t > 0,\ \mu = 0,$$

$$H = +it \textstyle\sum_j (\gamma_{2j}\gamma_{2j+1})$$

2D-pwave

$$H_{2\mathrm{D}} = \sum_{m,n} -t\left(c^\dagger_{m+1,n}c_{m,n} + h.c.\right) - t\left(c^\dagger_{m,n+1}c_{m,n} + h.c.\right) - (\mu - 4t)c^\dagger_{m,n}c_{m,n}c_j$$
$$+ \left(\Delta c^\dagger_{m+1,n}c^\dagger_{m,n} + \Delta^* c_{m,n}c_{m+1,n}\right) + \left(i\Delta c^\dagger_{m,n+1}c^\dagger_{m,n} - i\Delta^* c_{m,n}c_{m,n+1}\right)$$

$$H_{2\mathrm{D}}(\mathbf{k}) = (2 - \mu - \cos(k_x) - \cos(k_y))\tau_z - 2|\Delta|\sin(k_x)\tau_y - 2|\Delta|\sin(k_y)\tau_x$$

$$E_\pm(\mathbf{k}) = \pm\sqrt{(2 - \mu - \cos(k_x) - \cos(k_y))^2 + 4|\Delta|^2(\sin^2(k_x) + \sin^2(k_y))}.$$

trivial phases are found at $\mu < 0$ and $\mu > 4$ while the topologically nontrivial phases of opposite chirality are found at $0 < \mu < 2$ and $2 < \mu < 4$, respectively.

2D-Shiba lattice

$$
\begin{aligned}
H_{\mathrm{SC}} = & -t \sum_{\langle \mathbf{r}\mathbf{r}'\rangle,\sigma} (c^\dagger_{\mathbf{r},\sigma} c_{\mathbf{r}',\sigma} + \mathrm{H.c.}) - \mu \sum_{\mathbf{r},\sigma} c^\dagger_{\mathbf{r},\sigma} c_{\mathbf{r},\sigma} \\
& + i\alpha \sum_{\mathbf{r},\sigma,\sigma'} \left(c^\dagger_{\mathbf{r},\sigma} \sigma^2_{\sigma\sigma'} c_{\mathbf{r}+\hat{x},\sigma'} - c^\dagger_{\mathbf{r},\sigma} \sigma^1_{\sigma\sigma'} c_{\mathbf{r}+\hat{y},\sigma'} + \mathrm{H.c.}\right) \\
& + J \sum_{\mathbf{R},\sigma,\sigma'} c^\dagger_{\mathbf{R},\sigma} \sigma^3_{\sigma\sigma'} c_{\mathbf{R},\sigma'} + \Delta_s \sum_{\mathbf{r}} (c^\dagger_{\mathbf{r},\uparrow} c^\dagger_{\mathbf{r},\downarrow} + \mathrm{H.c.}) \\
& - t_{\mathrm{tip}} \sum_{\sigma} (c^\dagger_{\mathbf{r},\sigma} d_\sigma + \mathrm{H.c.}), \qquad (1)
\end{aligned}
$$

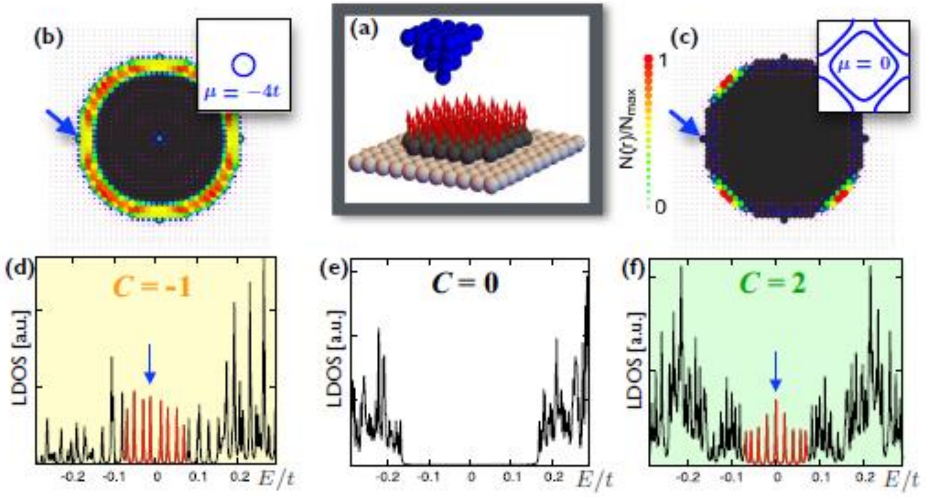

FIG. 1. (a) Sketch of a Shiba island with STS tip. The LDOS is shown for $\mu = -4t$ ($\mathcal{C} = -1$) in (b),(d), for $\mu = -2t$ ($\mathcal{C} = 0$) in (e), and for $\mu = 0$ ($\mathcal{C} = +2$) in (c),(f). Panels (d)–(f) display the energy-resolved spectra at the location marked by arrows in (b),(c); equally spaced in-gap states are clearly visible in the topological phases in (d) and (f). Panels (b),(c) show the spatial weight distribution (color coded) of the low-energy in-gap states marked by arrows in (d),(f); the insets display the corresponding normal-state Fermi surfaces. Parameters here and below are $(\alpha, \Delta_s, J) = (0.2, 0.3, 0.5)t$.

1D

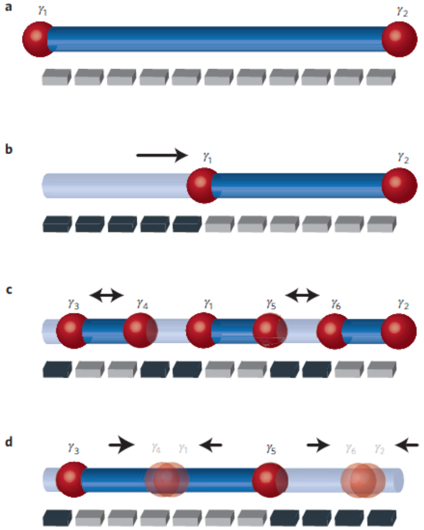

Figure 2 | Applying a 'keyboard' of individually tunable gates to the wire allows local control of which regions are topological (dark blue) and non-topological (light blue), and hence manipulate Majorana fermions while maintaining the bulk gap. As **a** and **b** illustrate, sequentially applying the leftmost gates drives the left end of the wire non-topological, thereby transporting γ_1 rightward. Nucleating a topological section of the wire from an ordinary region or vice versa creates pairs of Majorana fermions out of the vacuum as in **c**. Similarly, removing a topological region entirely or connecting two topological regions as sketched in **d** fuses Majorana fermions into either the vacuum or a finite-energy quasiparticle.

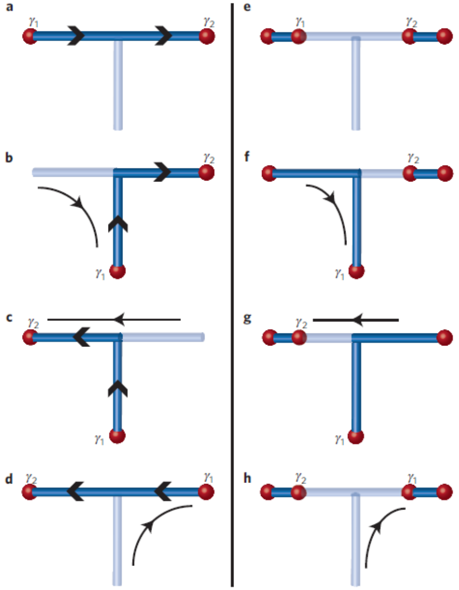

Figure 3 | A T-junction provides the simplest wire network that enables meaningful adiabatic exchange of Majorana fermions. Using the methods of Fig. 2, one can braid Majoranas bridged by either a topological region (dark blue lines) as in **a–d**, or a non-topological region (light blue lines) as in **e–h**. The arrows along the topological regions in **a–d** are useful for understanding the non-Abelian statistics, as outlined in the main text.

PHYSICAL REVIEW RESEARCH **2**, 023205 (2020)

Vortex Majorana braiding in a finite time

Thore Posske,[1] Ching-Kai Chiu,[2] and Michael Thorwart[1]
[1] *I. Institut für Theoretische Physik, Universität Hamburg, Jungiusstraße 9, 20355 Hamburg, Germany*
[2] *Kavli Institute for Theoretical Sciences, University of Chinese Academy of Sciences, Beijing 100190, China*

(Received 9 August 2019; revised manuscript received 17 April 2020; accepted 20 April 2020; published 21 May 2020)

Abrikosov vortices in Fe-based superconductors are a promising platform for hosting Majorana zero-energy modes. Their adiabatic exchange is a key ingredient for Majorana-based quantum computing. However, the adiabatic braiding process cannot be realized in state-of-the-art experiments. We propose to replace the infinitely slow, long-path braiding by a procedure that only slightly moves vortices in a special geometry without actually physically exchanging the Majoranas, like a Majorana carousel. Although the resulting finite-time gate is not topologically protected, it is robust against variations in material-specific parameters and in the braiding speed. We prove this analytically. Our results carry over to Y junctions of Majorana wires.

DOI: 10.1103/PhysRevResearch.2.023205

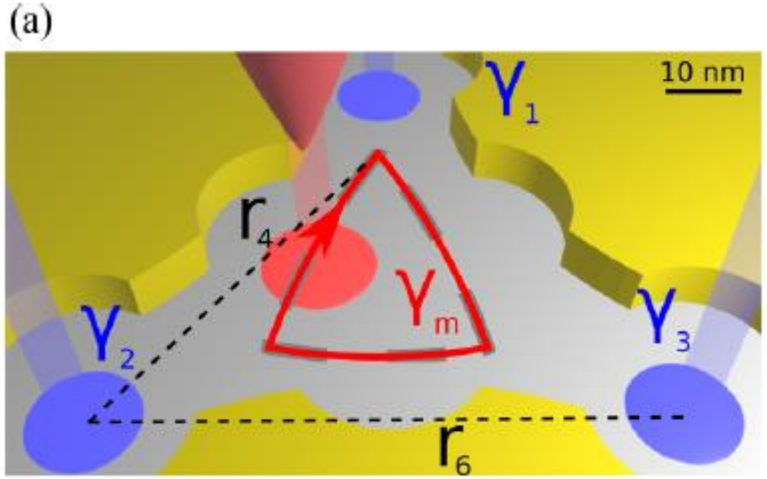

BSC

$$H_{\mathrm{BCS}} = \sum_{\mathbf{k},\sigma} \xi_{\mathbf{k}} n_{\mathbf{k},\sigma} + \sum_{\mathbf{k},\mathbf{l}} V_{\mathbf{k},\mathbf{l}} c^{\dagger}_{\mathbf{k}\uparrow} c^{\dagger}_{-\mathbf{k}\downarrow} c_{-\mathbf{l}\downarrow} c_{\mathbf{l}\uparrow}$$

$$H_{\mathrm{MeanBCS}} = \sum_{\mathbf{k},\sigma} \xi_{\mathbf{k}} n_{\mathbf{k},\sigma} - \sum_{\mathbf{k}} \left(\Delta_{\mathbf{k}} c^{\dagger}_{\mathbf{k}\uparrow} c^{\dagger}_{-\mathbf{k}\downarrow} + \Delta^{\dagger}_{\mathbf{k}} c_{-\mathbf{k}\downarrow} c_{\mathbf{k}\uparrow} - \Delta_{\mathbf{k}} b^{\dagger}_{\mathbf{k}} \right)$$

$$\Psi(\mathbf{k}) = \left[c_{\mathbf{k}\uparrow}, c^{\dagger}_{-\mathbf{k}\downarrow} \right]^{T}$$

$$c_{\mathbf{k}\uparrow} = u^{\dagger}_{\mathbf{k}} \gamma_{\mathbf{k}0} + v_{\mathbf{k}} \gamma^{\dagger}_{\mathbf{k}l},$$
$$c^{\dagger}_{-\mathbf{k}\downarrow} = -v^{\dagger}_{\mathbf{k}} \gamma_{\mathbf{k}0} + u_{\mathbf{k}} \gamma^{\dagger}_{\mathbf{k}l},$$

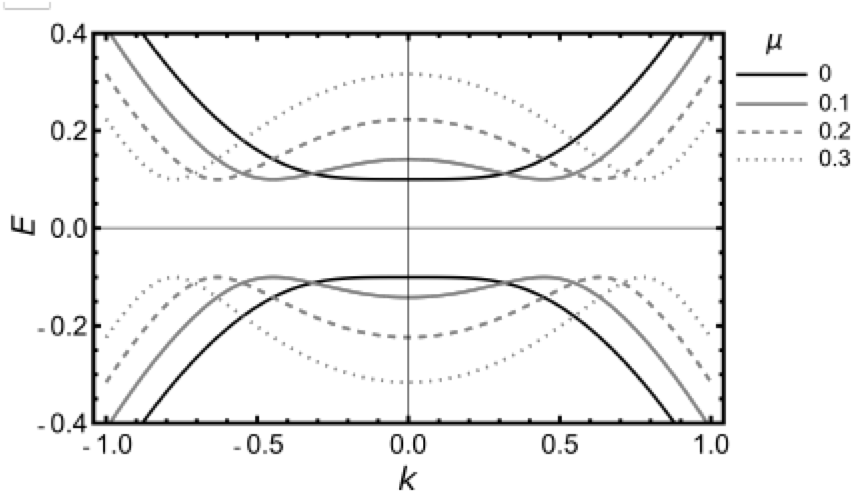

$$; E_{\pm} = \pm\sqrt{\left(\frac{\hbar^2 k^2}{2m} - \mu\right)^2 + |\Delta_{\mathbf{k}}|^2}$$

$$E_{\mathbf{k}\pm} = \pm\sqrt{\xi_{\mathbf{k}}^2 + |\Delta_{\mathbf{k}}|^2}$$

$$H = \left(\frac{k^2}{2m} - \mu + \alpha k \sigma_x - \mu\right)\tau_z - B\sigma_z + \Delta\tau_z$$

$$E_\pm = \frac{k^2}{2m} - \mu \pm \sqrt{(\alpha k)^2 + B}$$